

THE INTERACTION OF A FINITE
AMPLITUDE ACOUSTIC WAVE WITH
SMALL OBSTACLES AND ORIFICES

by

PETER J. WESTERVELT

B.S., Massachusetts Institute of Technology
(1947)

M.S., Massachusetts Institute of Technology
(1949)

SUBMITTED IN PARTIAL FULFILLMENT OF THE
REQUIREMENTS FOR THE DEGREE OF
DOCTOR OF PHILOSOPHY
(1951)

Signature of Author.....
Department of Physics, January 6, 1951

Certified by.....
Thesis Supervisor

.....
Chairman, Departmental Committee on Graduate Students

ABSTRACT

The principal objective of this research has been to test the applicability of hydrodynamic laws to large amplitude acoustic interaction phenomena. In particular the interaction of large amplitude acoustic waves with circular orifices and small objects is investigated from the point of view of steady state classical hydrodynamics. The laws of hydrodynamics do not comprise linear relations alone and it is the quadratic deviations from linearity of these relations which are considered here.

Two theoretical relations are drawn from hydrodynamics in treating the behavior of spheres and orifices. These relations are inherently non-linear and explain most of the experiments reported here. For the sphere the starting relation is Oseen's second order correction to the drag force on a sphere moving through a fluid. For the orifice Bernoulli's law explains qualitatively most of the non-linear phenomena evident in orifices. In some cases these two concepts, Oseen's drag correction for the sphere and Bernoulli's law for the orifice yield relations in fair agreement with the results of acoustical experiments, and it is the points of departure from exact agreement which

present new problems which have yet to be resolved.

A few striking effects have been encountered in the course of this investigation. For example forces many orders of magnitude greater than those due to radiation pressure have been observed on spheres in a sound field consisting of a sinusoidal fundamental plus a second harmonic component. These forces can be explained in terms of the non-linear hydrodynamic drag theory.

A technique is outlined for finding the force caused by radiation pressure arising from the interaction of a collimated beam of sound with an object. The force is evaluated in terms of a surface integral of asymptotic scattering functions for the object. The expression for the force is valid for objects of any shape having arbitrary non-uniform normal boundary impedance. In addition, the method is simpler in its application than King's method. Specific expressions are derived for rigid spheres and cylinders of infinite and zero mass.

It is shown that the effects of ordinary viscous and thermal losses at the surface of small objects may give rise to extra forces, induced by radiation pressure, which are several orders of magnitude greater than the classical values calculated by King. The exact value of the force on the object cannot be obtained directly since part is due indirectly to a transfer of momentum associated

with the medium streaming by the object. The streaming is caused by the wave momentum absorbed in the viscous and thermal boundary layer surrounding the object.

It is also shown that the migration of particles under any force whatsoever cannot be governed by Stokes' law if the particle is at the same time exposed to a strong sound field. A modified form of Stokes' law is given for this case. The absorption cross section of spheres, small compared to the wavelength of sound, is shown to depend upon whether the sphere has a steady component of velocity along the propagation direction of the sound wave. The absorption cross section of small spheres is shown to depend upon the amplitude of the sound. These absorption effects have not been directly measured but are predicted in a simple manner from the same theory which explains the steady forces on the sphere. Two terms are introduced to describe these two absorption effects, the differential cross section σ_D , and the non-linear cross section σ_{NL} .

The non-linear behavior of orifices has been found to be quite similar in many respects to that of spheres. The relation is in a sense a reciprocal one, relating the force on the sphere to the velocity through the orifice. For example if a second harmonic wave is superposed on a sinusoidal sound wave, a small steady flow through the orifice is generated; the converse is also true. The acoustic

resistance of orifices with a superposed unidirectional flow has been called the differential resistance R_D . Measurements of the differential resistance have been obtained and correlated with measurements of flow resistance and non-linear resistance of the orifice. It has been found possible to modify a hydrodynamic treatment due to Sivian which originally explained the non-linear resistance of very small orifices in terms of kinetic energy loss, so that in its present form the theory accounts for most of the observed phenomena. The modifications of Sivian's theory consist in including the effects of contraction, and viscosity.

Bolt, Labate and Ingard found that the reactance of an orifice is materially reduced at large amplitude oscillations. We have found that the acoustic reactance for small amplitude oscillations can also be considerably decreased by forcing a steady flow of air through the orifice. A theory has been developed which accounts for the observed reduction in mass. The theory predicts approximately the value of the non-linear reactance, which experiments show to be a constant. The theory is also capable of specifying at what particle displacement amplitude the reactance attains its constant non-linear value.

The results of a large number of measurements of the

harmonics generated by small orifices and nozzles are reported. Harmonics as high as the 25th have been measured.

ACKNOWLEDGMENTS

The author wishes to acknowledge with gratitude the guidance given him by Professor R. H. Bolt in the conduct of this research.

Mr. Peter W. Sieck and Mr. Keith Hoyt assisted the author in the experimental work, and their contributions are specifically mentioned in the body of this report.

TABLE OF CONTENTS

ABSTRACT

ACKNOWLEDGMENTS

TABLE OF CONTENTS

LIST OF FIGURES

CHAPTER I - BASIC CONSIDERATIONS Page

1. Introduction.....	1
2. The Objects.....	1
3. The Phenomena.....	2
4. The Experimental Conditions.....	4
5. The Theory.....	6

CHAPTER II - A BRIEF REVIEW OF THE ORIFICE PROBLEM

1. Introduction.....	8
2. Steady Flow Characteristics.....	10
3. Sivian's Measurements and Theory.....	15
4. Non-Linear Reactance.....	18
5. The Author's Previous Work.....	19
6. The Results of Ingard and Labate.....	20

CHAPTER III - THE THEORY OF NON-STEADY FLOW THROUGH AN ORIFICE

1. Introduction.....	25
2. The Non-Linear Resistance.....	26
3. The Differential Resistance and Reactance.....	29
4. The Orifice as a Rectifier.....	33
5. The Maximum Available Momentum Flux.....	35

CHAPTER IV - THE ORIFICE---EXPERIMENTAL RESULTS

1. Introduction.....	38
2. General Experimental Technique.....	38
3. Flow Resistance.....	40
4. The Measurement of Non-Linear Resistance.....	43
5. Measurements of Differential Acoustic Resistance.....	46
6. The Influence of Steady Flow and Large Amplitudes on the Reactance.....	48
7. The Generation of Harmonics by Small Circular Orifices.....	50
8. The Pumping Action of the Orifice.....	53

CHAPTER V THE THEORY OF STEADY FORCES CAUSED BY SOUND WAVES

1. Introduction.....	54
2. The Wave Drag Coefficient.....	57

3.	Forces Produced by Acoustical Radiation Pressure.....	58
4.	The Oseen-Type Forces.....	66

CHAPTER VI - AN EXPERIMENTAL DETERMINATION OF THE WAVE
DRAG COEFFICIENT ON SPHERES AND CYLINDERS

1.	Introduction.....	77
2.	Experimental Technique.....	78
3.	Early Experimental Results.....	81
4.	The Variation of $-\log d_3$ with f and ϕ	84
5.	The Wave Drag Coefficient Versus Sound Pressure Level and Frequency...	86

CHAPTER VII - SIGNIFICANCE OF THE RESULTS

1.	The Virtual Mass of an Oscillating Sphere..	91
2.	The Non-Linear and Differential Absorption Cross Section of a Small Sphere.....	95
3.	Floating Particles with Sound.....	96
4.	Free Fall Velocity in a Sound Field.....	97
5.	Recommendations for Future Work.....	98

APPENDIX I - A DERIVATION OF NON LINEAR RESISTANCE
FOR THE ORIFICE 100

APPENDIX II - ACOUSTICAL IMPEDANCE IN TERMS OF ENERGY
FUNCTIONS 102

APPENDIX III - CALCULATION OF THE OSEEN TYPE AVERAGE 108

APPENDIX IV - MAXIMIZING THE OSEEN TYPE MOMENT 109

APPENDIX V - THE GENERATION OF HARMONICS BY ORIFICES 113

BIBLIOGRAPHY

BIOGRAPHICAL NOTE

LIST OF FIGURES

Figure Numbers	Title
1.	Orifice in Tube
2.	Coefficient of Discharge
3.	Orifice Harmonics
4.	One-half ^{Power} Dependence of Fundamental /
5-8.	Ingard and Labate's Phase Diagrams
9-11.	Ingard and Labate's Resistance Measurements
13.	Ingard and Labate's Kinetic Mass Measurements
14.	Waveform with Square Root Moment
15.	Resistance Defined
16.	Momentum Flux from Orifice
17.	Block Diagram of Orifice Test Apparatus
18.	Photograph of Equipment
19.	Typical Flow Characteristics Curve
20.	Flow Resistance of 0.5 cm Orifices
21.	Flow Resistance of 0.357 cm Orifices
22.	Typical Transmission Loss through Orifice
23.	Sound Pressure Level for Onset of Non-Linear Transmission Loss
24.	Non-Linear Resistance for 0.5 cm Orifices
25.	Non-Linear Resistance for 0.357 cm Orifices
26.	Non-Linear Resistance and Flow Resistance Compared
27.	Differential Resistance for 0.5 cm Orifice

Figure Numbers	Title
28.	Differential Resistance for 0.357 cm Orifice
29.	Differential Resistance and Reactance for 0.5 cm Orifice
30.	Hydrodynamic Drag on a Sphere
31.	Hydrodynamic Drag on a Cylinder
32.	Wave Form with Oseen-Type Moment
33.	Normalized Oseen Moment vs. Harmonic Fraction
34.	Normalized Oseen Moment vs. Steady Flow Fraction
35.	The Partial Drag Coefficients Compared
36.	Rectangular Wave with an Oseen Moment
37.	Block Diagram of Obstacle Test Apparatus
38.	Schematic Diagram of Frequency Doublers and the Phase Shifter
39.	Maximum Available Particle Displacement Amplitude
40.	Early Measurement of Oseen-Type Force
41.	Oseen-Type Force in a Stationary Wave
42.	The Polar Dependence of $-\log d_3$
43.	$-\log D_W$ vs. Harmonic Fraction
44.	$-\log D_W$ vs. Phase Angle
45.	$-\log D_W$ vs. Sound Pressure Level
46.	$-\log D_W$ vs. Traveling Wave Sound Pressure Level in the Presence of Steady Flow
47.	$-\log D_W$ vs. Stand Wave Sound Pressure Level in the Presence of Steady Flow
48.	$-\log D_W$ for a 1 Micron Cylinder vs. Sound Pressure Level
49.	$-\log D_W$ for a 14 Micron Cylinder vs. Sound Pressure Level

Figure
Numbers

Title

- 50. Vibration Amplitude Ratio for 1 Micron Cylinder
- 51. Vibration Amplitude Ratio for 14 Micron Cylinder
- 52. A Comparison of the Drag Coefficient Ratios for Spheres and the Incremental Reactance for Orifices.
- 53. Theoretical Sound Pressure Level Required to Float Sphere
- 54. Theoretical Reduction of Terminal Velocity
- 55. Theoretical Reduction of Terminal Velocity
- 56. Peak Reynold's Number vs. Sound Pressure Level
- 57-60. Waveform of a Wave with Second Harmonic Distortion
- 61-71 Spectral Distribution of Harmonics from Orifices
- 72. Orifice Harmonics
- 73. Dip in Second Harmonic
- 74. Decay Slope of the Odd Harmonics

CHAPTER I
BASIC CONSIDERATIONS

1. Introduction

In this report phenomena are discussed which are best explained by combining certain concepts derived from acoustics on one hand and from the hydrodynamic theory of real fluids on the other hand. We are interested in explaining certain effects, arising from the interaction of large amplitude compressional waves with objects. This explanation is sought in the application of steady flow theory. The point of view adopted throughout the report is that the steady flow equations are instantaneously valid for periodic flow. The variety and accuracy of the predictions stemming from such a point of view are investigated experimentally in air for frequencies between 0 and 800 cycles.

Attention is given in this chapter to some of the phenomena which have been measured; their origin are discussed from a physical point of view in terms of the properties of the medium.

2. The Objects

The objects investigated in this study were spheres, cylinders, and sharp-edged orifices. Thick orifices (called nozzles) were also used. In all cases the objects

are assumed to be small in comparison with the shortest wavelength component of the interacting wave. Orifices and nozzles are treated in Chapters II to IV; spheres and cylinders in Chapters V and VI; while in Chapter VII the points of similarity between apertures and obstacles are discussed and certain applications of our findings are suggested.

3. The Phenomena

The interaction of a wave and an object can be described in terms of energy and momentum considerations. For this description it is necessary to know the rate at which energy and field momentum are abstracted from the wave. It is also necessary to know how much of this momentum and energy is divided between the object, the medium, and the scattered wave. Momentum transmitted to the medium in general results in a streaming of the fluid medium. If the object is not free to move, no mechanical energy will be communicated to it; however, a force may be exerted on the object. The complete specification of how energy and momentum divide appears to be an extremely difficult problem. We shall consider separate idealized problems in an attempt to reach approximate answers.

We shall deal only with average quantities such as complex power, average momentum flux, and steady forces.

Though the behavior of either the obstacle or the orifice can be specified in equivalent terms, it turns out to be simpler, from the experimental point of view, to determine the energy behavior of orifices on the one hand and the momentum behavior of obstacles on the other hand. Adopting this operational point of view then, the quantities of immediate interest are:

- (1) The complex power transformed by the orifice to the medium.
- (2) The average rate at which the obstacle absorbs momentum from the medium (not all this momentum need come from the wave, and the wave need not be sinusoidal.)

It is obvious here that the words "orifice" and "obstacle" can be interchanged. As discussed in Chapter VII, energy relations can be obtained from momentum measurements and vice versa. The availability of both energy and momentum measurements can serve to check the consistency of the results.

The behavior of the orifice is ascertained by measuring its acoustic impedance. Acoustic impedance is the complex power absorbed by the orifice divided by the square of the fundamental volume velocity amplitude. The units of acoustic impedance are acoustic ohms or, in cgs units,

(dynes-sec)/cm⁵. The orifice is studied only in the non-linear region where its operation is essentially jet-like. The power abstracted by means of the orifice is communicated to the medium by way of the jet.

The behavior of the obstacle is ascertained by measuring the total steady force acting upon it. This force is the momentum abstracted from the medium. The origin of this force is studied theoretically in both the low amplitude and the high amplitude regions. In the small particle displacement region, two mechanisms are responsible for forces stronger than the force due to classical radiation pressure. One of these mechanisms depends upon losses in the boundary layer and hence is influenced by viscosity and heat conduction, two properties of real fluids. The other mechanism, based on the temperature dependence of the viscosity has been treated elsewhere⁽¹⁾ by the author and thus it will not be developed in this paper. None of these forces which occur in the linear region has been measured by us.

Two further mechanisms leading to forces in the non-linear region of large particle displacements are discussed.

4. The Experimental Conditions

It turns out experimentally that certain effects do not occur very strongly unless the particle displacement amplitude exceeds a characteristic linear dimension of the

object by about one order of magnitude. For this reason we arbitrarily speak of the low amplitude region as one for which the particle displacement amplitude is considerably less than the characteristic length of the object, projected in the direction of the vibration vector. For example, in dealing with the sphere, the ratio of the particle displacement amplitude ξ_0 to the radius a , ξ_0/a can be adopted as a convenient dimensionless quantity. In general if $\xi_0 > a$, strong forces exist which disappear when $\xi_0 < a$. The author has previously suggested⁽²⁾ that this ratio is a convenient one for describing the behavior of orifices. This ratio is also inversely proportional to the dimensionless frequency, v' , a number used by aerodynamicists in connection with flutter phenomena. The dimensionless frequency is given by

$$v' = \frac{v\ell}{v}$$

where v is the frequency, ℓ a characteristic length and v the velocity amplitude. Most of our experimental work with orifices was obtained for a v' much less than 0.1, in the jet region of operation. The experiments with spheres and cylinders were performed at a v' in the vicinity of 0.1

In all experiments with obstacles, the peak Reynold's number for the obstacle was in every case less than 50 and in most cases less than 20, while the peak particle velocities were less than 300 cm/sec. Peak Reynold's numbers as low as .02 were investigated.

Most of the experiments with orifices were carried out at a peak Reynold's number of about 10^4 . The peak mach number in the throat of the orifice was usually less than 0.1, so that compressibility effects could be neglected.

5. The Theory

The theoretical work reported in Chapters III and V is for the most part purely adaptive. The results of existing steady flow theory are applied to non-steady phenomena without inquiring into the basic limitations of such an approach. In some instances the steady flow theory is so complicated (Oseen's theory for example) that its extension to non-steady flow does not seem imminent.

One way of modifying the steady flow theory is suggested from dimensional analysis. For example, it is possible to show⁽³⁾ that the relation between the force F on a sphere moving with velocity u and acceleration \dot{u} must have the form

$$F = \rho u^2 a^2 g\left(\frac{2ua}{\nu}, \frac{\dot{u}a}{u^2}\right). \quad (1)$$

where ρ and ν are the density and kinematic viscosity of the medium and a is the radius of the sphere. Now if u is periodic with frequency, n , we see that g becomes a function of the Reynold's number R and the reduced frequency ν' .

This suggests that the dependence of the average drag coefficient might properly be expressed as a function of the Reynold's number, and the reduced frequency. This is standard procedure, in the limit of zero frequency, as is illustrated in Figs.30, and 31. Our experimental results in Chapter VI can be considered to yield this functional dependence, for which there does not yet appear to be an adequate theoretical development.

CHAPTER II

A BRIEF REVIEW OF THE ORIFICE PROBLEM

1. Introduction

The orifice is a precision instrument used frequently in laboratories and in industrial processes for accurately metering the flow of fluids. In view of its widespread use a large body of literature exists, pertaining predominantly to the steady flow characteristics of the orifice. The most authoritative information may be found in the A.S.M.E. Fluid Meters Report⁽⁴⁾. A less detailed discussion of the sharp-edged orifice adequate for an understanding of the present problem may be found in "Unit Operations"⁽⁵⁾. Since our problem is to interpret how the orifice responds to periodic driving forces, in terms of its steady flow characteristics, these characteristics will first be briefly reviewed.

Sivian⁽⁶⁾, in the year 1935, appears to have been the first person to have made a systematic study of the large amplitude alternating flow characteristics of the orifice. Sivian's pioneer measurements of the acoustic resistance of orifices for large particle velocities will be reviewed. His measurements indicated that the non-linear resistance was fundamentally attributable to the jet forming property of the orifice, and that in general the resistance had a first power dependence on the particle velocity amplitude. He found the non-linear resistance essentially

independent of frequency; however his measurements were not carried out over as wide a range of conditions as was done later by Ingard and Labate.⁽⁷⁾ The latter found operating regions for which the resistance was strongly frequency-dependent.

Sivian's attempt to apply hydrodynamic theory to the non-linear acoustical performance of orifices is analyzed and the importance of friction and contraction, two factors neglected in his theory, will be emphasized. R. Clark Jones⁽⁸⁾ mentioned the need to consider contraction in specifying non-linear resistance. Jones treated the problem of a siren in which the port area varied periodically with time and due to the complexity of this problem, he did not take contraction into account.

The author's⁽²⁾ earlier explanation of non-linear resistance in terms of the generation of harmonics is shown in general not to apply. Later evidence obtained by him in support of the jet mechanism is discussed.

Some recent measurements performed by Ingard and Labate⁽⁷⁾ of the non-linear resistance and reactance of orifices will be discussed. Their extremely accurate work carried out in conjunction with a detailed study of steady flow phenomena in the neighborhood of the orifice demonstrates graphically certain regions in which a classical hydrodynamic approach is justified.

2. Steady Flow Characteristics

Consider the arrangement in Fig.1 depicting two cylindrical pipes of equal cross-sectional area S_1 , separated by a thin circular orifice of cross-sectional area S_2 . Fluid flows from left to right. A reasonable distance to the left of the orifice the pressure P_1 and velocity V_1 are considered to be uniform. The streamlines converge as they approach the orifice. The fluid issues from the orifice in the form of a jet into a region where, for the present, the absolute pressure will be assumed zero. Close to the plane of the orifice the jet has a minimum area S_2' called the vena contracta. The ratio of the minimum jet area to the orifice area S_2 is called the coefficient of contraction C_c . A knowledge of this coefficient, which turns out to be a function of geometry as well as the Reynold's number for the orifice, is essential to the discussion of jet-like flow. The exact magnitude of this coefficient has not been obtained theoretically for an orifice situated in a pipe; it is a function of the ratio of the diameter of the orifice to that of the pipe. When the orifice is small in comparison with the diameter of the pipe and provided friction losses are neglected, this coefficient may be obtained approximately by applying the principles of conservation of energy and momentum. The exact formal expression for C_c may be set up by applying the

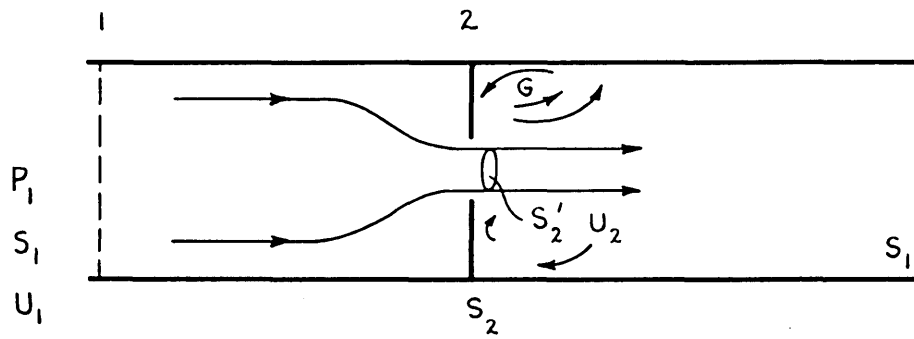


FIG. 1 - ORIFICE IN TUBE

principle of continuity of the flux of momentum to the cross sections 1 and 2 in Fig. 1:

$$P_1 S_1 = \int_{S_1-S_2} p dA = \rho u_2^2 S_2' \quad (1)$$

where ρ is the density of the fluid. Conservation of energy leads to:

$$P_1 u_1 S_1 = \frac{\rho u_2^3}{2} \quad (2)$$

Continuity of incompressible matter, $u_1 S_1 = u_2 S_2'$, allows Eq.(2) to be rewritten

$$P_1 = \frac{\rho u_2^2}{2} \quad (3)$$

Eq. (3) is a statement of Bernoulli's principle which, in connection with Eq.(1), determines the coefficient C_c :

$$C_c = \frac{S_1'}{S_2} = \frac{P_1 S_1 - \int_{S_1-S_2} p dA}{2 P_1 S_2} \quad (4)$$

The integral in the above equation is not evaluated for the orifice in a pipe. If the approximation is made that the pressure at point 2 is uniform over the cross section and equal to P_1 , it follows from Eq.(4) that $C_c = 1/2$. If the velocity is assumed to be uniformly distributed over hemispheres concentric with the center of the orifice, the analysis gives $C_c = 0.535$. The methods of hydrodynamics give 0.61 as the coefficient of contraction for a long narrow slot.

Bernoulli's equation (3) may be written in terms of Q , the volume velocity through the orifice, the orifice area S_2 , and C_c :

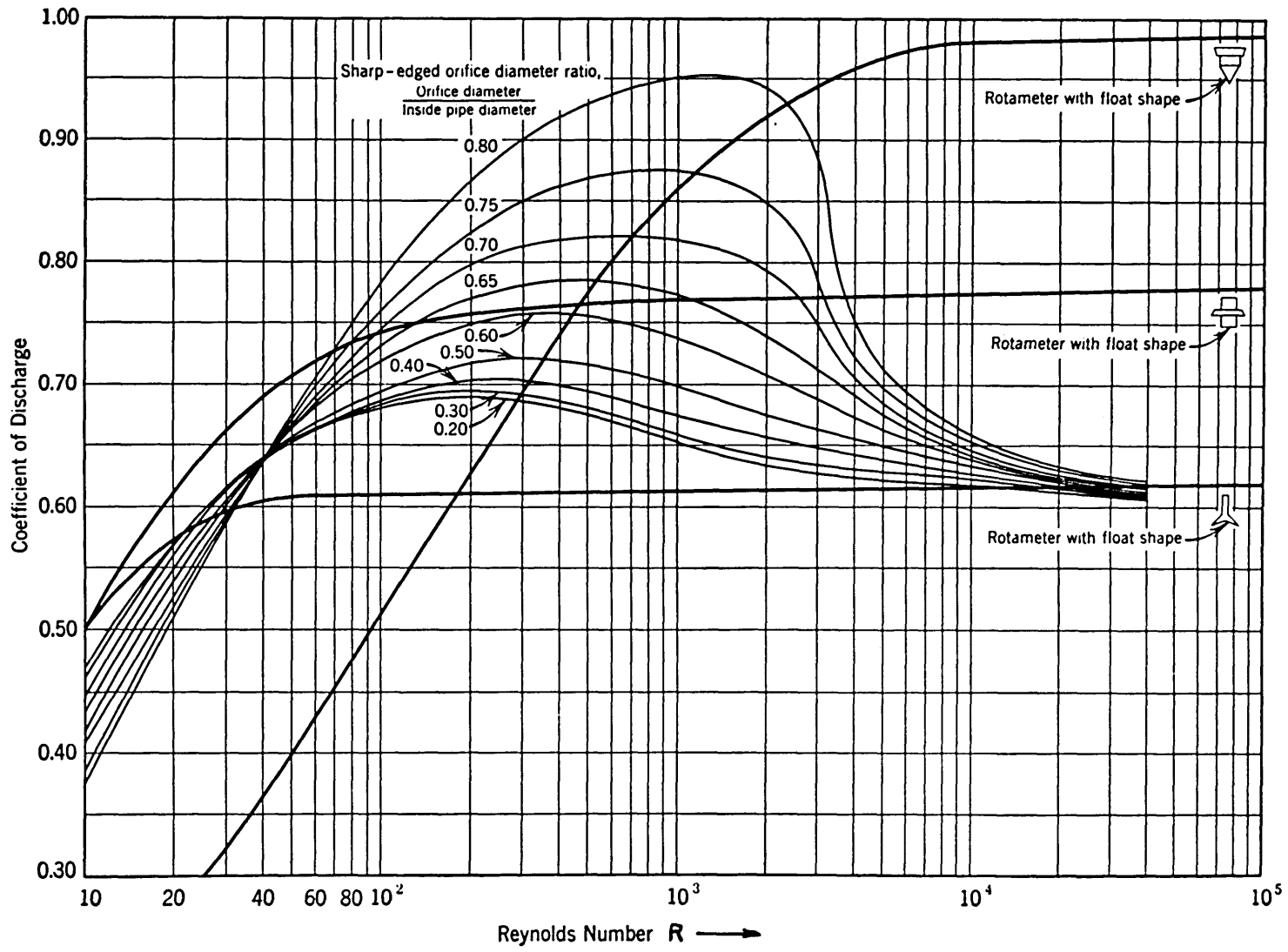
$$Q = C_c S_2 \sqrt{\frac{2p}{\rho}} \quad (5)$$

Now were it not for frictional losses in the orifice Eq.(5) would relate the observed volume flow to the pressure head p . Due to frictional effects the actual flow will be reduced by a factor C_v , called the coefficient of velocity, which is less than unity. It is conventional practice to call the product of the two orifice coefficients ($C_c C_v$) the coefficient of discharge which is designated C_d . All three of these coefficients vary with the character of the liquid, the roughness of the orifice, and the Reynold's number for the orifice. Eq.(5) may be written so as to include the effects of contraction and viscosity:

$$Q = C_d S_2 \sqrt{\frac{2p}{\rho}} \quad (6)$$

Experimental values of C_d vary with the Reynold's number of the orifice $R = \frac{2ur}{\nu}$, where r is the radius of the orifice and ν the kinematic viscosity. Representative data (reproduced from "Unit Operations"⁽⁵⁾ taken in a pipe are illustrated in Fig.(2). The range of Reynold's number spanned in our experiments extends from 100 to 4000.

Measurements were made in the course of this investigation from which the value of the discharge coefficients of our orifices could be determined. These results appear in



Variation of discharge coefficient with Reynolds number for sharp-edged orifices and rotameters.

FIG. 2

Chapter IV. The d-c characteristics were evaluated in terms of the flow resistance R_F which is defined as the ratio of the d-c pressure p to the steady volume velocity Q . The flow resistance comes directly from Eq.(6) and is*

$$R_F = \frac{p}{Q} = \frac{\rho Q}{2(SC_d)^2} \quad (7)$$

It is not engineering practice to present orifice data in terms familiar to the acoustician. We shall not be interested in the exact value of the more widely used coefficient of discharge as long as our experiments yield values which form reasonable extrapolations of previously existing data. From Eq.(7) it is seen that measurements of R_F as a function of the volume velocity through the orifice, enables the coefficient of discharge to be evaluated. In addition to the experimentally determined values of R_F presented in the Figs. 20 and 21 in Chapter IV, there is plotted (in heavy solid line) the value of R_F obtained from Eq.(7) by choosing $\sqrt{\frac{1.1}{2}}$ for the coefficient of discharge. It is fairly evident that the coefficient of discharge varies among orifices of equal area but differing thickness, and the reason for this is discussed next.

The effects of thickness and finite width on orifices may be discussed in terms of the behavior of a nozzle. A

* Henceforth, unless specifically mentioned S stands for the actual area of the orifice.

nozzle is an orifice with an added discharge section which confines the jet, causing the vena contracta to have the same area as the discharge end of the nozzle. The orifice equations apply to the nozzle provided the constants are modified appropriately. For example, the coefficient of contraction C_c of a nozzle with a thickness to diameter ratio three or more is unity.⁽⁹⁾ On the other hand, it is to be expected that the coefficient of velocity C_v should increase with the thickness of the orifice (length of the nozzle), since viscous losses vary approximately in direct proportion to the inner cylindrical surface of the orifice. Thus the coefficient of discharge C_d which is the produce of C_c and C_v might be expected to have a maximum value for a thickness which corresponds approximately to the thickness for which contraction is completely suppressed; we shall call this the critical thickness. The critical thickness would be expected to increase with the Reynold's number. Hence, for a constant average velocity through the orifice the critical thickness will become greater for orifices of large diameter.

We have observed this effect quite clearly; it shows up if one plots the measured d-c flow resistance against the thickness of the orifice. Such a curve is given in Fig. 26 of Chapter IV. In this figure the flow resistance is observed first to decrease with increasing thickness, an effect attributable to a suppressed contraction. A minimum in the resistance of the 0.5 cm diameter orifice is seen to be followed by an

increase brought about by friction.

In our work, discussed in Chapter IV, we have found that the response of the orifice to alternating flow follows closely its steady flow behavior. For examples, the non-linear acoustic resistance varies in the same manner as the d-c flow resistance with the orifice thickness. Ingard's phase diagrams (see Figs. 5-8 of this Chapter), when plotted against orifice thickness, correlate closely with the d-c flow resistance curves provided the latter are inverted.

However, before discussing these regions of agreement in detail, it is advisable to review Sivian's attempt to correlate his steady flow and alternating flow measurements with hydrodynamic theory.

3. Sivian's Measurements and Theory

L. J. Sivian⁽⁶⁾ in 1935 presented the results of acoustic resistance measurements which he and R.T. Jenkins had made in 1930 on three circular orifices varying in diameter between .25 cm and 1.0 cm and having a thickness to diameter ratio of 0.2 or less. This group of orifices he called Group B. In the same article Sivian gave more recent data he had obtained pertaining to four circular orifices .034 cm in diameter with the length to diameter ratio varying from about .15 to 1.5. He used a resonator technique which enabled him to measure the resistance down into the approximately linear region. His data are given as plots of Acoustic

Resistance versus rms particle velocity averaged over the orifice. We have extrapolated the non-linear part of his curves to a value pertaining to a peak velocity of 500 cm/sec and subsequently tabulated this value in Table I along with his theoretical values (see Eq.(7) of next section.) The per cent deviation of his theory from the extrapolated values has been listed. In the last column is tabulated the power of the dependence $R\propto U^n$. The power n was estimated from Sivian's experimental curves. The first groups of 5 orifices, group B, were all measured at 100 cps, whereas the first and third listed orifices in this group were also measured at 500 cps. No noticeable frequency dependence was noted. No frequency was stated for the measurements of the orifices in group A.

TABLE I

diam. (cm)	thick. (cm)	R(meas.) ohms	R(theo.) ohms	per cent dev.	n
.034	.005	400	250	-38	1
.034	.013	poor data			1.8
.034	.025	400	250	-38	0.8
.051	.034	insufficient data			
.071	.013	90	56	-38	1
.25	.051	8	4.2	-47	1
.5	.051	2.6	1.1	-58	1.3
1.0	.051	1	.28	-70	1.5

Two points of significance about the results, which were not emphasized by Sivian, are the apparent increase in the exponential dependence n with increasing diameter, and the rather poor agreement of theory and experiment. These features will be discussed later.

Sivian noted that, to a first approximation, the growth of the observed resistance at high velocities appears to be a velocity effect. This justified his viewing the matter from the standpoint of d-c air flow. His theoretical treatment consisted essentially in applying conservation of energy to the flow through the orifice. We shall review in detail what we believe to be his theoretical approach. This is done because there is some ambiguity in the exact procedure presented in the original article. We start by quoting Sivian directly:

"We shall estimate the effect of the kinetic energy (K.E.) acquired by the air in an orifice on the resistance of the latter. Simplifying the problem still further, consider the case of an orifice S joining two semi-infinite tubes, T_1 and T_2 whose cross sections are much larger than that of S . Let the gas pressure in T_1 and T_2 be p_1 and p_2 respectively. The tubes are assumed so large that p_1 and p_2 remain sensibly constant while the velocity, V , of flow through S , is being observed. Also, the velocity of the air in the tubes is so small compared with the speed in the orifice, that its K. E. may be neglected. We further assume: (1) turbulence is negligible; (2) the flow is adiabatic; (3) the velocity is uniform over any cross section of the jet; (4) there is no internal dissipation. Then the air flow through the orifice is isentropic, and as shown

in thermodynamic texts,

$$\frac{1}{2}\rho U^2 = p_1(p_1^\alpha - p_2^\alpha)/\alpha p_1^\alpha \quad (8)$$

where U = linear velocity and $\alpha = (\gamma - 1)$. We shall apply this equation to an orifice in which viscosity and heat conductivity are effective even though that somewhat violates conditions (2), (3) and (4). Denoting the orifice area by A , and remembering that in practically all cases of acoustic interest, $(p_1 - p_2)/p_1 \ll 1$, we have to a first approximation

$$R_1 = R + 1/2(\rho U/S)$$

where R_1 is the new orifice resistance and R is the "low velocity" resistance. If this equation is to be used with slowly alternating flow, we should write

$$R_1 = R + \frac{1}{2}(\rho \cdot |U|)/S \quad .'' \quad (9)$$

This ends the quotation from Sivian. There are several points which bear consideration. In Eq.(8) it is important to realize that U signifies the linear velocity in the vena contracta, a fact neglected by Sivian.

Sivian does not state explicitly that Eq.(9) is the relation which is supposed to represent the acoustic resistance. Furthermore it is not evident from the text just quoted what is implied by U . Suffice to say that if $|U|$ is chosen the rms particle velocity, Eq. (9) agrees with Sivian's theoretical curves.

4. Non-Linear Reactance

Sivian, in his work discussed in the last section,

reported that the reactive component of the impedance of orifices was substantially independent of velocity. This result was contradicted in a recent paper⁽¹⁰⁾ by Bolt, Labate and Ingard. Bolt, et al, found that the reactance decreases strikingly with particle velocity. Later substantiation of this discovery by Ingard will be discussed in Section 6 of this Chapter.

5. The Author's Previous Work

The author made a study of large amplitude acoustic waves in 1947 and applied some of his results to the behavior of orifices. He studied the non-linear compressibility effects associated with the spherically diverging wave which issues from the orifice under high intensity conditions. His measurements confirmed for the first time the presence of strong odd harmonics Sivian⁽⁶⁾ had predicted should exist, but was unable to measure. An example of the relative strength of the first three harmonics is given in Fig. 3. Fig. 4 illustrates the $1/2$ power dependence of the fundamental on the driving pressure. These two curves were taken from the author's Master's thesis. The author attempted to explain the variation both in resistance and reactance in terms of compressibility effects. The increase in resistance he attributed to the power abstracted by the harmonics whose strength relative to the fundamental frequency

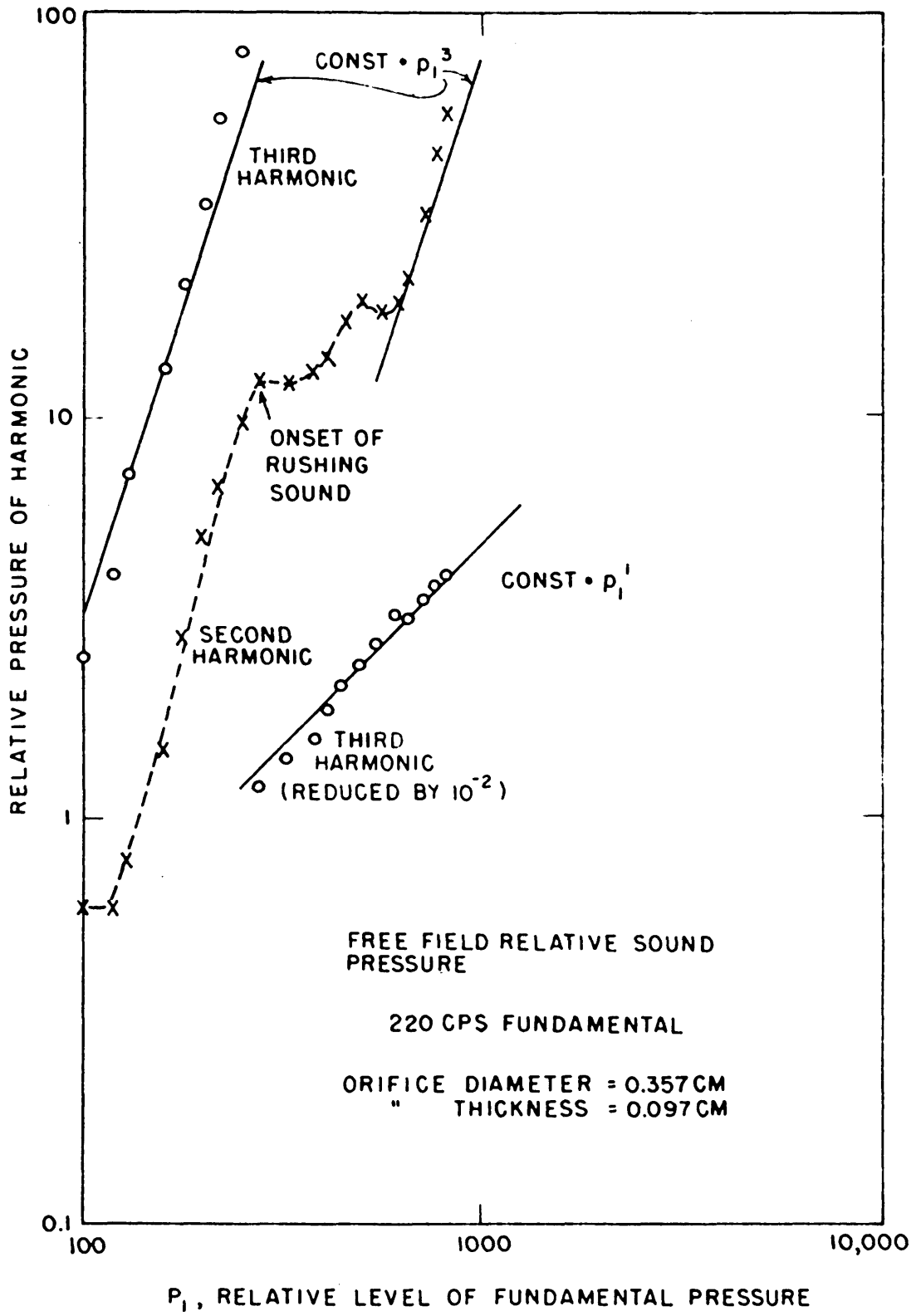


FIG. 3

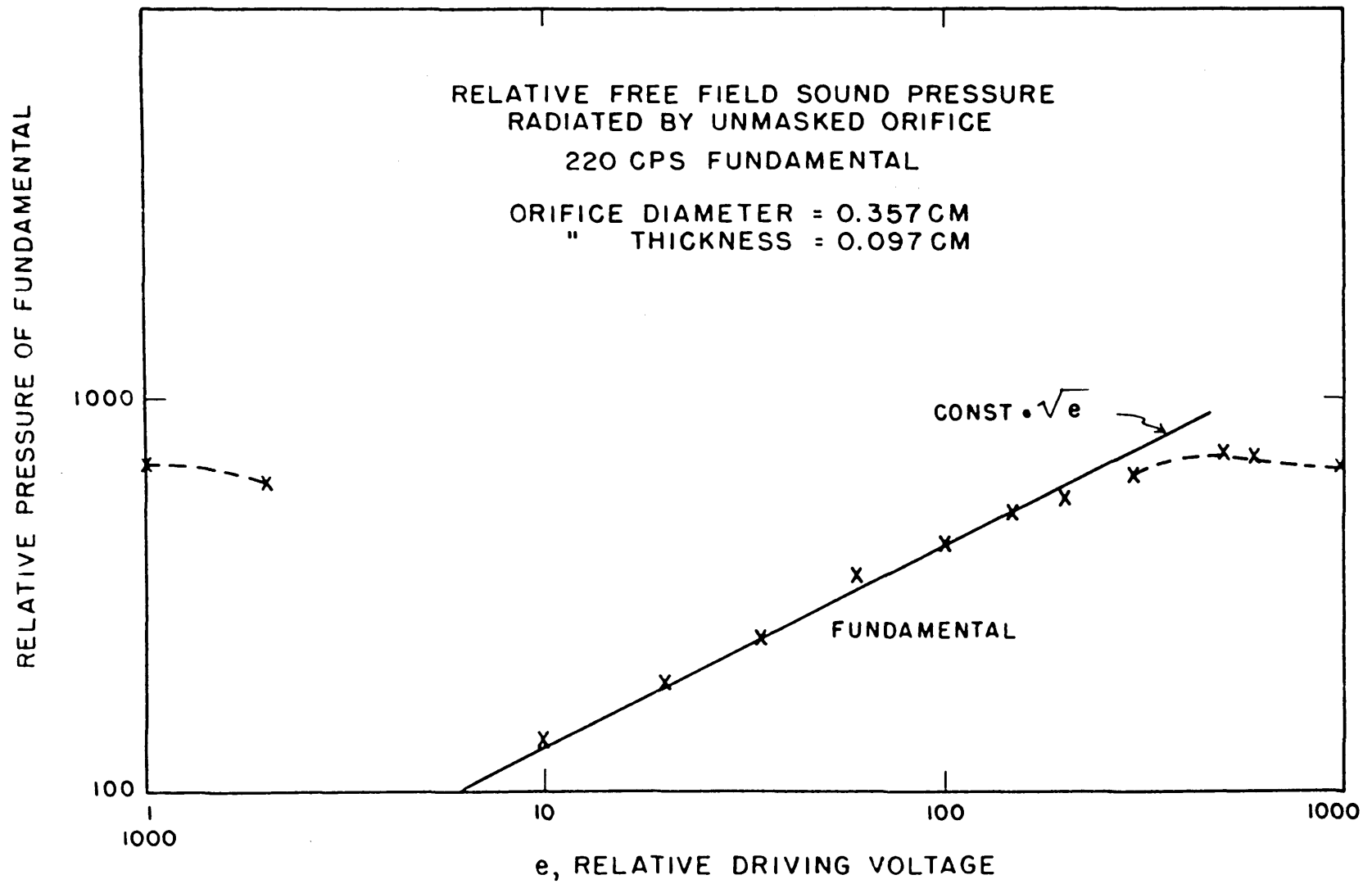


FIG. 4

component increased according to N^n , N being the ratio of the particle displacement amplitude to orifice radius and n the order of harmonic.

The validity of this mechanism was thrown into considerable doubt when⁽²⁾, at the author's suggestion, he and H. Harrison viewed the jet issuing from the orifice under stroboscopic illumination. Smoke on one side of the orifice was observed to issue from the other side as discrete pulses, which frequently assumed the nature of vortex rings. Later work by Ingard and Labate⁽¹¹⁾ showed conclusively that this jet was predominantly responsible for the resistance. Later measurements by the author indicated that only under special circumstances, could harmonic generation contribute measurably to the dissipation. Thus it became clear that orifice non-linearity was basically, as postulated by Sivian, a hydrodynamic problem, and that further work could most profitably be carried out by modifying Sivian's initial methods so as to bring them into agreement with the well established engineering behavior of orifices under steady flow conditions.

6. The Results of Ingard and Labate

The non-linear acoustic behavior of orifices has most recently⁽¹¹⁾ been examined by Ingard and Labate. They studied the circulation patterns generated in the vicinity of the

orifice and correlated changes in the nature of these patterns with measured values of the impedance. The circulation was conveniently described by them in terms of contour plots separating from each other the four different circulation regions they have defined. These "phase diagrams" are plotted by them in terms of the peak particle velocity, averaged over the orifice; either the frequency of the sound or the thickness of the orifice provides a second independent variable. Several such diagrams which will be useful in our later discussion are shown in Figs. 5 to 8. A description in their own words of the different circulation regions is given:

Region 1: A low particle velocity region with steady circulation; the flow is directed out from the aperture along the axis.

Region 2: A region of steady circulation in which the direction of flow is along the axis toward the aperture, i.e., the reverse of that in Region 1.

Region 3: A region characterized by the onset of turbulence.

Region 4: A high particle velocity region characterized by the appearance of jets and vortex rings. The jet is pulsatory and is made up of air pulses contributed by each cycle of the sound wave. It appears symmetrically on each side of the aperture.

The reader will do well to refer to the original article

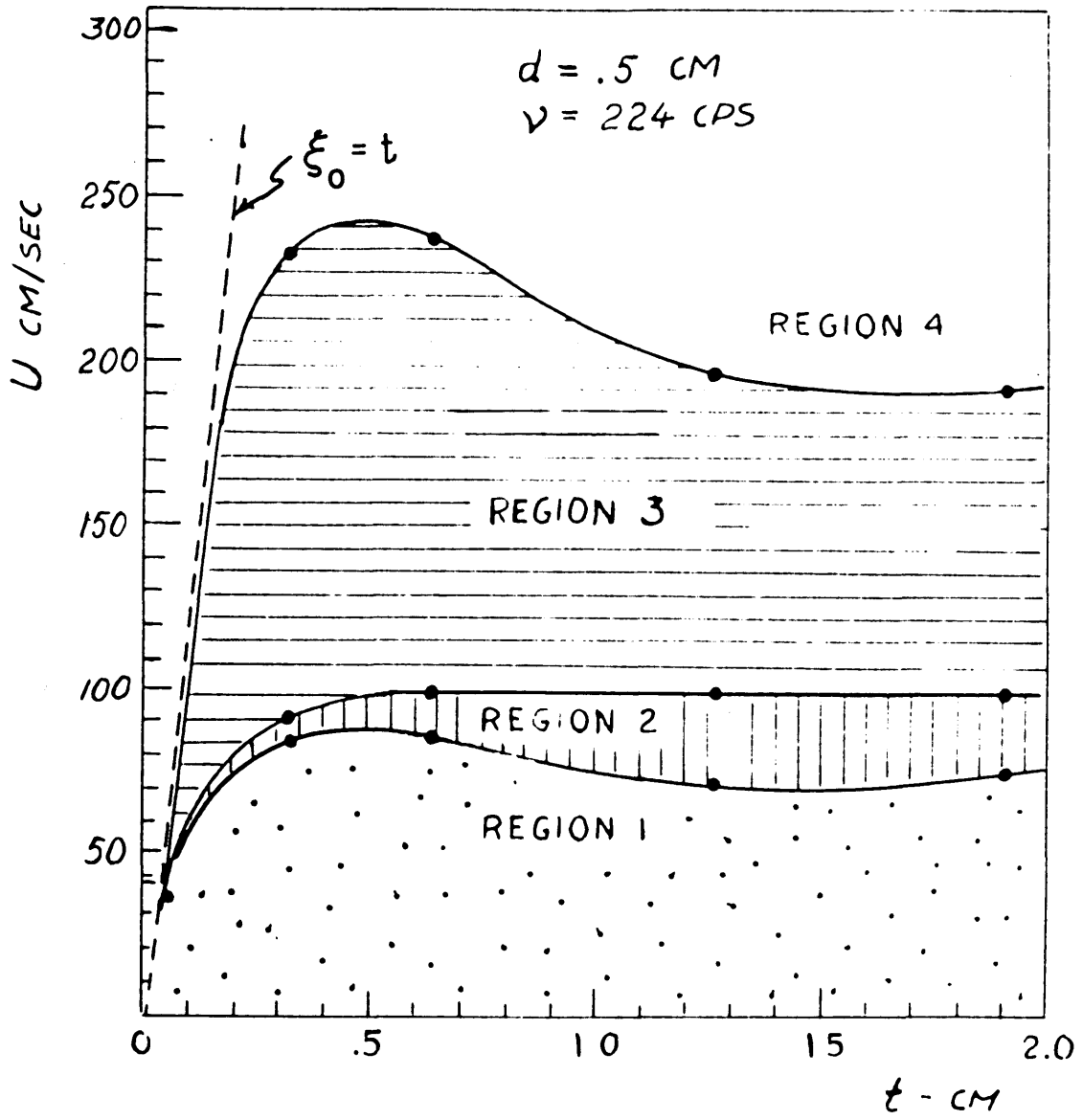


FIG. 5

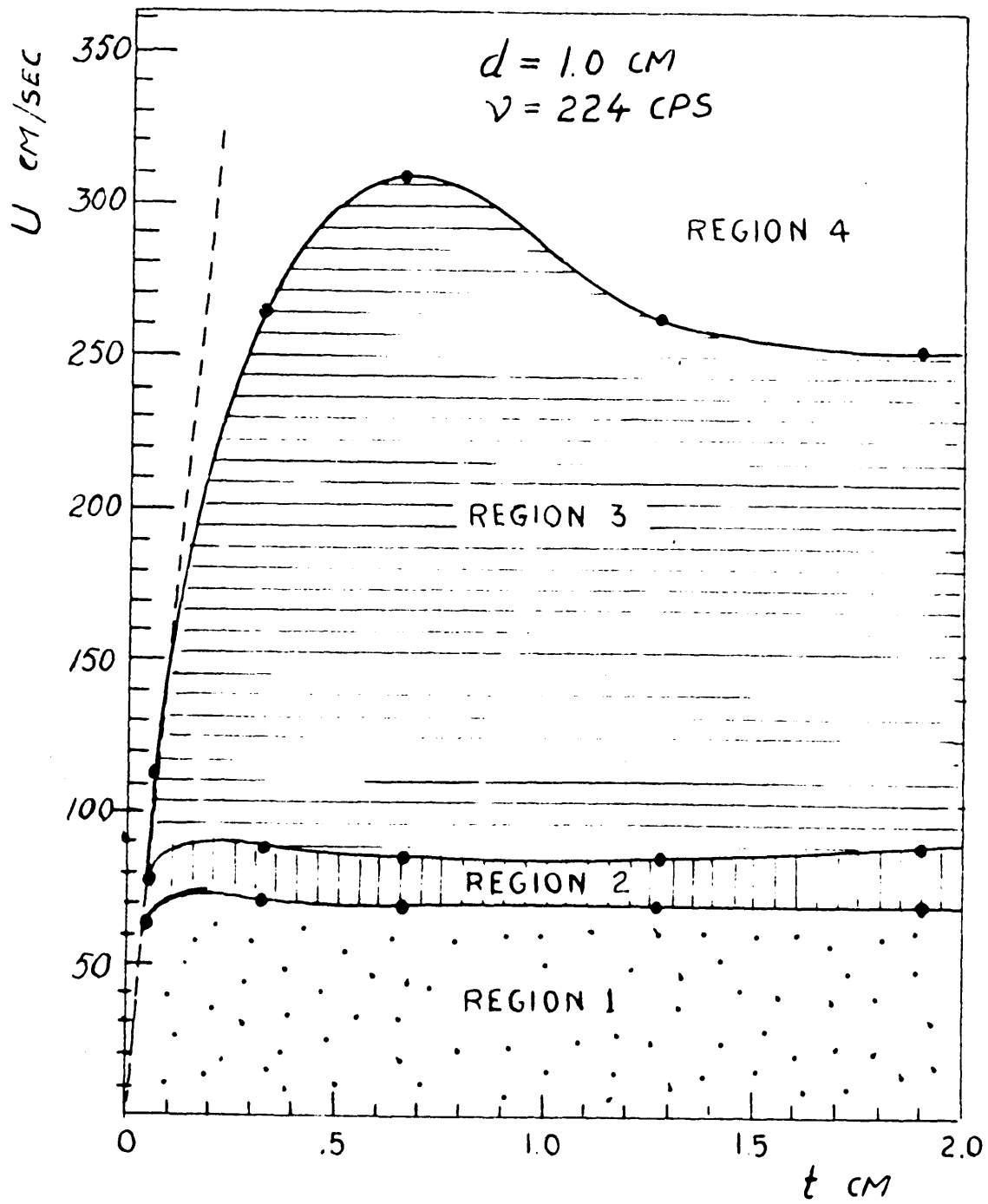


FIG. 6

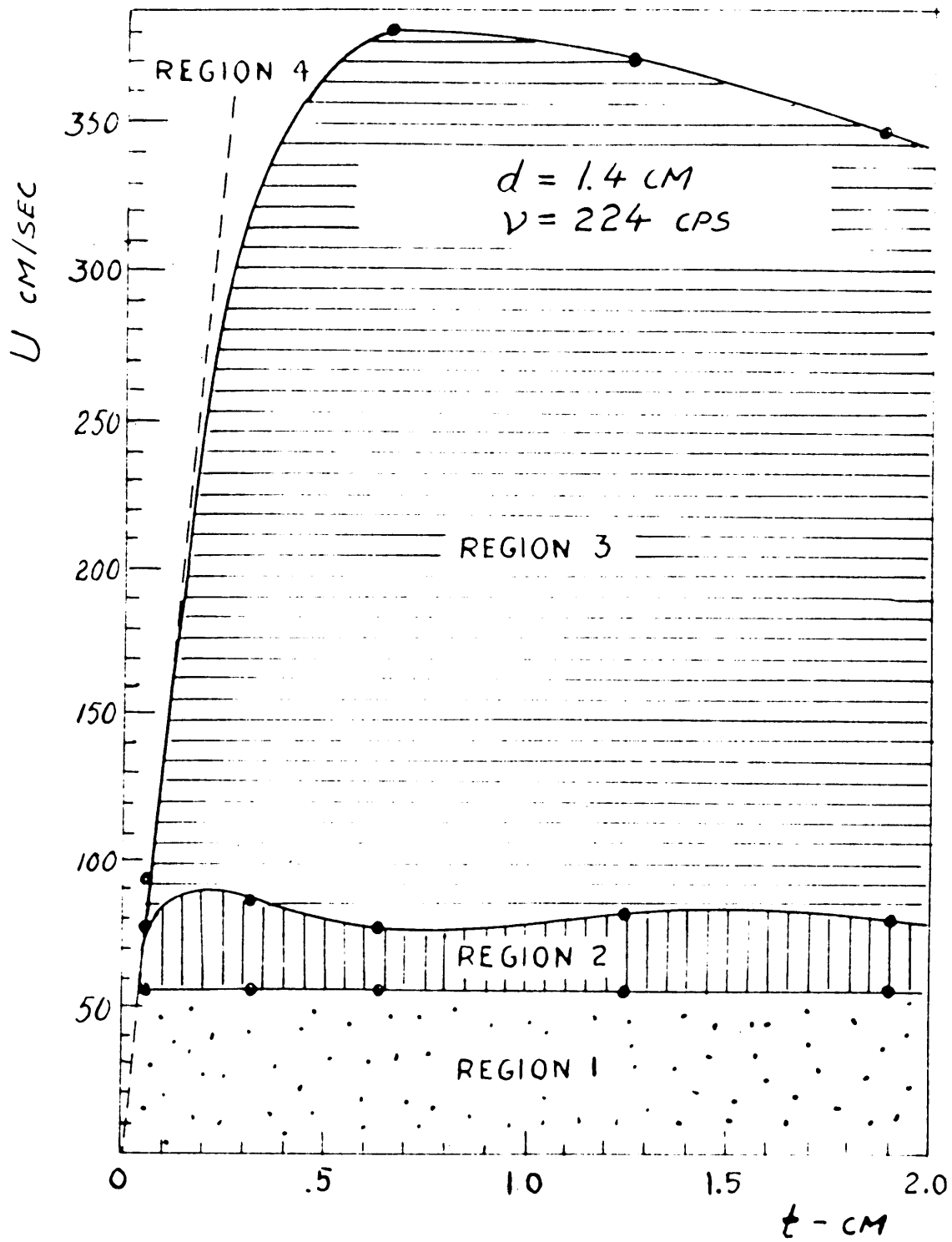


FIG. 7

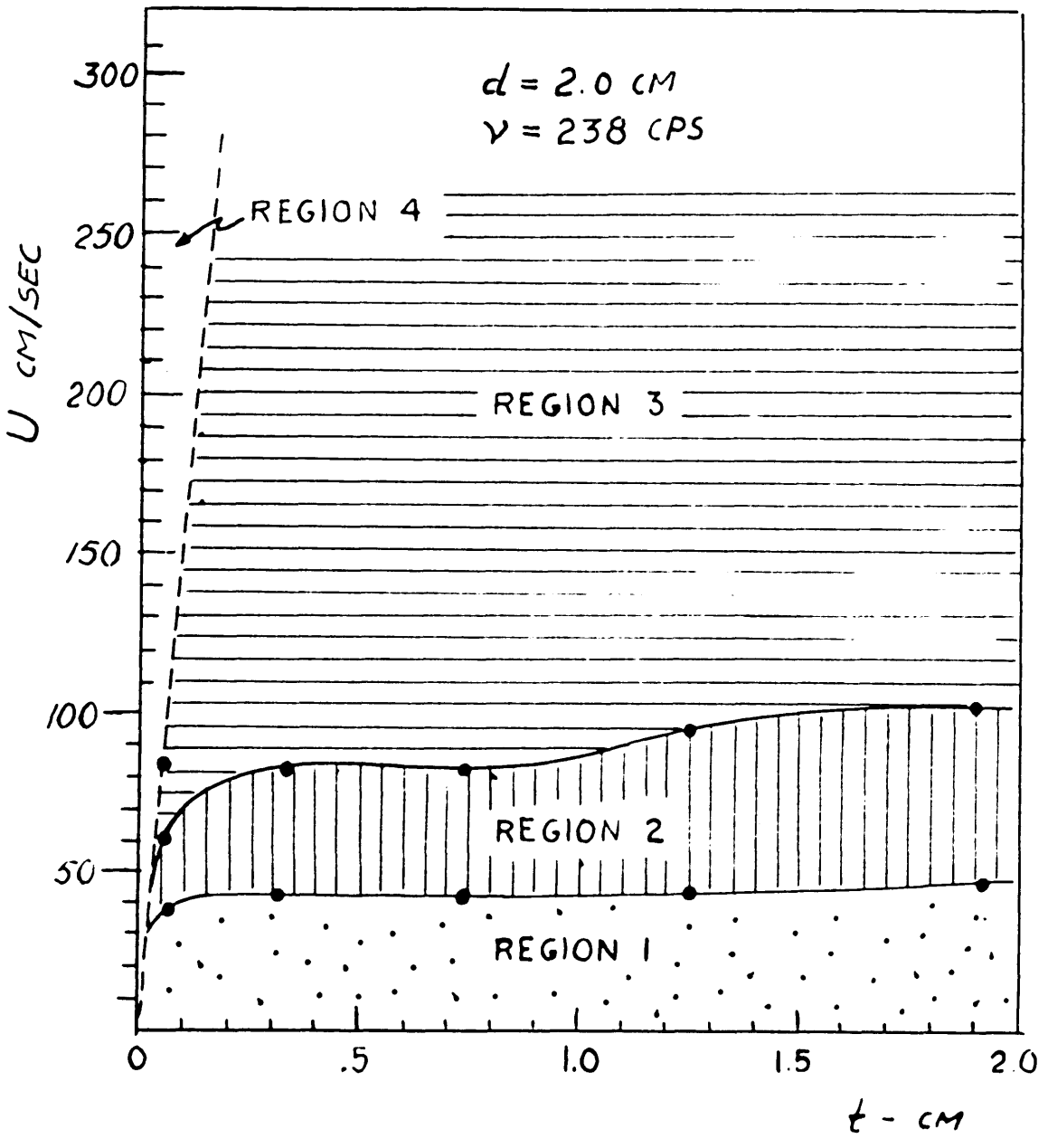


FIG. 8

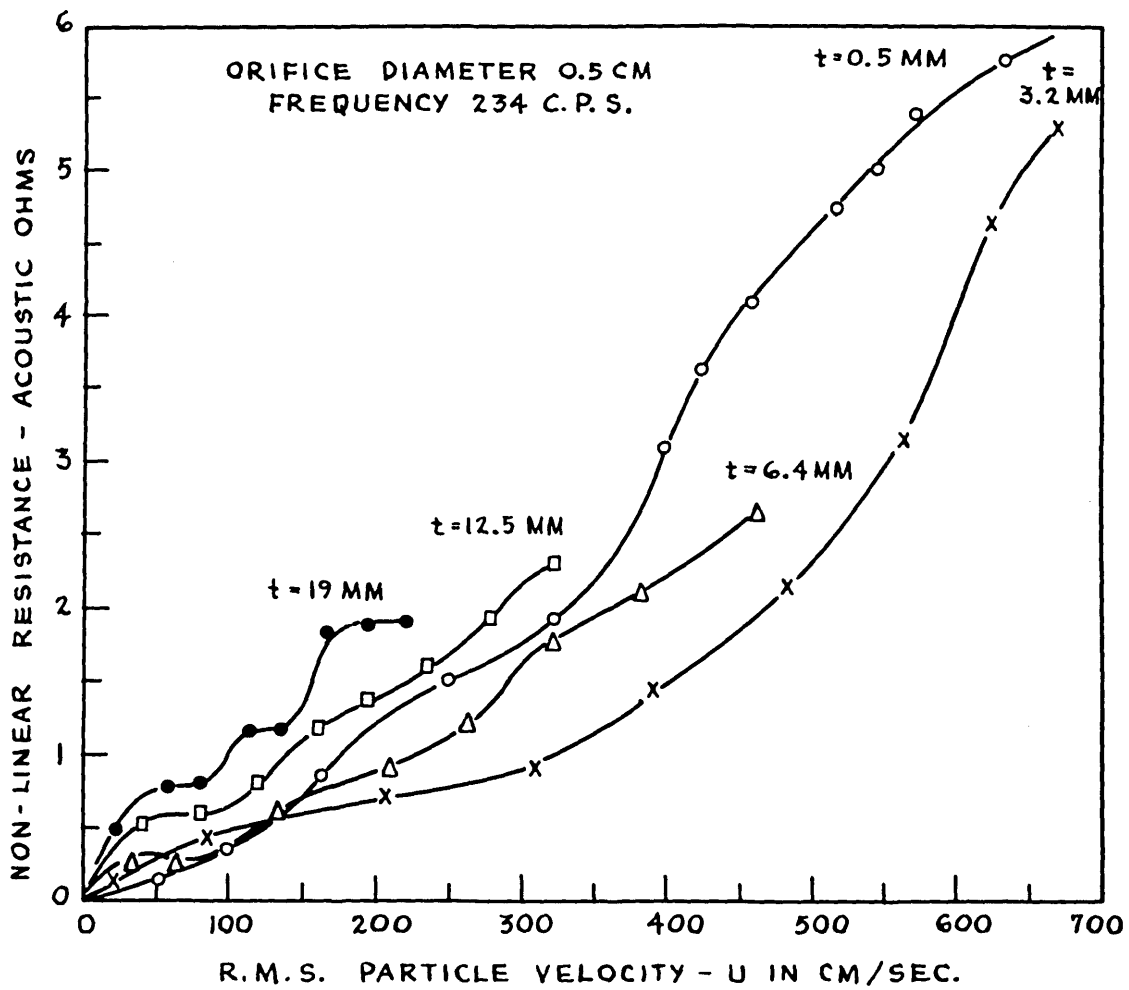


FIG. 9 - NON-LINEAR ACOUSTIC RESISTANCE OF AN ORIFICE AS A FUNCTION OF THE PARTICLE VELOCITY IN THE ORIFICE.

for a fuller description of these circulatory effects which are illustrated by a remarkable sequence of photographs of the streaming, made visible by means of smoke particles.

We will find that a close correlation exists between the shape of Ingard's phase diagrams, which are plotted with thickness as one variable, and the variation thickness of the d-c flow resistance for the orifice. We shall also see that the hydrodynamic interpretation of non-linear a-c resistance is valid primarily in Region 4 of the diagram.

Ingard and Labate made extensive measurements of the resistance of orifices for all conditions of circulation. An analysis of their results discloses that the logarithm of the resistance plotted against the logarithm of the particle velocity amplitude suffers in general two broad discontinuities in slope. A typical plot is shown in Fig. 10 where a quantity proportional to the resistance, $\frac{\Delta_{NL}}{d} = \frac{4S R_{NL}}{.84 \times 10^{-3} \sqrt{v}}$ has been plotted against $\frac{S_0}{t}$ the ratio of the particle displacement amplitude to the thickness of the orifice. Here S is the orifice area in cm^2 , v the frequency in cps. For orifices of small radius, the two changes in slope merge to form a broad inflection at a $\frac{S_0}{t}$ of about unity, correlating approximately with the transition from circulation Region 3 to 4.

A point of more significance to our problem is the fact that if the particle displacement amplitude exceeds thickness

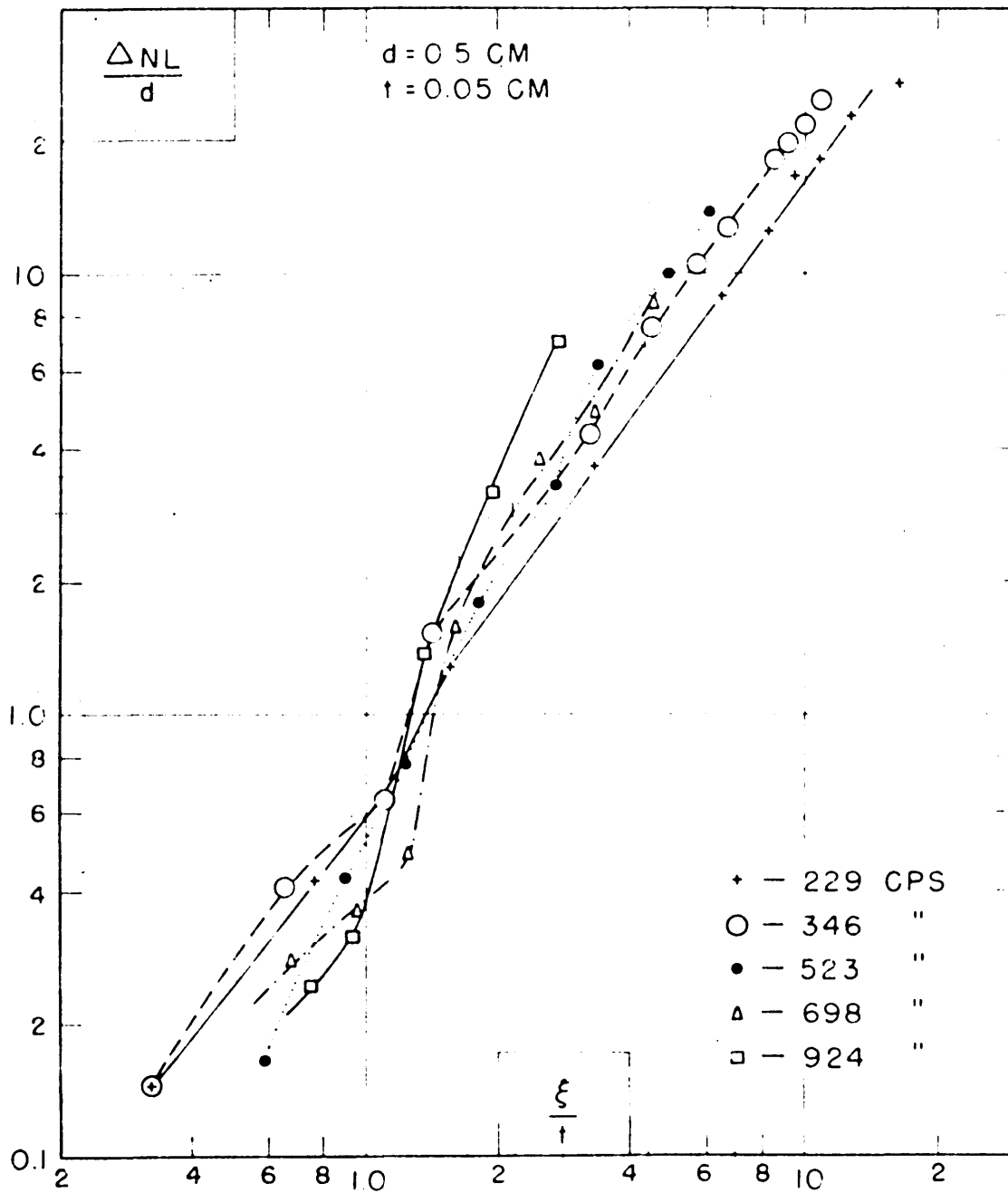


FIG. 10

by an order of magnitude or if the velocity exceeds the value defining the boundary between Regions 3 and 4, the resistance becomes roughly a function of the first power of the velocity. If neither of these criteria is met, the resistance varies with a power of the velocity greater than the second. Put another way, for low velocities or particle displacements the non-linear resistance is less than would be predicted by linearly extrapolating the high velocity value down to the low velocity. This fact is in accord with the exponents pertaining to Sivian's data tabulated in I. Approximate values of the exponent n taken from Ingard's curves in the similar velocity range are tabulated below:

TABLE II

Fig.	11b	9	10	12				11a	
diam. (cm)	.36	.5	.5	1	1	1.4	1.4	2	2
thick- ness (cm)	.09	.05	.05	.05		.05		.05	
n	1.3	1.0	1.5	1.3	1.6	1.6	1.6	1	2

In general the thin orifices have an n value approaching unity. Thick apertures of small diameter also have an n close to 1.

Our experiments have confirmed the fact that the resistance remains essentially a linear function of the velocity for velocity amplitudes about ten times greater than that achieved by Ingard. It is within this operating region that we will expect the hydrodynamic analogies to hold

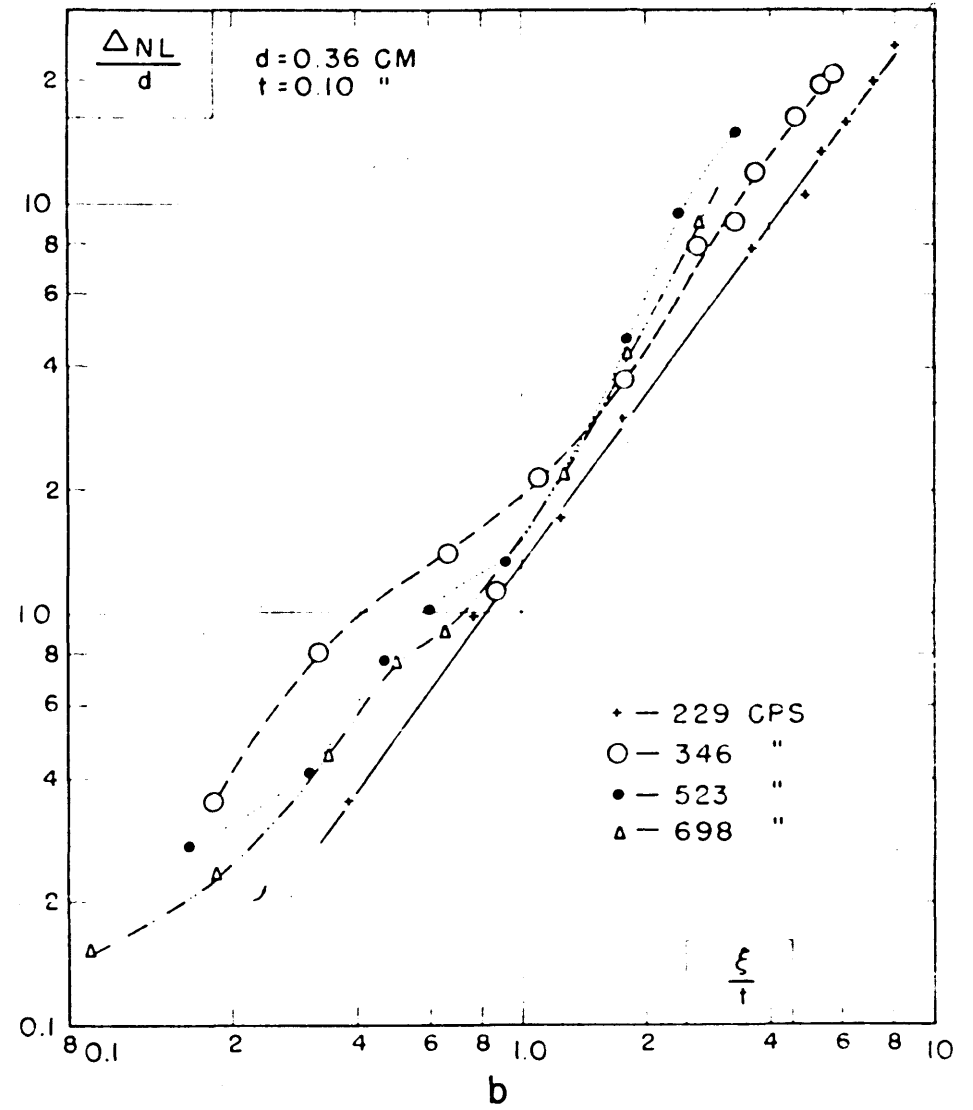
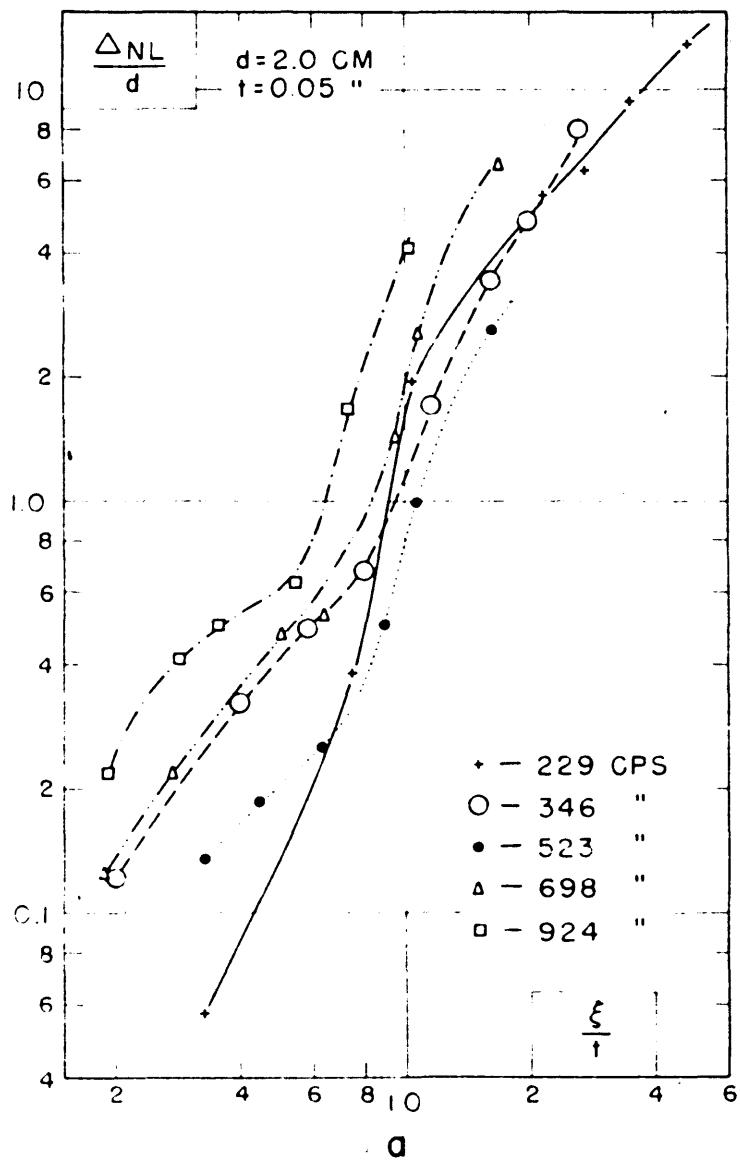


FIG. II

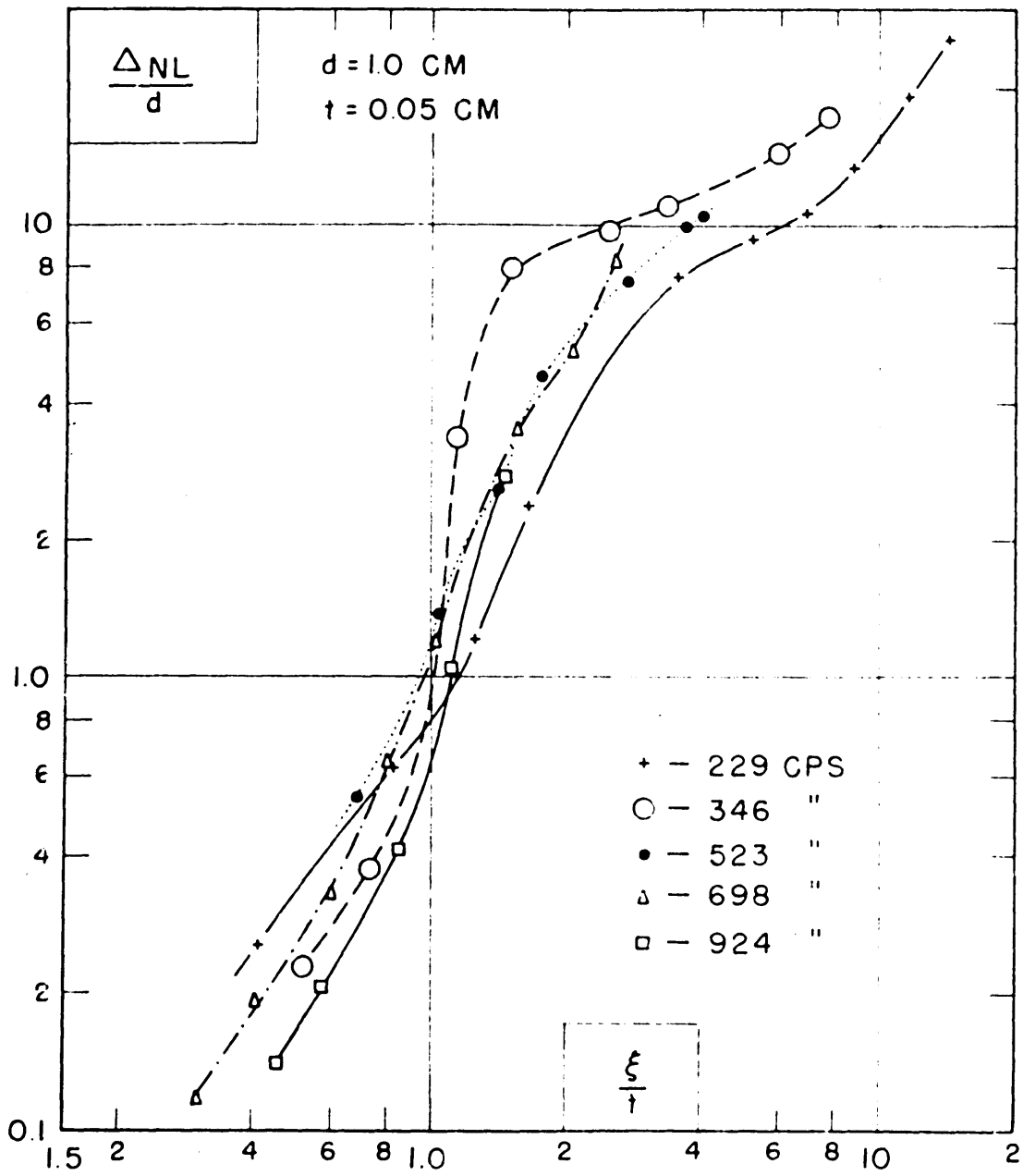


FIG. 12

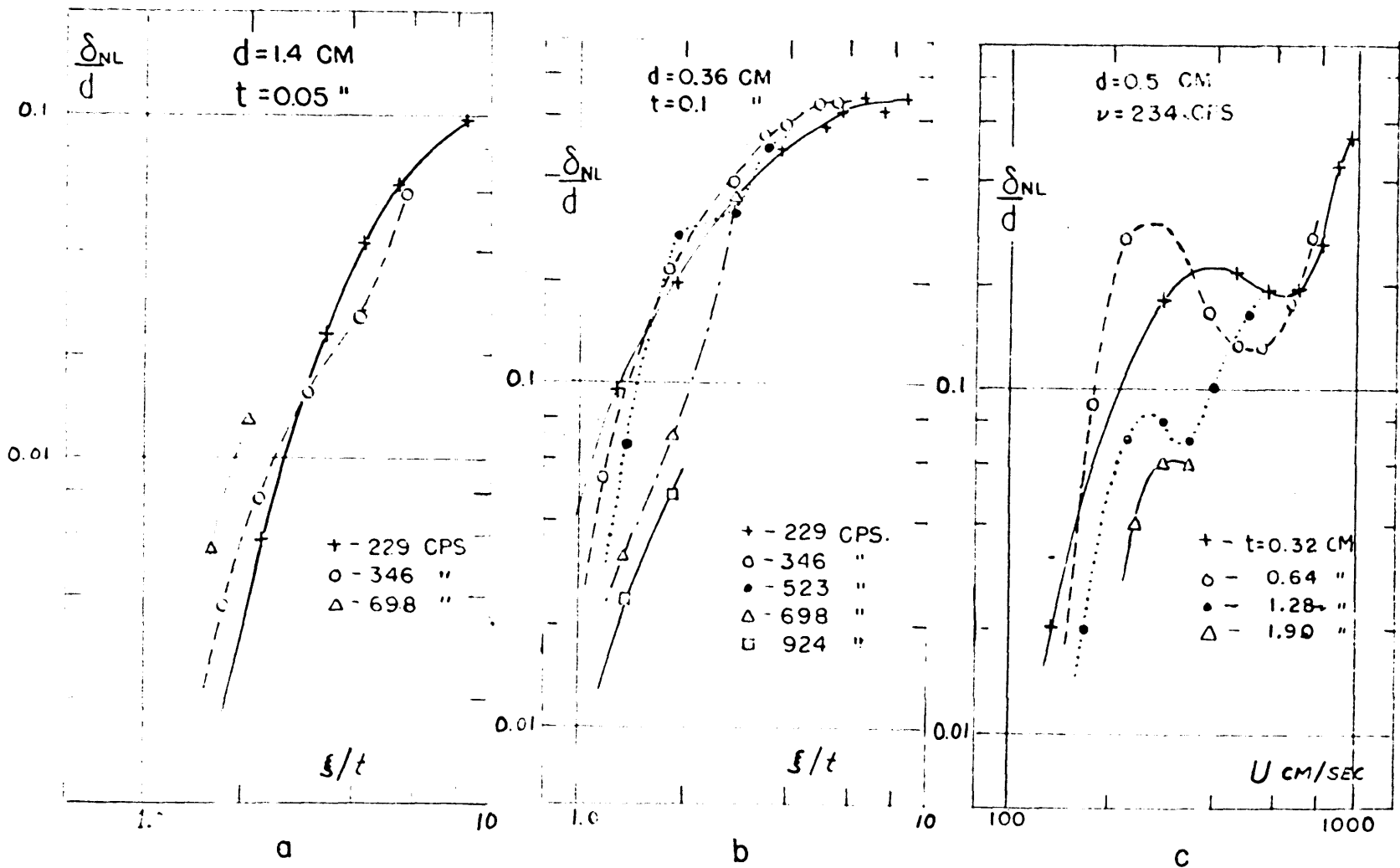


FIG. 13

reasonably well.

Ingard and Labate determined the kinetic energy carried by the vortices issuing from the orifice by measuring the momentum and velocity of the vortex stream. They obtained the momentum by finding the force caused by the vortices in striking a torsion balance. They claim to have obtained a surprisingly close agreement between their measured values of resistance and the value expected, assuming the loss of energy to be that carried away by the vortices. Unfortunately, we find that their measured value of momentum is twice as great as the maximum value it could possibly have from the momentum conservation principle. In order to justify their force measurements it is necessary to postulate that the vortex element rebounds elastically from a flat surface; if this is true, the power carried by the vortices is one-half the value they calculate.

Ingard has also measured the variation of the kinetic mass of the orifice with amplitude. These extremely interesting results are plotted in Fig. 13, in terms of an equivalent ^{end} and correction for the orifice. We shall present a theory in the following chapter which interprets the reduction in kinetic mass in terms of the destruction in the coherence of the mass associated with the near field of the orifice.

CHAPTER III

THE THEORY OF NON-STEADY FLOW THROUGH AN ORIFICE

1. Introduction

We develop in this chapter a theory of the response of the orifice (and nozzle) in terms of its steady state behavior, as outlined in Section 2 of the previous chapter. We shall not assume, as did Sivian, that the velocity is uniform over the cross section of the orifice, but we will consider the effects of contraction. Losses within the orifice due to friction and turbulence will be lumped together in their effect, and represented by the coefficient of velocity.

The coefficient of contraction is assumed to be a constant. This assumption in addition to the assumption of incompressible flow allows a theoretical expression for non-linear resistance to be derived which can be expressed in terms of the d-c flow resistance.

Next the transmission of sound through an aperture which supports a steady flow of gas is investigated by means of a trivial extension of flow resistance theory. The differential resistance, R_D is introduced as a measure of the acoustic resistance of apertures carrying air flow. The inverse problem, that of the modification of the d-c flow resistance by an intense acoustic wave is mentioned briefly.

The rectifier-like properties of the orifice are considered qualitatively. It is shown that the orifice may be made to support a steady difference in pressure provided it is excited with an asymmetric pressure wave whose square root moment $\overline{p|p|^{-1/2}}$ differs from zero. This pressure difference can be used to pump fluid through the orifice in a direction which is determined by the sign of $\overline{p|p|^{1/2}}$. Harmonic generation by the orifice is discussed briefly. Sivian's prediction of the existence of odd harmonics is reviewed. Second harmonics are shown to be generated by superposed d-c flow.

Finally, the maximum available flux of momentum from one side of an orifice is discussed. A calculation of this quantity for an orifice driven by a simple harmonic pressure is compared with Ingard and Labate's measurements of the stagnation pressure of emitted vortices. The measured force appears to be high by a factor of two.

2. The Non-Linear Resistance

If the pressure difference across the orifice is less than 1 per cent of atmospheric⁽⁴⁾, it is sufficiently accurate to consider the orifice flow to be governed by the equation for incompressible flow. In this case Eq.(8) in Chapter II reduces to the ideal flow equation:

$$p = p_1 - p_2 = \frac{\rho Q_1^2}{2S^2} \quad (1)$$

where p_1 is the pressure on the upstream side of the orifice and p_2 that on the downstream side, ρ is the density of the gas, Q is the ideal theoretical volume velocity through the orifice which has a cross section S . Eq.(1) neglects the effects of friction and contraction which will be considered later. If we now assume that Eq.(1) is instantaneously valid, and that p varies sinusoidally, it is a simple matter to compute the average power dissipated (see Appendix 1). This power divided by one-half the square of the peak volume velocity results in an expression for the non-linear resistance,

$$R_{NL} = \frac{1.1 \rho Q}{2S^2} \quad (2)$$

where Q is the peak volume velocity. Eq.(2) may be expressed in terms of u_{rms} the rms average particle velocity through the orifice

$$R_{NL} = \frac{1.1 \rho u_{rms}}{\sqrt{2}S} \quad (3)$$

Unfortunately Eq.(2) disagrees by a factor of $1.1/\sqrt{2}$ with the non-linear term in Sivian's equation (9) in Chapter II for resistance. It is therefore difficult to justify Sivian's equation, and we conclude that sufficient caution was not exercised in its derivation.

Eqs.(2) and (3) could have been derived just as easily from the equation for incompressible flow which has been

properly corrected for contraction and losses (see Eq.(6) in Chapter II). This procedure is only valid if the coefficient of discharge C_d is a constant independent of the velocity. The experimental results discussed in Chapter IV justify assuming C_d constant. Inasmuch as the correct flow equation differs from Eq.(1) which neglects contraction by the constant factor C_d^{-2} , we may write immediately the correct expression for the non-linear resistance

$$R_{NL} = \frac{1.1\rho Q}{2(SC_d)^2} \quad (4)$$

We have already seen (Eq. 7, Chapter II) that the flow resistance is

$$R_F = \frac{\rho Q}{2(SC_d)^2}$$

so that we may express the non-linear acoustic resistance in terms of the flow resistance

$$R_{NL} = 1.1 R_F \quad (5)$$

Eq.(5) will represent the facts if the coefficient discharge has the same value for steady flow as for alternating flow, a situation found not true within the experimentally available frequency range. As will be seen in the following chapter, the experimental data on thin orifices taken above 200 cps was found to agree fairly well with the relation

$$R_{NL} = .6 R_F \quad (6)$$

indicating that the a-c flow coefficient is about $(.6)^{-1/2} = 1.3$ times larger than the d-c coefficient.

It is necessary to justify our having neglected the reactance of the orifice in the preceding treatment. This point is considered in more detail in the following section on differential resistance where we shall merely give a physically plausible reason for neglecting reactance. In any event, as can be seen from Ingard and Labate's experimental results in Fig. 13 that the reactance of the orifice decreases appreciably in the region where hydrodynamic laws become applicable.

3. The Differential Resistance and Reactance

In general, when there is an average transport of matter through a small aperture, the acoustic conductivity of the aperture decreases. This phenomenon can be discussed in terms of the acoustic resistance of the aperture under steady flow conditions; this resistance we shall call the differential acoustic resistance. Strictly speaking it is the complex impedance of the aperture which should be specified. Since, however, even for moderate flow velocities, the impedance of the orifice becomes essentially real, so that the differential resistance is a useful quantity. To see this, we

first examine the basic origin of kinetic mass.

The acoustic reactance (see Appendix II) of a system driven at a single point can be expressed in terms of the time average of ~~where~~ L , is the Lagrange function for the system evaluated for unit terminal volume velocity amplitude. To a first approximation a small orifice (and the tube to which it is coupled) is a system whose behavior can be expressed in terms of the driving pressure, p , on one side of the orifice and Q , the volume velocity through the orifice. Thus, neglecting interaction between the incident wave and the scattered wave from the orifice, we have for reactance X of the orifice

$$X \approx 4 j\omega [L_{AV}]_{Q=1} \quad (7)$$

If all boundaries are rigid, L_{AV} can be expressed in terms of volume integrals of the average kinetic and potential energy densities t_{av} and v_{av}

$$L_{AV} = \int (t_{av} - v_{av}) d\tau \quad (8)$$

where the integral extends throughout the region occupied by the field. It is shown in Appendix II that reactance of a small orifice in a tube is given approximately by (7) provided the orifice is considered to scatter as a simple source. In this case the integral in Eq.(8) is taken over a spherical volume concentric with the orifice and extending to a radius r_t , where r_t is the radius of the tube. An

examination of the integral (8) shows that in the limit when the orifice radius r_o is very small compared with the tube radius r_t , and for wavelengths long compared with the tube radius, Eq.(8) approaches:

$$L_{AV} \rightarrow T_{AV} \approx (3 + 5) \frac{\rho Q_o^2}{48\pi r_o} \quad (9)$$

The number 3 in the bracket represents the kinetic energy in the region outside the hemispherical caps covering the orifice, while 5 represents the kinetic energy inside.

If a steady stream is superimposed on the sound field, the jet of gas issuing from one side of the orifice will destroy the coherence of the mass contained inside the hemispherical cap on the exit side.

This will remove 1/2 of 5/8 of the kinetic mass of a thin orifice. It is not known how to determine the destroyed fraction of kinetic mass on the inflow side. Assuming for lack of alternative, that the same loss of mass occurs on both sides, we could expect the reactance, under flow conditions to be 3/8 of its normal value. This reduction is in accord with recent measurements reported in the next chapter.

We next derive the expression for differential resistance, R_D . This is facilitated by reference to Fig. 15, which serves to summarize compactly the three kinds of resistance, and some approximations involved in their derivation. The pressure-volume velocity curve is drawn assuming a constant

coefficient of contraction. If we consider the response to a small signal superposed on a relatively large steady flow, we see the differential resistance is defined to be (just like the dynamic resistance of a vacuum tube) the slope of the p-Q curve at the operating point established by the steady flow velocity. Thus the differential resistance is obtained by differentiating the flow equation (6) of Chapter II,

$$R_D = \frac{\partial p}{\partial Q} = \frac{\rho Q^2}{(SC_d)^2} \quad (10)$$

We have already seen (Eq.(7) in Chapter II) that the flow resistance is

$$R_F = \frac{\rho Q}{2(SC_d)^2}$$

so that we may express the differential acoustic resistance in terms of the flow resistance:

$$R_D = 2 R_F \quad (11)$$

Eq.(11) will represent the facts if the coefficient of discharge has the same value for steady flow as for pulsating flow. We have verified Eq.(11) experimentally.

A differential flow resistance (not to be confused with the differential acoustic resistance) can be defined which specifies the d-c flow resistance of the orifice when an alternating flow is superposed. The problem of modulated flow through an orifice has received some engineering

attention because of the errors caused by pulsations in orifice-type flow meters. By straightforward means Lindahl⁽¹²⁾ has obtained an expression relating the average flow through an orifice under a pressure head $p = P + \delta p \sin \omega t$ where $\delta p \ll P_0$. His relation, expressed in our notation is

$$Q_{av} = C_d \sqrt{\frac{2P_0}{\rho}} \left[1 - \frac{p^2}{16P_0^2} - \frac{15}{1024} \frac{p^4}{P_0^4} \right] \quad (12)$$

The differential flow resistance is

$$R_{DF} = \frac{p_0}{Q_{AV}}$$

which is, from (12) and remembering that $p \ll P_0$:

$$R_{DF} = \frac{\rho Q^2}{2(C_d)^2} \left[1 + 1/8 \left(\frac{p}{P_0}\right)^2 + \frac{11}{1024} \left(\frac{p}{P_0}\right)^4 \right] \quad (13)$$

The bracketed term is obviously a correction factor to the steady flow resistance R_F , which must be applied when there exists a small sinusoidal pressure disturbance. The relation for R_{DF} has not received experimental confirmation.

4. The Orifice as a Rectifier

The distortion products and steady flow terms produced by an orifice are briefly investigated in this section. We proceed to obtain an expression for the third, and predominant harmonic. Starting from a quadratic pressure-velocity relation

$p = KQ^2$, we look for the first two Fourier components of Q when p is sinusoidal. If we say

$$p = P_0 \sin \omega t,$$

and $Q = a \sin \omega t + b \sin 3\omega t$

the coefficients a and b are

$$a = \frac{2K^{-1}\sqrt{P_0}}{\pi} \int_0^\pi (\sin \omega t)^{3/2} d\omega t = \frac{2K^{-1}\sqrt{P_0}}{\sqrt{\pi}} \frac{\Gamma(5/4)}{\Gamma(7/4)}$$

and

$$b = \frac{2K^{-1}\sqrt{P_0}}{\pi} \int_0^\pi \sin 3\omega t (\sin \omega t)^{1/2} d\omega t = 3a - \frac{8K^{-1}\sqrt{P_0}}{\sqrt{\pi}} \frac{\Gamma(9/4)}{\Gamma(11/4)}$$

Thus the ratio of the third harmonic velocity component to the fundamental is

$$\frac{b}{a} = 1/7 \quad (14)$$

This is equivalent to a third harmonic that lies $16.92 \approx 17$ db below the fundamental, a result in accord with certain experiments reported in Section 7 of Chapter IV.

The second harmonic component, usually weak in comparison with the third, becomes predominant if a steady flow is superposed on the a-c signal. This is most easily seen by expanding directly the expression for velocity

$$Q = K^{-1}(P_{dc} + P_{ac} \sin \omega t)^{1/2}$$

considering P_{ac} P_{dc}

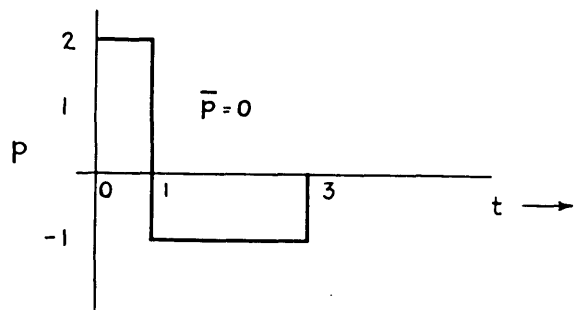
$$Q = K^{-1}P_{dc}^{1/2} \left[1 + \frac{P_{ac}}{2P_{dc}} \sin \omega t - \frac{1}{8} \left(\frac{P_{ac}}{P_{dc}} \right)^2 \sin^2 \omega t + \frac{1}{16} \left(\frac{P_{ac}}{P_{dc}} \right)^3 \sin^3 \omega t \dots \right] \quad (15)$$

From Eq.(15) it is evident that the second harmonic term is greater than the third by a factor of at least P_{ac}/P_{dc} . This effect is easily observed experimentally.

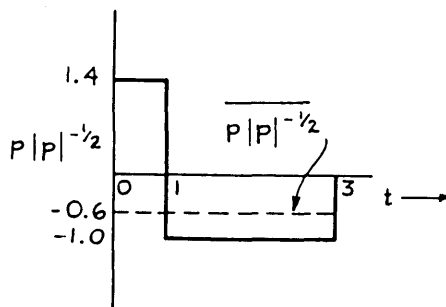
Finally we consider the effect of driving the orifice with an asymmetric wave form such as that depicted in Fig. (14a). While this wave form has a zero average value, its square root moment $\overline{p|p|^{1/2}}$ differs from zero as is demonstrated in Fig.(14b). The average volume velocity is proportional to $\overline{p|p|^{1/2}}$ so that the orifice is seen to behave as a pump. Experimentally it has been possible to derive enough power from this action to drive a mechanical wet-test flow meter. Details are given in the next chapter.

5. The Maximum Available Momentum Flux

The instantaneous flux of momentum transmitted through the orifice is the product of p , the instantaneous pressure difference across the orifice with S , the area of the orifice. In the positive half cycle of the driving pressure a certain quantity of momentum J is transmitted through in one direction, while during the negative half cycle an



(a)



(b)

FIG. 14 - A WAVE FORM WITH A SQUARE ROOT TYPE MOMENT

equivalent quantity returns. The total magnitude of momentum which passes in the positive or negative half cycle is

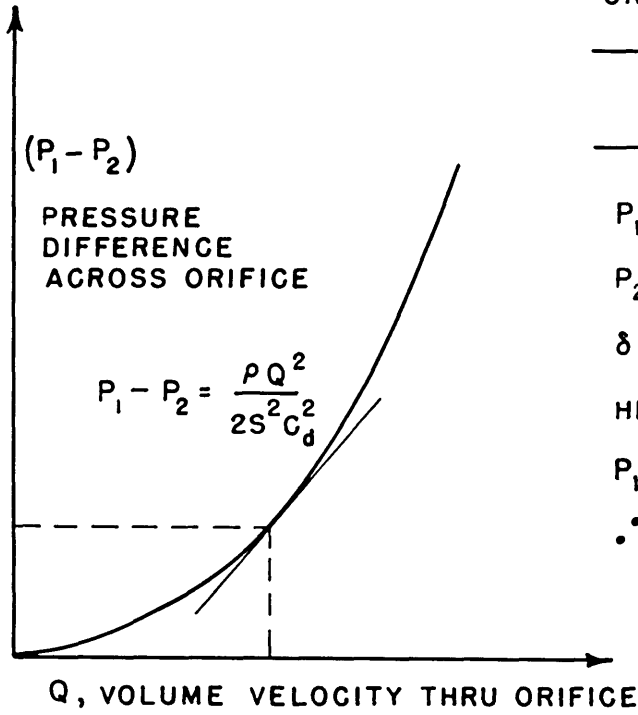
$$J = S \int_0^{T/2} p dt = \frac{SP_0 T}{\pi} \quad (16)$$

where T is the period of the wave and P_0 the peak driving pressure. If it is assumed that all this momentum is carried away by vortex rings which detach themselves at a frequency $\frac{1}{T}$, the maximum momentum flux carried away by the vortices on one side of the orifice is $\frac{SP_0}{\pi}$. This momentum may be expressed in terms of the non-linear resistance and u_{rms} the rms particle velocity, averaged over the orifice

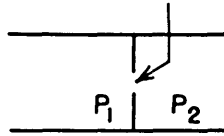
$$\text{maximum momentum flux} = F = \frac{\sqrt{2}S^2}{\pi} R_{NL} u_{rms} \quad (17)$$

The stagnation force of the vortices incident normally on plane surface would not be expected to exceed F unless the impact were partially elastic. Ingard and Labate⁽⁴⁾ have measured both the resistance R_{NL} and the force F of the issuing vortices for one orifice. Their results do not agree with Eq.(17) as may be seen by referring to Fig. 16 which compares the direct measurement with the value computed from Eq.(17). The measured force appears to be two times greater than the value arrived at indirectly. It is difficult to explain this inconsistency, particularly since the energy carried away by the vortices would be, if

DEFINITIONS



ORIFICE, AREA S



$$P_1 = P_0 + \delta p_1$$

$$P_2 = P_0 + \delta p_2$$

$$\delta p_2 \ll \delta p_1 \ll P_0$$

HENCE

$$P_1 - P_2 = \delta p_1 - \delta p_2 = p$$

∴ TREAT AS INCOMPRESSIBLE FLUID

$$\text{ANALOGOUS FLOW RESISTANCE} = R_F = \frac{P}{Q} = \frac{\rho Q}{2S^2 C_d^2}$$

$$\text{DIFFERENTIAL RESISTANCE} = R_D = \frac{\partial P}{\partial Q} = \frac{\rho Q}{S^2 C_d^2} = 2R_F$$

$$\text{NON LINEAR RESISTANCE}^* = R_{NL} = \frac{1.1\rho Q}{2S^2 C_d^2}$$

* NOTE THAT FLOW COEFFICIENTS ARE NOT SIMILAR IN D-C AND A-C CASE

FIG. 15

anything, less than the total power expended at the orifice, a consideration which leads to further disagreement. Unfortunately these results have only been found recently so that no experimental attempt has been made to resolve the dilemma.

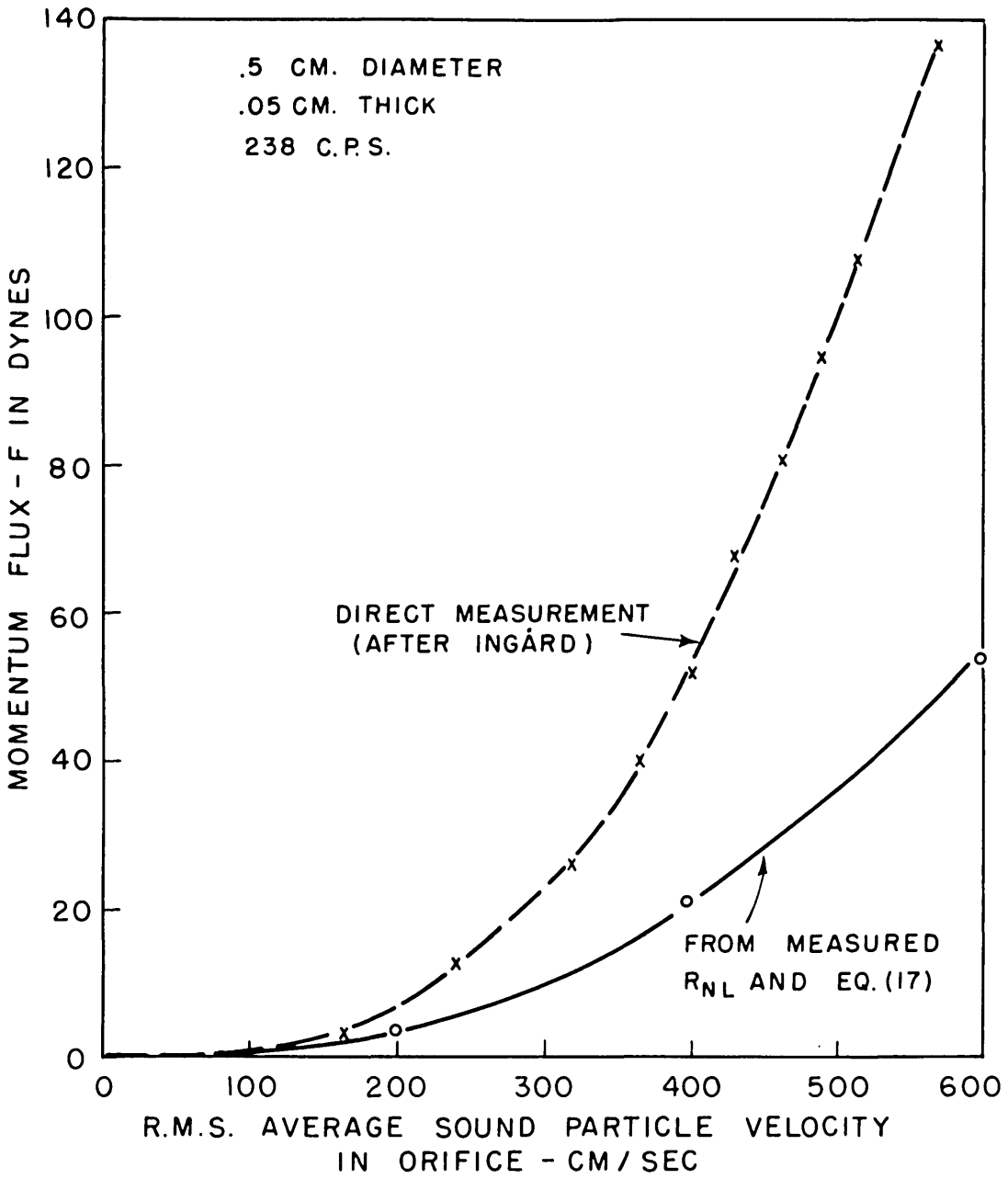


FIG. 16 - MOMENTUM FLUX ISSUING FROM AN ORIFICE.

CHAPTER IV

THE ORIFICE--EXPERIMENTAL RESULTS

1. Introduction

The following properties of orifices have been measured and they are discussed in the designated sections: The d-c flow resistance in Section 3; the non-linear acoustic resistance in Section 4; the differential acoustic resistance in Section 5; the influence of steady flow on the reactance in Section 6; the spectral distribution of harmonics in Section 7; the pumping action in Section 8. In section 2 certain general features common to most of the experiments are outlined. Preliminary results on the measurements of harmonics have been reported by the author⁽¹³⁾. The author was assisted in all other measurements discussed in this chapter by Mr. Peter Sieck with whom he has also presented a preliminary report of this work⁽¹⁴⁾⁽¹⁵⁾.

2. General Experimental Technique

The orifices studied in this work are small sharp-edged circular orifices whose diameters are at least two orders of magnitude smaller than the wavelengths of sound used. The principal results were obtained using orifices having diameters of 0.357 cm and 0.5 cm. The range of thickness extended from 0.05 cm to 1.25 cm. The orifices used were also those employed by Dr. Ingard in connection with

his thesis. When radius and diameter conform, the orifices used by us are also the same ones that were employed by Bolt, Labate and Ingard⁽¹⁰⁾, as well as by Ingard and Labate⁽¹¹⁾ in their recent work which has been reported in the literature.

All measurements, with the exception of the harmonic analyses, were performed with the orifice situated axially between two tubes, one having an inner diameter of three inches, the other two inches. Fig. 17 is a block diagram of the principal ingredients of the experiment with the exception of the conventional oscillators, amplifiers, etc. The equipment appears in a photograph in Fig. 18. The driving cavity to the left of the orifice was made as small as possible so that high alternating pressures could be generated within by the high powered western electric horn driver unit. The coupling cavity was 2" long with an inside diameter of two inches. The output side of the orifice was coupled by means of a 1-meter long steel tube of 3" inside diameter to a Fiberglas cone whose normal incidence absorption coefficient was 0.99+.

Acoustic resistance was determined by a transmission loss technique. The incident driving pressure was measured by the upstream sound-cell while the a-c volume velocity through the orifice was indirectly determined by the downstream sound cell. The upstream sound cell was placed sufficiently close to the orifice so that no wave correction

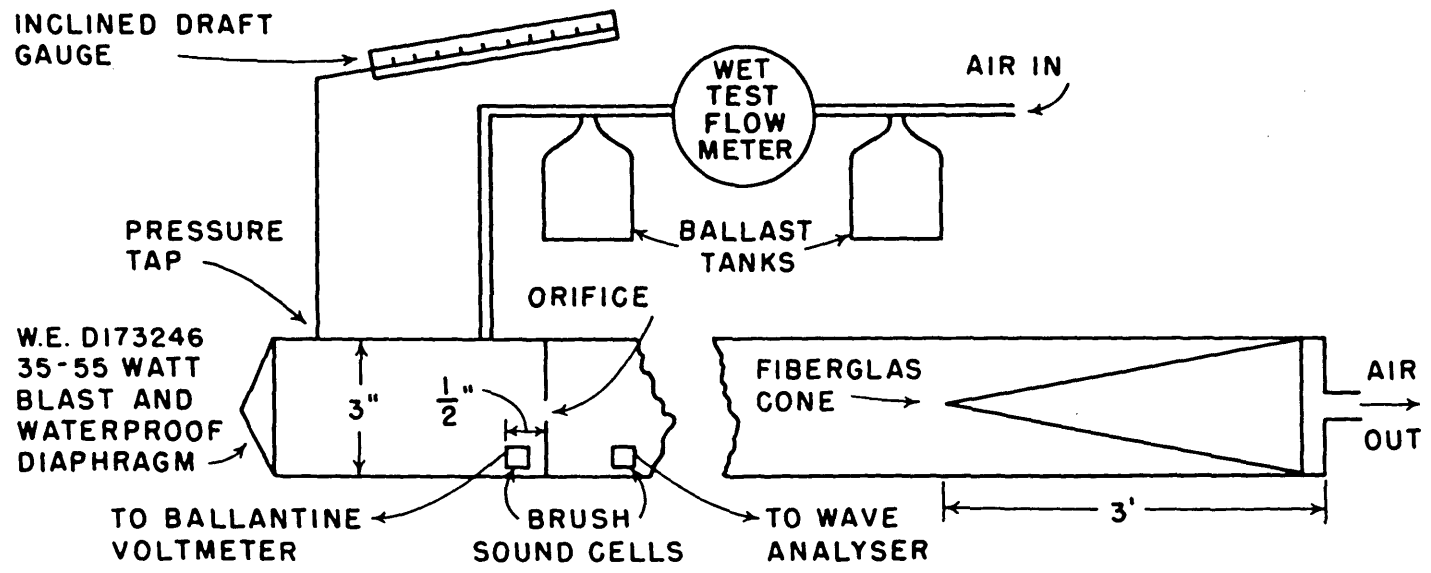
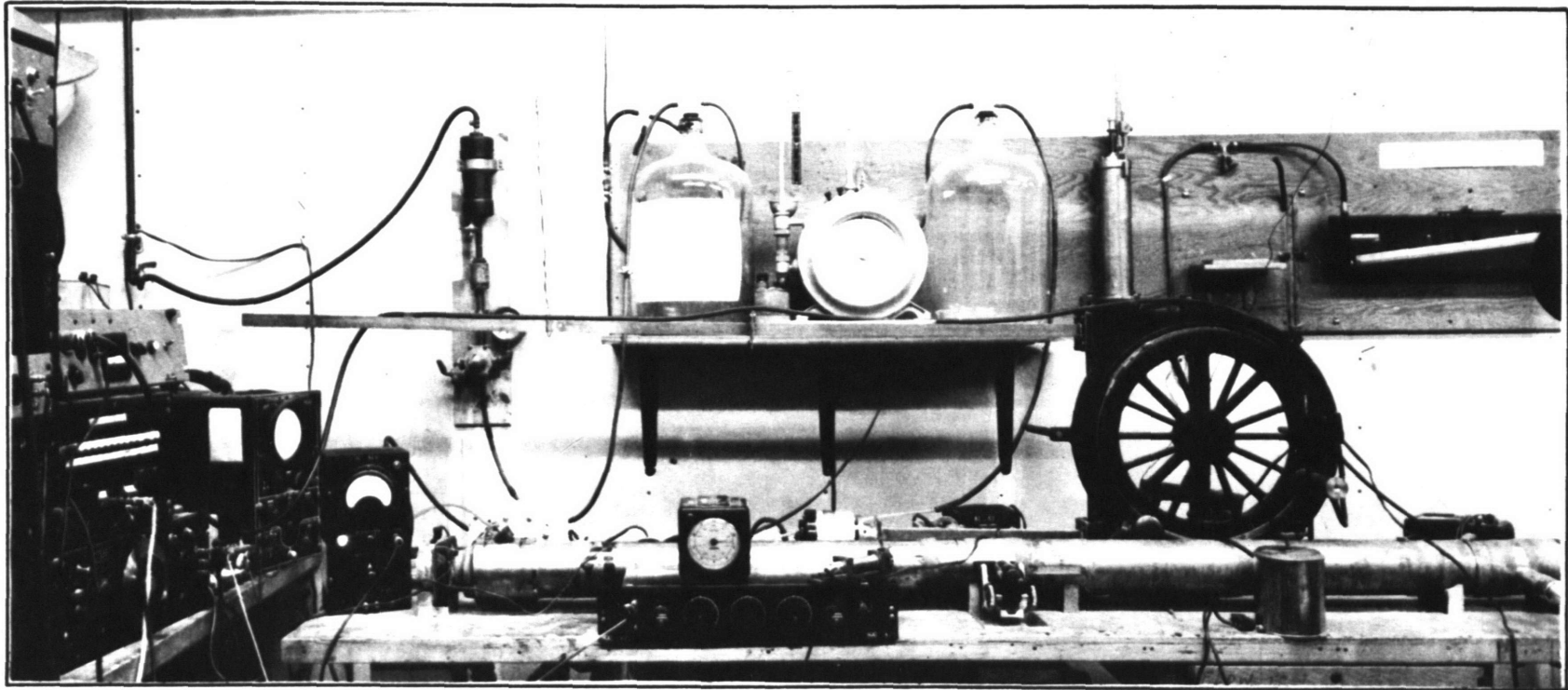


FIG. 17



EQUIPMENT USED IN EXPERIMENTS ON THE INTERACTION OF SOUND WITH OBSTACLES AND ORIFICES

FIG. 18

had to be applied to its readings. Interference from higher order modes was non-existent by virtue of the large values of resistance which were encountered.

Flow resistance was obtained by measuring the time required for a metered quantity of air to flow through the orifice under a fixed pressure head. Within the approximations set forth in Fig. 15, the d-c pressure head is measured by the inclined draft gauge. No static pressure tap was used on the down-stream side of the orifice; the orifice was sufficiently small in relation to the tube so that the discharge could be considered to be into atmospheric pressure.

3. Flow Resistance

A typical plot of the measured pressure-volume velocity characteristics of an orifice is given in Fig. 19. Data of this kind were obtained for each of the orifices tested. It was noticed that the logarithm of the pressure plotted against the logarithm of the volume velocity fell extremely closely on a straight line, provided U , the average particle velocity through the orifice exceeded about 150 cm/sec. Above 150 cm/sec the exponent in the proportionality $p \propto U^n$ was very close to two as can be seen from the values tabulated below:

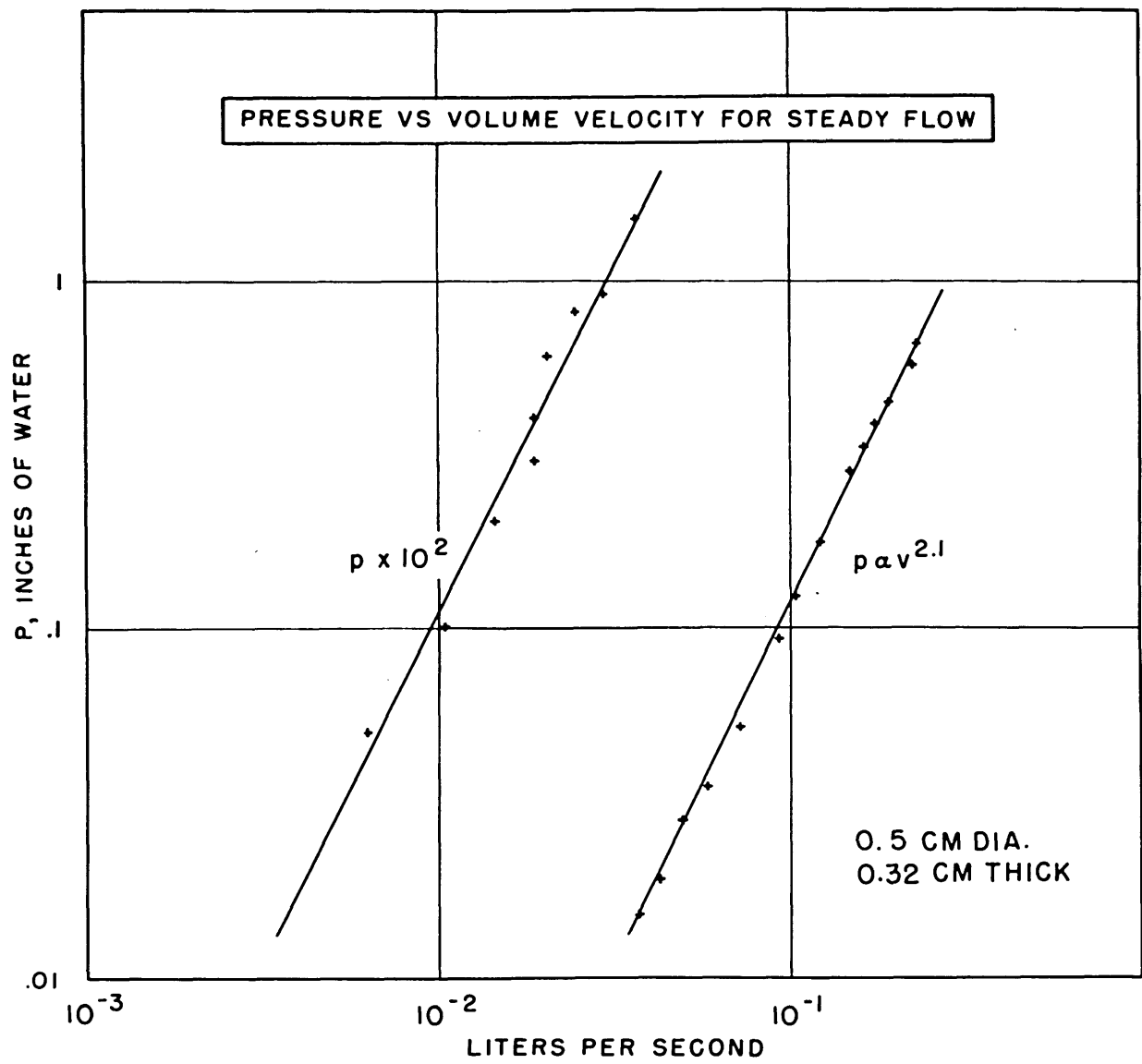


FIG. 19

TABLE III

diameter cm	thickness cm	n
.357	.09	2.05
.5	.05	1.96
.5	.32	2.10
.5	.64	2.00
.5	1.25	1.96
.5	1.9	1.92
.5	2.54	1.88

For flow velocities less than 150 cm/sec the log p - log Q relation appears to fluctuate appreciably from a straight line characteristic, a definite tendency to break up being noticed at about 100 cm/sec.

The data have been correlated and expressed in terms of the d-c flow resistance by obtaining the ratio of the pressure to the volume velocity from curves similar to those shown in Fig. 19. The data are given in acoustic ohms which have the dimensions of dyne-sec/cm⁵ or gm-sec/cm⁴.

The measured values of flow resistance are given in Figs. 20 and 21. Plotted for comparison is the value of flow resistance computed from formula (3) of Chapter III. A discharge coefficient $\sqrt{\frac{1.1}{2}} = .74$ was chosen. This value of the coefficient is roughly consistent with values given in the literature (see Fig. 2) and it enables the flow resistance to be written in a simple way

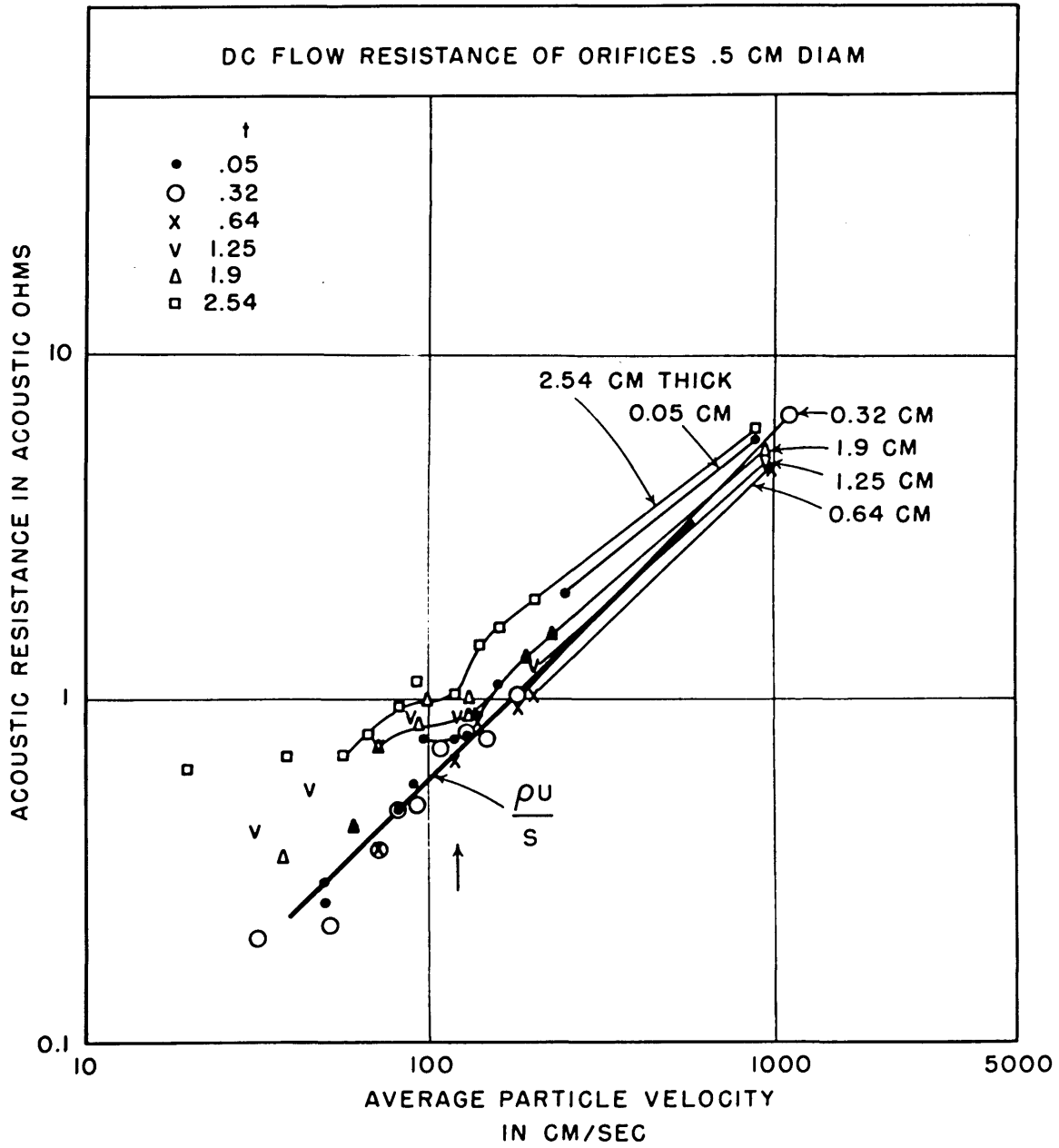


FIG. 20

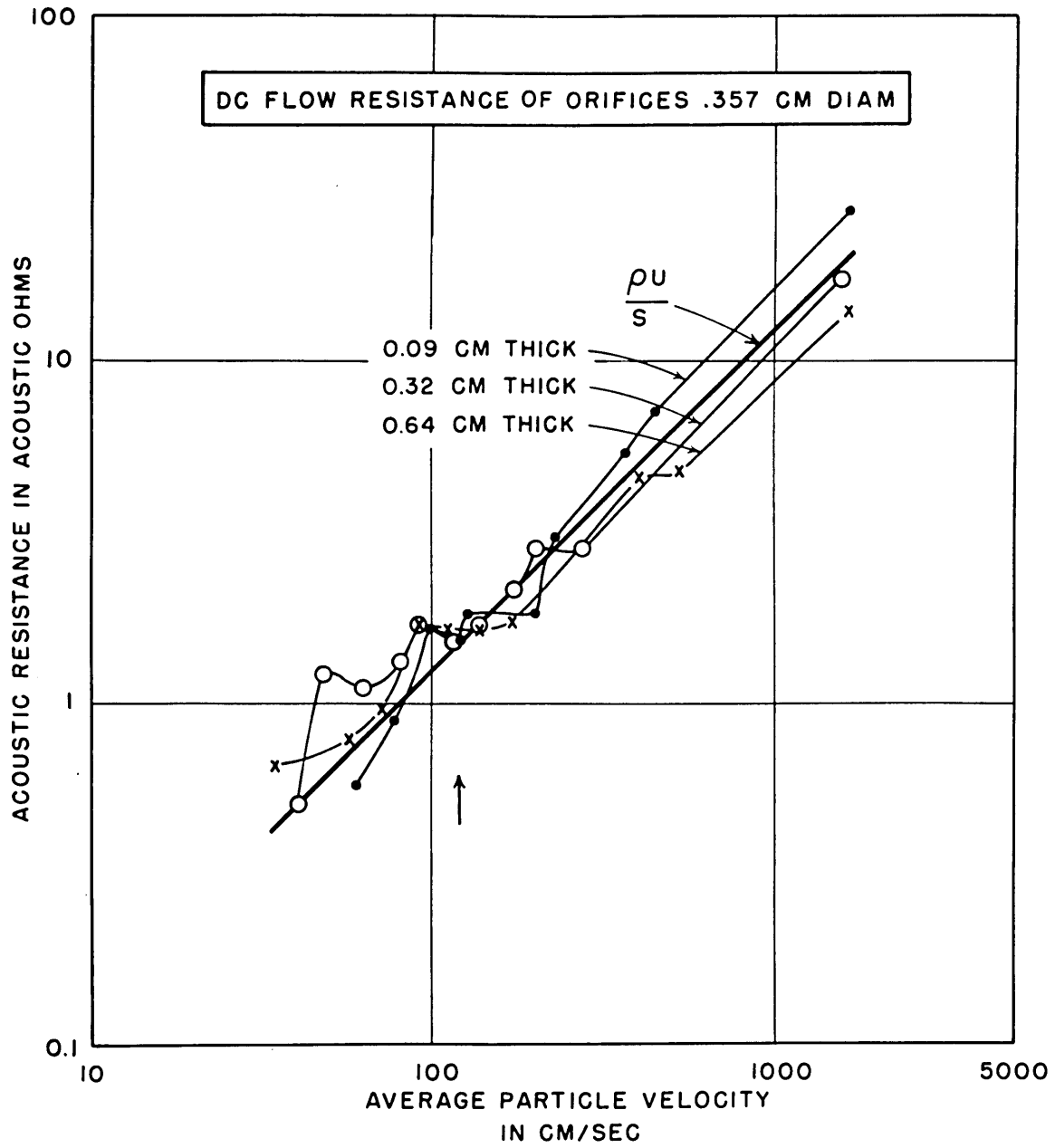


FIG. 21

$$\text{For } C = \sqrt{\frac{1.1}{2}}, R_F = \frac{1.1\rho Q}{2(SC_d)^2} = \frac{\rho Q}{S^2} = \frac{\rho U}{S} \quad (1)$$

in terms of the average velocity through the orifice U , the orifice area S and the density of air ρ . The measured value of the discharge coefficient is obtained by equating

$$(R_F)_{\text{meas.}} = \frac{1.1\rho Q}{2(SC_d)^2}$$

hence

$$C_d = \sqrt{\frac{1.1\rho Q}{(2S^2 R_F)_{\text{meas.}}}} = .74 \sqrt{\frac{\rho v/S}{(R_F)_{\text{meas.}}}}$$

The quantity under the radical is the ratio of the resistance obtained from the heavy curve, of $\frac{\rho U}{S}$, divided by the experimental values drawn in lighter lines. Thus the actual coefficient of discharge, evaluated at 500 cm/sec for the thin orifices turns out to be

$$C_d = .74 \frac{2.8}{3.5} = .66 \quad \text{for the .5 cm orifice}$$

$$C_d = .74 \frac{6.2}{7.9} = .66 \quad \text{for the .357 cm orifice}$$

These values agree almost exactly with the value .67 obtained from Fig. 2 for an orifice whose diameter is .2 times the pipe diameter.

A similar computation carried out at 500 cm/sec leads to a value of .87 for both the orifices which are .064 cm thick. These larger values of the coefficient obtained for thick orifices result from a decrease in the contraction as

discussed in Section 2 of Chapter II. A similar computation for the 2.54 cm orifice would indicate that the discharge coefficient for the .5 cm diameter orifice had passed through a maximum, the coefficient now being reduced by the increasing importance of friction in thicker orifices.

The variation of the measured flow resistance with the thickness of the orifice has been plotted in Fig. 26. The non-linear resistance, discussed in the next section, has also been plotted in Fig. 26 for comparison.

4. The Measurement of Non-Linear Resistance

The transmission loss through a small orifice can be divided into two regions; a low amplitude region in which the transmission loss is independent of the amplitude of the incident sound level and a high amplitude region in which the transmission loss depends considerably on the incident sound pressure. In the low amplitude, or linear region, the transmission loss is controlled mainly by the mass reactance of the aperture. In the non-linear region the loss is governed by the non-linear resistance of the orifice.

Fig. 22 depicts a typical measurement of the sound pressure level transmitted into a three-inch pipe, plotted as a function of the incident sound pressure level. The onset of non-linearity is clearly defined by the abrupt change

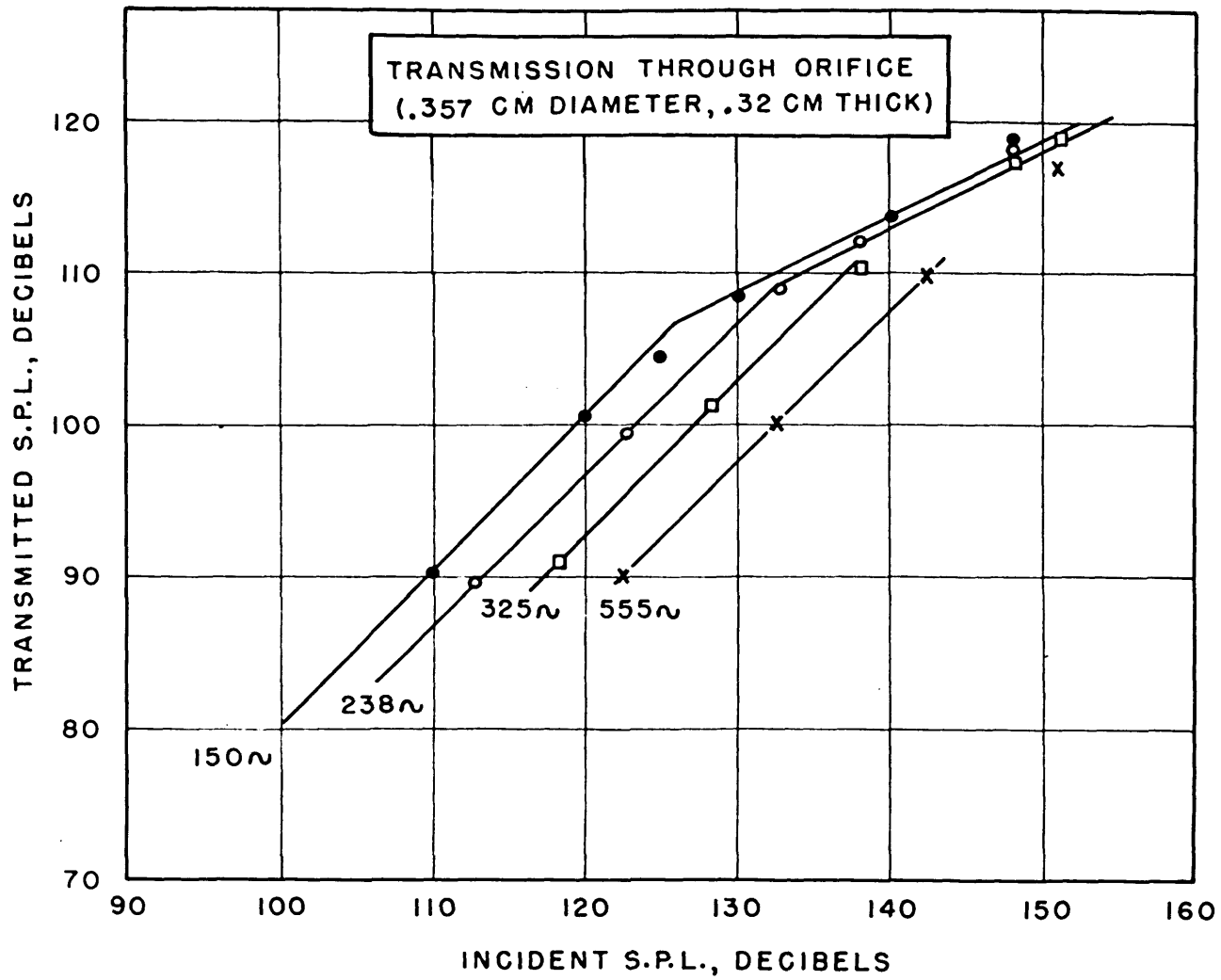
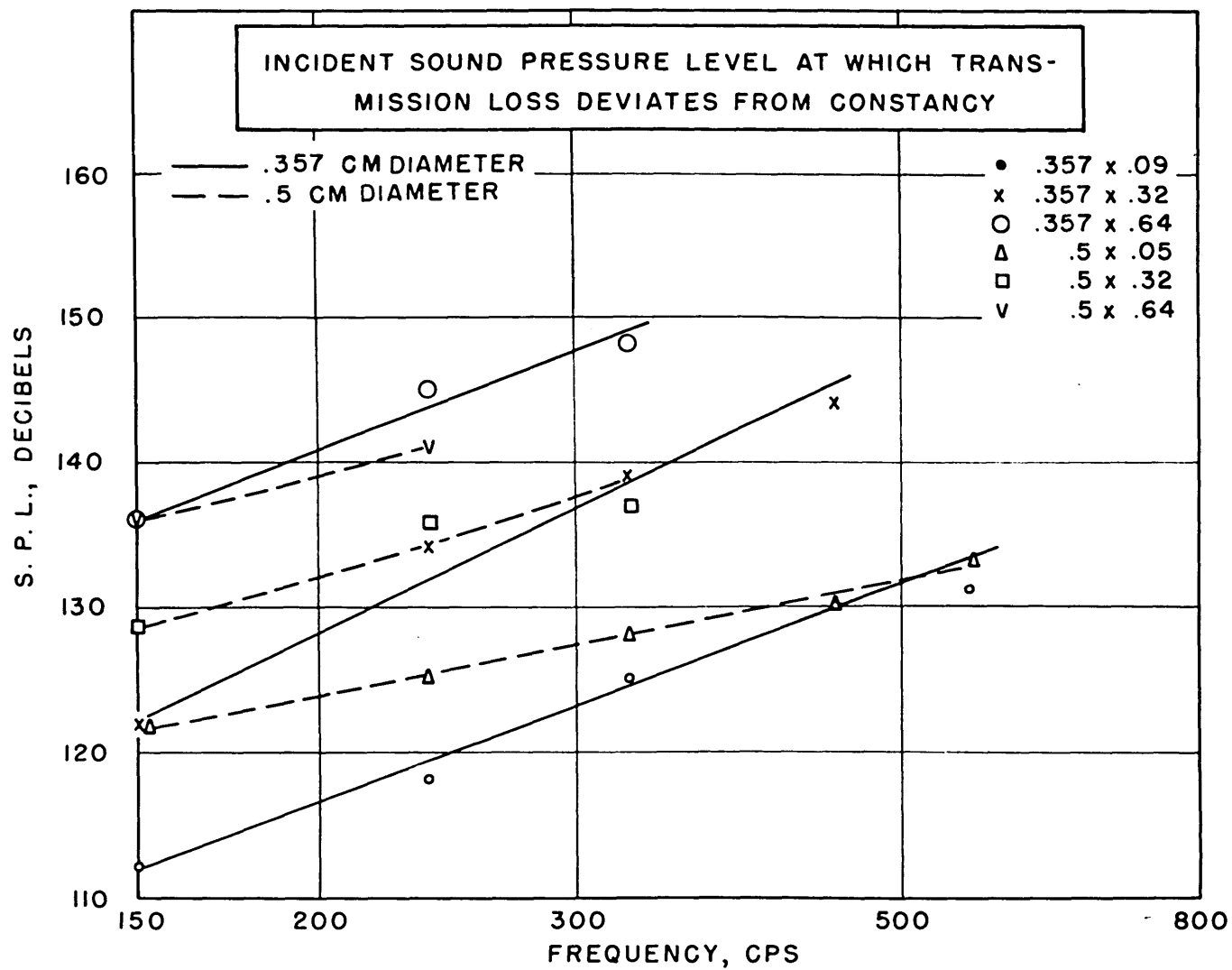


FIG. 22

in the slope of the curves plotted in Fig. 22. In the linear region the slope is 1 db per db; in the non-linear region it is 1/2 db per db. This is consistent with previously obtained results indicated in Fig. 4. The influence of mass reactance shows up clearly in the linear region of Fig. (22). The transmission loss is seen to increase directly with the frequency at low sound levels. In the non-linear region the curves approach each other and can be represented by a single line. The exact point at which non-linearity sets in is a function both of the frequency and the geometry of the orifice. The critical sound pressure level at which the transmission loss deviates from constancy is presented in Fig. 23. This critical sound pressure level increases about six db per octave for the orifice of .5 diameter and roughly about 12 db per octave for the .357 cm orifice. of the particle displacement amplitude.

The values of the non-linear resistance obtained by the transmission loss measurement technique are plotted in Fig. 24 and 25. The data are given in acoustic ohms which have the dimensions dyne-sec/cm^5 or gm-sec/cm^4 . The data were obtained over a frequency range extending from 150 cps to 800 cps. For comparison, the flow resistance has been plotted at zero cps. The non-linear resistance was measured at particle velocity amplitudes between 2000 and 7000 cm/sec; the values plotted have been linearly



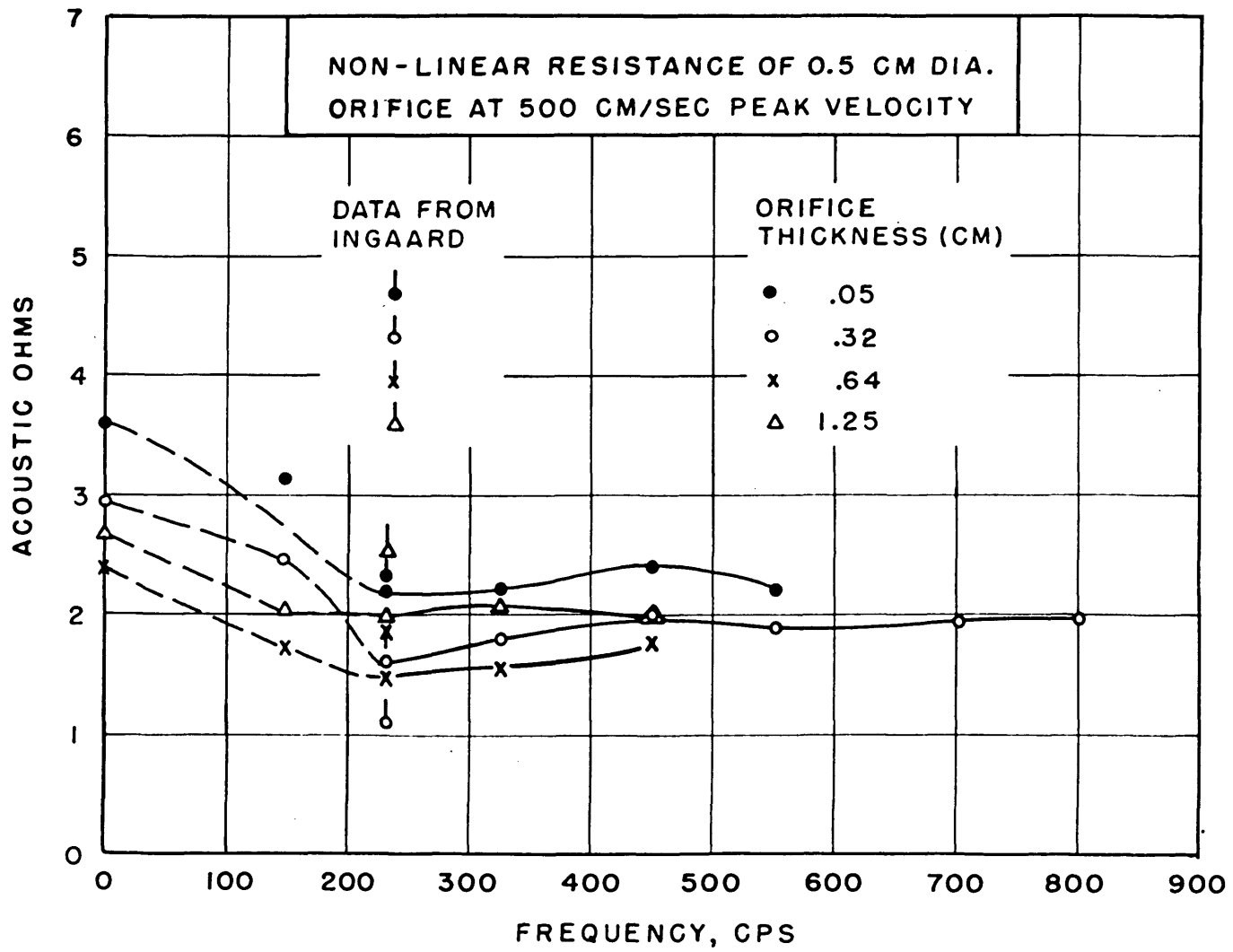


FIG. 24

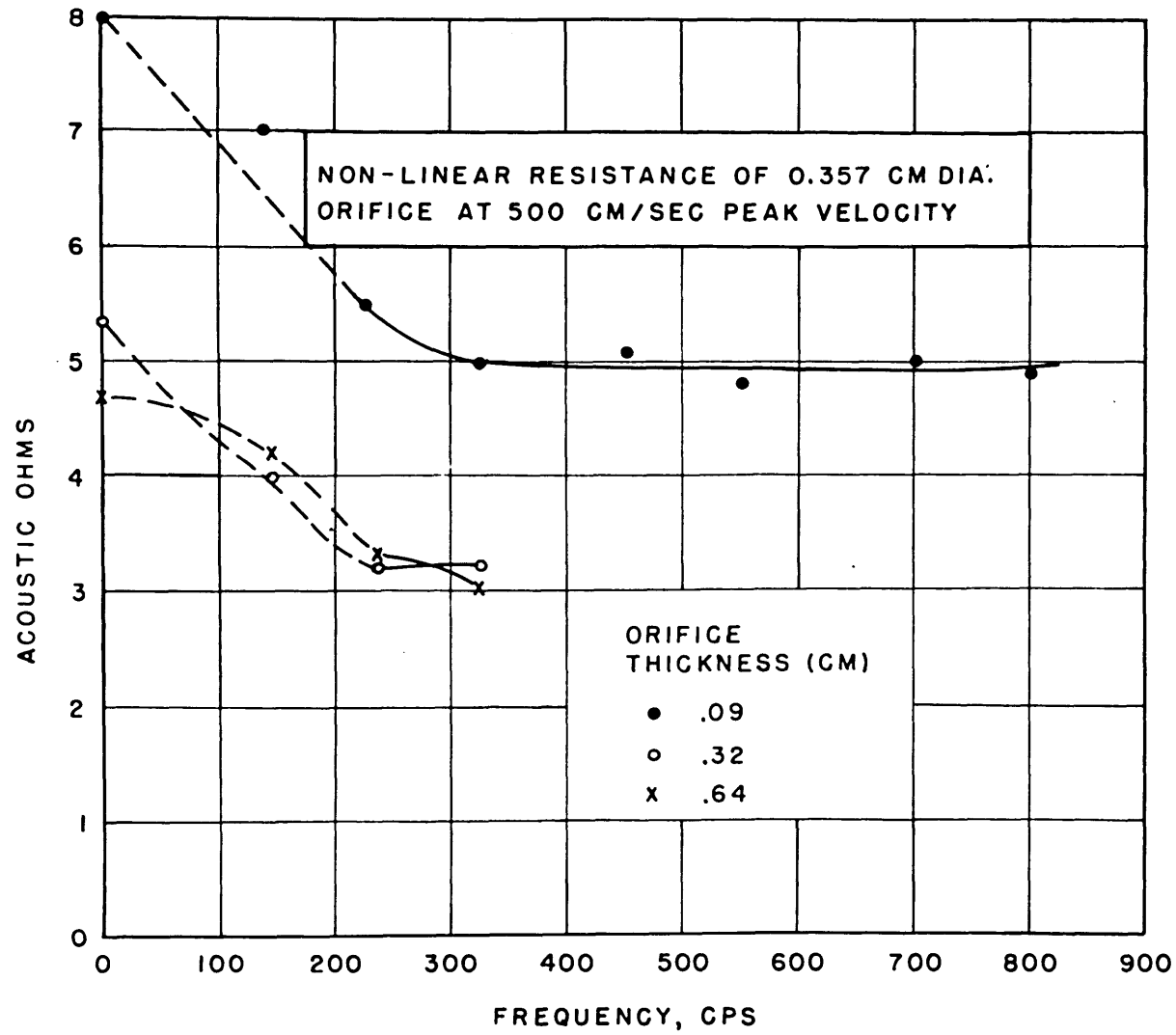


FIG. 25

extrapolated to a particle velocity amplitude of 500 cm/sec.

The resistance appears to increase to its d-c value. It was not possible to determine whether this increase was monotonic as measurements were not obtained at frequencies below the cut-off of the pc termination.

It is important to emphasize the fact that the values of resistance given in Fig. 24 were not measured at the peak velocity of 500 cm/sec. These data will agree with measurements obtained at 500 cm/sec provided the frequency of low measurement is enough to insure that the orifice is in Ingard's jet region.

It is evident that a high degree of correlation exists between the measurements of non-linear and flow resistance. This correlation is even more evident when the two kinds of resistance are plotted for various values of the orifice thickness as is done in Fig. 26. It is particularly clear that the effects of reduced contraction influence the non-linear resistance. According to Eq. (5) of Chapter III, the non-linear resistance should be 10 per cent greater than the flow resistance provided the same coefficient of discharge is applicable in both cases. It is evident that the non-linear resistance for thin orifices is considerably less than Eq. (5) predicts. This implies that the coefficient of contraction is greater for alternating flow (by about 30 per cent) than it is for steady flow. For thicker

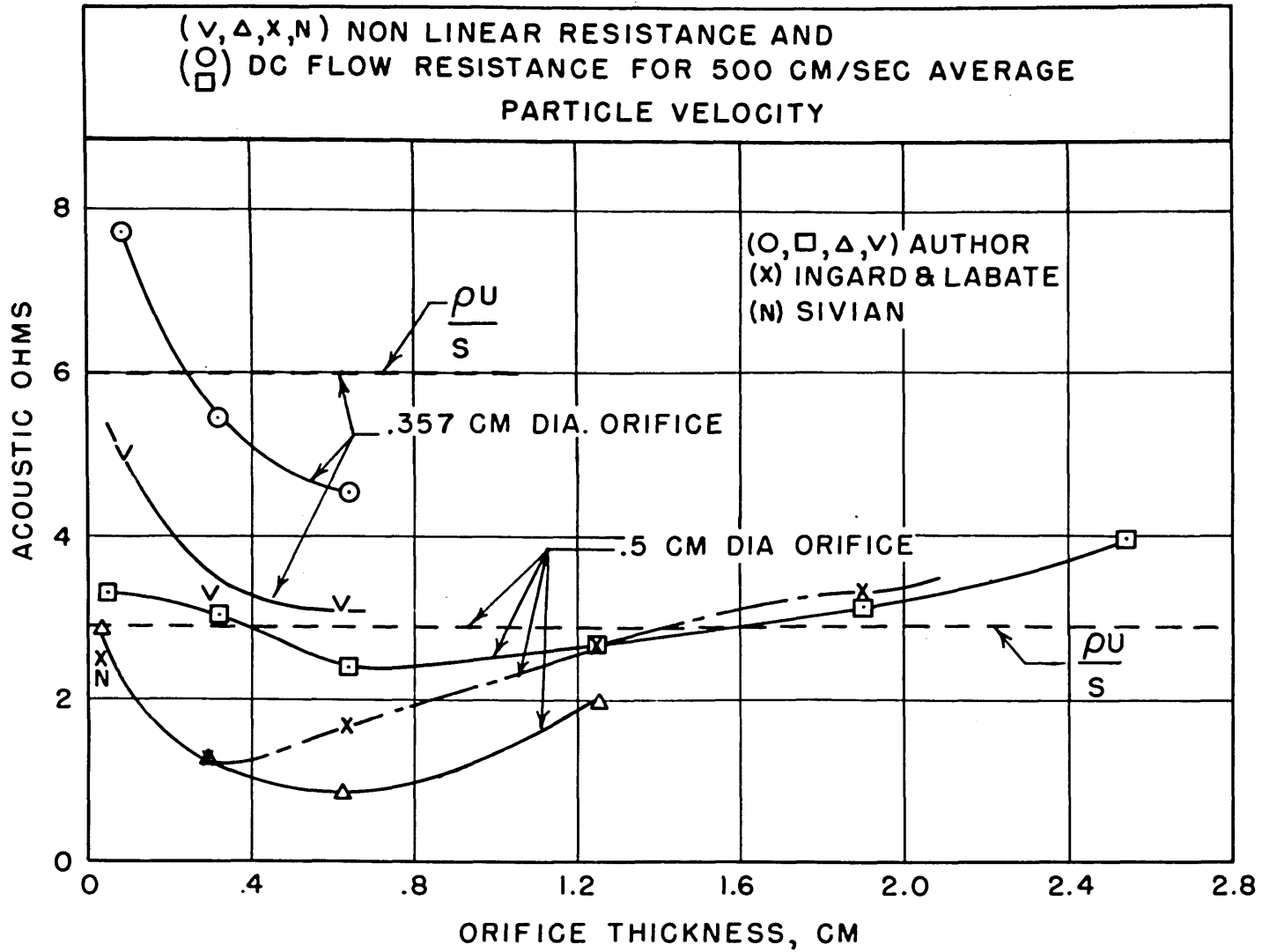


FIG. 26

orifices, the non-linear resistance and the flow resistance are very closely equal. This result agrees with our assumption of a suppressed contraction in the case of orifices whose thickness-to-diameter ratio exceeds about 2.

5. Measurements of Differential Acoustic Resistance

The differential resistance for two thin orifices of diameter 0.5 and 0.357 cm have been measured by techniques similar to those employed in the previous section. These results are given in Figs. 27 and 28, in terms of acoustic resistance which has the dimensions of dyne-sec/cm⁵ or gm-sec/cm⁴. The measured values of flow resistance multiplied by 2 are plotted for comparison as well as the equation (10) of Chapter III:

$$R_D = \frac{\rho Q^2}{(SC_d)^2} \quad C_d = \sqrt{\frac{1.1}{2}} \rightarrow \frac{2\rho U}{S} \quad (2)$$

In general the measured differential resistance is less than the flow resistance times 2, and greater than the value calculated directly from the above equation. The measured points corresponding to twice the flow resistance have been omitted from the plot since they would fall on the given solid line. In obtaining the differential resistance, R_D , the a-c velocity amplitude is always considerably less than the superposed d-c particle velocity. As can be seen from Fig. 21, the direction of the d-c flow does not influence

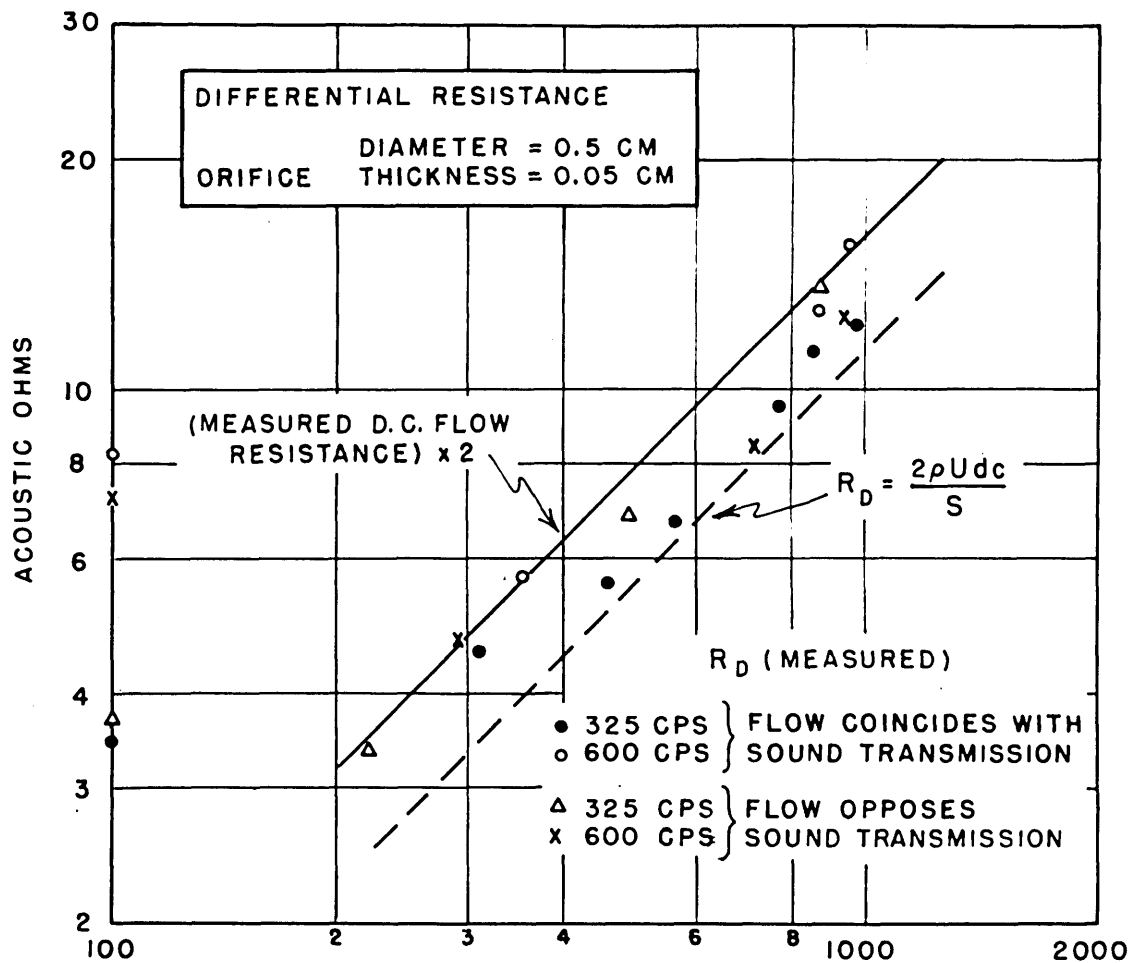


FIG. 27

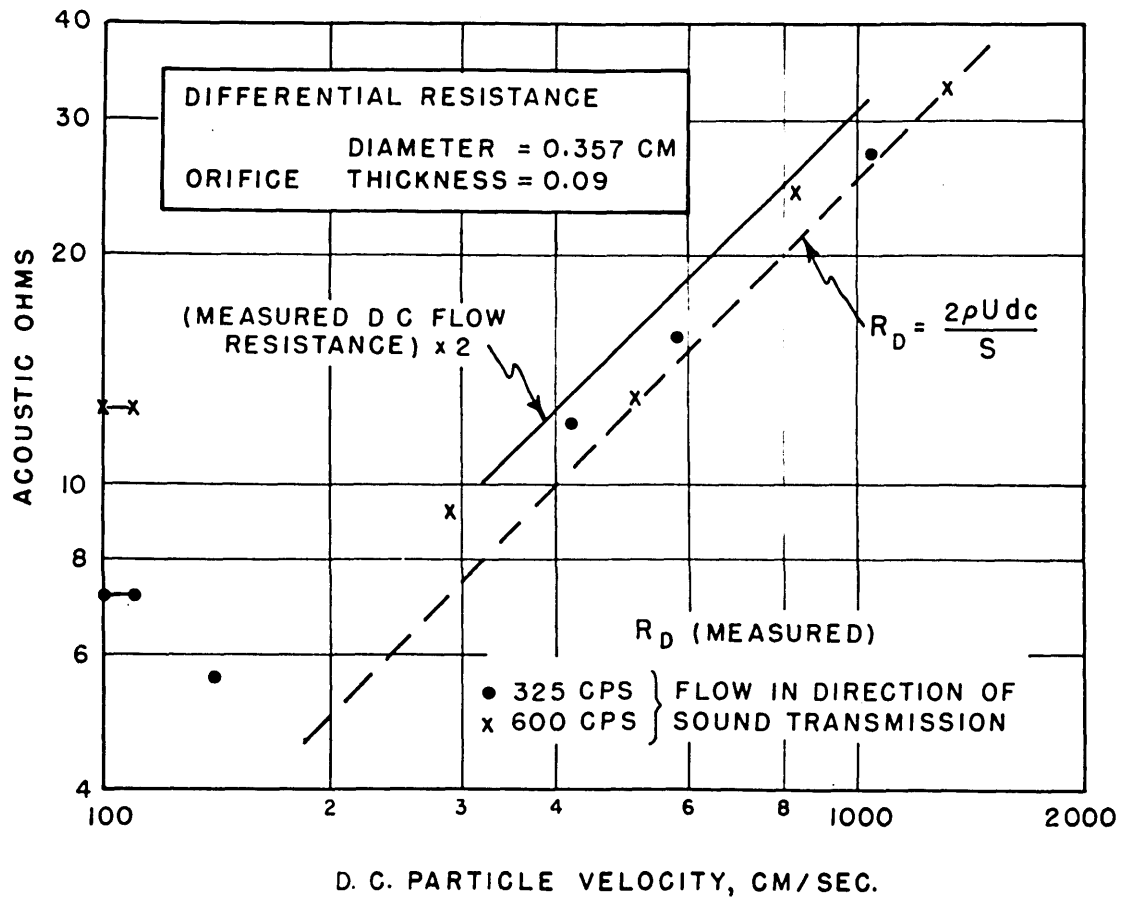


FIG. 28

the results within the estimated experimental error, which is about 20 per cent.

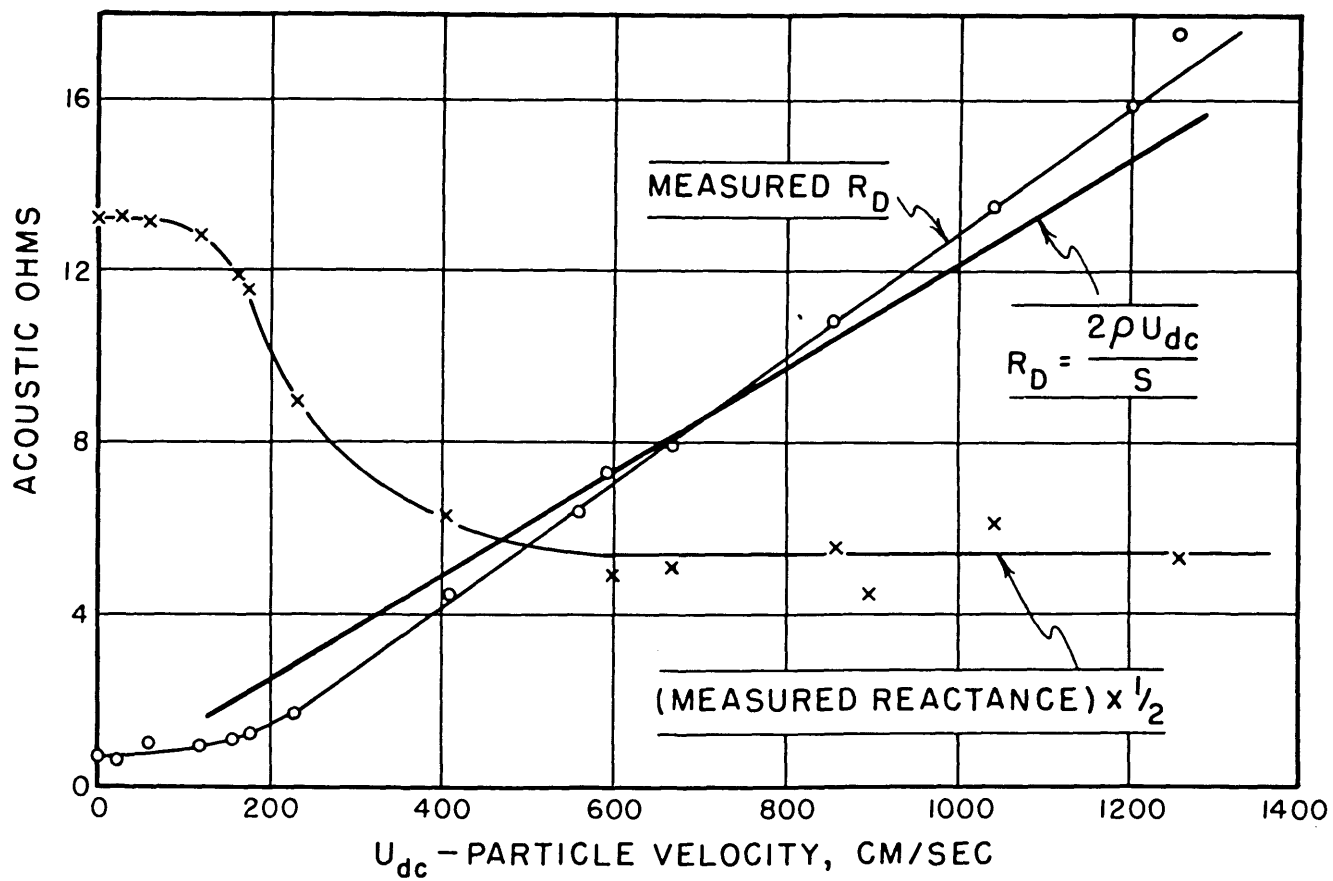
For sufficiently low values of the d-c flow velocity the magnitude of the orifice impedance becomes independent of the d-c velocity. These constant magnitudes of the impedance have been plotted arbitrarily at 100 cm/sec on the abscissas of Figs. 27 and 28. It is of interest to note that for flow velocities of the order of 200 cm/sec the differential resistance is less than the magnitude of the impedance at lower velocities. This means that the acoustic conductance reaches a maximum value and thereafter decreases approximately linearly with a further increase in flow velocity. This behavior may be qualitatively explained in terms of the mass reactance of the orifice. At low flow velocities the conductance is determined primarily by the mass reactance which, for the orifices considered, was greater than the resistance. As the d-c flow increases the coherence of the air mass that contributes to the reactance is destroyed, resulting in a decreased mass reactance and therefore an increased conductance. A further increase in the flow velocity increases the differential resistance so that ultimately the resistance overrides the effect of a reduction in reactance. The quantity, $(-\frac{NI}{\rho})$ plotted in Fig. 13 is the reduction in the acoustic mass of the orifice expressed in terms of the equivalent end correction for that orifice.

The transmission loss technique is inherently incapable of measuring the differential resistance unless this resistance exceeds the magnitude of the reactance. Conversely the reactance may be measured by this method only when its magnitude exceeds that of the resistance. More accurate measurements of the differential resistance and of the dependence of the reactance on flow have subsequently been made by McAuliffe⁽¹⁶⁾ with the precision impedance tube.⁽¹⁷⁾ In Fig. 29 McAuliffe's results for the differential resistance of a .5 cm orifice are compared with our Eq.(2). The reactance is discussed in the following section.

6. The Influence of Steady Flow and Large Amplitudes on the Reactance

The reactance is observed to decrease considerably with the initial increase in flow velocity. It thereupon levels off to a constant fraction of its former value. It is observed from Fig. 29 that the reactance drops from 26 ohms at zero flow velocity to about 11 ohms at high velocities. This is a fractional reduction in the kinetic mass of $11/26 = .42$, which is to be compared with the fraction $5/8 \approx .38$, derived from the approximate theory presented in Section 3 of Chapter III.

Similar considerations might be applied to interpret the behavior of non-linear reactance depicted in Ingard's



DIFFERENTIAL RESISTANCE AND REACTANCE

ORIFICE DIAMETER = 0.5 CM
 THICKNESS = 0.05 CM

FIG. 29

curves reproduced in Fig. 13. The quantity, $(\frac{\delta_{NL}}{d})$ plotted in Fig. 13 is the reduction in the acoustic mass of the orifice expressed in terms of the equivalent end correction for that orifice. The asymptotic approach of the non-linear kinetic mass to a constant value, for high particle velocities, cannot be explained in terms of the mass transferred to the jet⁽¹¹⁾. The reason for this is that the mass ejected by the orifice continues to increase, after the reactance has stabilized to a constant value.

We consider briefly now what we meant in Section 5 by the Statement "... the jet of gas issuing from one side of the orifice will destroy the coherence of the mass contained inside the hemispherical cap on the exit side". We adopt the criteria that an element of mass is coherent if it remains within the region bounded by the hemispherical caps on either side of the orifice during one complete period; otherwise it is incoherent. This leads to the following critical relation between the frequency f , the radius r_0 and thickness t of the orifice and the maximum flow velocity v_d of the particles:

$$v_c = f(2r_0 + t) \quad (3)$$

Applied to the data of Fig. 29 which was obtained at 400 cps, we obtain a critical velocity of 220 cm/sec, which is about one-half the velocity at which the experimentally determined reactance has reached its stable value for high flow velocities.

In Fig. 52 of Chapter VII this criteria is applied in a slightly different way to the data of Fig. 29 as well as to some additional data. We now use the above concept to estimate the velocity at which a constant non-linear reactance is attained. From considerations similar to those used in the steady flow criterion, we assume the critical particle displacement amplitude in the orifice to be $\xi_c = (2r_o + t)$. Then if u_c is the critical velocity amplitude in the orifice, we have for alternating flow:

$$\xi_c = (2r_o + t) \tag{4}$$

or

$$u_c = 2\pi f(2r_o + t)$$

We apply these last two relations to Ingard's measurements (see Fig. 13b) of the non-linear reactance. We note that the reactance of the .357 orifice has stabilized by the time $\xi/t \approx 6$. Since this orifice is .1 cm thick, the critical displacement is 0.6 cm from experiment. From Eq.(4) we find:

$$\xi_c = (.357 + 0.1) \approx .46,$$

which is fair agreement.

This treatment cannot be applied to the measurements of Figs. 13a or 13c since in these cases sufficient amplitude was not attained to reduce the reactance to a constant value.

7. The Generation of Harmonics by Small Circular Orifices

The author has reported⁽²⁾⁽¹³⁾ measuring the harmonic

components generated by an orifice which was driven by high intensity sinusoidal pressure. Harmonics of the exciting pressure as high as the fortieth were detected. It was found for the .357 cm orifice that the first three harmonics, including the fundamental, behave as if they were emanating from a spherical source having a radius equal to the radius of the orifice. This observation was made on the orifice in an infinite baffle and while the orifice was operating in the jet region.

We have made further measurements of the spectral distribution of the harmonics. These measurements were obtained at a distance of 7.0 cm from the center of the orifice which was located centrally in a 4' x 6' rectangular baffle, yielding essentially free field conditions. The sound pressure level was recorded through a 640-AA coupled through an Erpi R-A 277 F Automatic Frequency Analyzer to a Bruel and Kjaer Sound Level Recorder. The 640-AA, without grill, was placed on the baffle in such a position that the sound from the orifice was received at grazing incidence. The orifice was driven in the manner described in Section 2 of this Chapter.

Because of their bulk the spectrum curves have been grouped together in Appendix IV where they appear as

This partially justifies the tacit assumption made in estimating the kinetic mass of the orifice (see Section 5 and Section 6) namely that the kinetic energy configuration outside the jet region is unperturbed by non-linear effects.

Figs. 61 to 71.

A simple addition of the power carried away in each of the first few harmonics would show how little acoustic power is radiated compared with the power conferred to the jet.

The author⁽²⁾ has previously noted that increasing the particle velocity amplitude causes the second harmonic to increase with the square of the fundamental low levels; then the second harmonic suffers a sharp minimum which is followed by an approximate fourth power recovery finally going into a third power rise. This behavior is illustrated in Figs. 3 and 72.

It has now been ascertained that this sharp dip in the second harmonic occurs when the particle displacement is approximately equal to the radius of the orifice. This is evident from a glance at Fig. 73 where the second harmonic relative to the fundamental level is plotted for orifices from .25 cm to 1 cm in diameter. Fig. 73 was plotted from values taken from Figs. 61 to 71. The independent variable N is the fundamental particle displacement amplitude of a spherical source (having the radius of the orifice) divided by the orifice radius.

The decay rate of the first few odd harmonics is given in Fig. 74 in terms of the number of decibels decrease per odd harmonic. In examining these results it is important to realize the orifice behaves like a point source; hence

the decay of the equivalent simple source will be 6 db per octave greater than the value obtained from Fig. 74.

At sufficiently high levels the third harmonic becomes directly proportional to the fundamental, as can be seen from Fig. 3. In this region the theory given in Section 4 of Chapter III can be used to predict the ratio of the third harmonic to the fundamental. According to this theory, the third harmonic pressure should be about 7 db below the fundamental.

A glance at the data taken at the highest levels, on the small and thin orifices (Figs. 61, 62, 65) shows that the third harmonic is very nearly 7 db below the fundamental. The other data cannot be used in making this comparison, since they do not represent data taken in the jet region. Neither can the results given in Fig. 74 be used in this comparison, since this decay in Fig. 74 represents an average over several harmonics and in the jet region the third harmonic is lower than would be predicted from the average decay.

8. The Pumping Action of the Orifice

In Section 4 of Chapter III it was shown that an orifice driven by a pressure wave having a non-zero square root moment should behave like a pump. This behavior was confirmed in a single experiment with the .357 diameter orifice having a thickness of .09 cm. With one obvious exception, the

experimental arrangement was equivalent to that utilized in obtaining the differential resistance. Instead of forcing airflow through the orifice, the orifice was called upon to pump air through the flow meter. The required pumping power could be estimated from the product of the pumping rate times the static head which also was measured. The desired waveform was obtained by combining a 600 cps tone with its second harmonic, both having the same sound pressure level, 152 decibels measured behind the orifice. The relative phase between the two waves was adjusted until the maximum pumping rate of .95 liters per minute was achieved against a pressure head of 4" which represents a working rate of the order of one milliwatt. The power π dissipated by the orifice can be estimated from the relations

$$\pi = Q_{rms}^2 R_{NL} = \frac{1.1 Q_{rms}^2 \rho Q_{peak}}{2(C_d S)^2}$$

and

$$\pi = P_{rms} Q_{rms}$$

from which we obtain

$$\pi = \sqrt{\frac{1.1}{1.1\rho}} C_d S P_{rms}^{3/2}$$

where the symbols have their usual meaning and P_{rms} is the pressure incident on the orifice. Using as an a-c coefficient one that is 30 per cent greater than the d-c coefficient (the d-c coefficient we found to be .66 in Section 3) we compute that 3 watts is dissipated in the orifice.

The mechanical efficiency of this pump is evidently less than one tenth of 1 per cent. Possibly this efficiency could be improved by altering the wave form. Thicker orifices of the same diameter were found to be less efficient pumps.

The fact that small orifices pump quantities of gas has meant that extreme care had to be taken to eliminate small leaks from the tube before valid measurements of the force on objects could be made.

CHAPTER V

THE THEORY OF STEADY FORCES CAUSED BY SOUND WAVES

1. Introduction

In general sound waves cause steady forces on objects with which the waves interact. The nature of these forces is understood provided one restricts the considerations to ideal fluids lacking viscosity, and heat conductivity. In these cases, if the object is not under steady translation, these forces are due to the well-known radiation pressure. On plane reflection and absorbing screens arising from radiation pressure, the forces have been thoroughly investigated by L. Brillouin⁽¹⁸⁾, whereas the forces on spheres have received a rather complete treatment at the hands of L. V. King.⁽¹⁹⁾

Brillouin, in 1925, noted the importance of the flux of momentum tensor specifying the radiation stress tensor, a tensor defined by Brillouin. Adopting Brillouin's point of view we shall derive in terms of the scattered and absorbed energy a general expression yielding the radiation pressure on an object of any shape and having arbitrary normal boundary impedance. This general description of radiation pressure enables the first step to be taken in accounting for the non-ideal character of the fluid. We define the boundary of the object to be the outer surface of its boundary layer which we assume, with Cremer⁽²⁰⁾, can

be specified by a normal impedance. The losses incurred within the boundary layer are shown to modify appreciably the forces due to radiation pressure, particularly in the case of spheres of small radii, and at low frequencies.

We next investigate forces which come about by virtue of the non-linear properties of the medium. The author has previously discussed⁽¹⁾ a force which exists by virtue of the temperature dependence of viscosity. This so-called Stokes-type force, which to date has not been measured, is exerted in the direction opposite to the wave normal and it depends upon the field intensity rather than upon the energy density. It now appears that this Stokes force may be just about cancelled by the modified radiation pressure force which for spheres always acts in the direction of the wave.

Consideration is next given to the influence of asymmetry in the velocity wave form of the medium. It is shown that asymmetry in the wave form will give rise to forces, which as in the case of the Stokes-type force, cannot be explained in terms of the concepts of radiation pressure, but which are caused by the non-ideal nature of real fluids. We have chosen to call the forces arising from asymmetry in the velocity the Oseen-type forces. This has been done in order to emphasize the connection between this force and the force resulting from steady flow which was investigated theoretically by Oseen.

The asymmetry in the velocity required to produce Oseen-type forces may be realized in several ways. We have chosen to examine in detail the effects of asymmetry obtained by combining two or more harmonically related waves. The asymmetry which results from endowing either the medium or the particle with a steady velocity in addition to the large amplitude harmonic disturbance is also studied. We have found that these forces which come about through the combined effects of a non-ideal fluid and an asymmetric wave form can be ten or more orders of magnitude greater than radiation pressure.

The non-ideality of the fluid is apparent in the force velocity relation, which is found to exist for bodies undergoing uniform translation. It is well known that an ideal inviscid fluid exerts no force on a body undergoing uniform translation. In a real fluid the force velocity relation is in general non-linear. Hence any treatment which does not take into account the real character of the fluid is apt to lead to unrealistic conclusions.

Such a treatment due to Nabarro has appeared this month (December 1950) in the literature.⁽²¹⁾ Nabarro in treating an ideal fluid deduces that there will be no force which arises specifically from the non-linear interaction of a sound field and the uniform velocity with which the body is assumed to move through the field. Nabarro does find, as

one would expect, that the classical radiation pressure forces are modified due to flux and doppler considerations. Because of his assumption, Nabarro's treatment is valid primarily in regions where the forces due to classical radiation pressure are large, that is for large spheres or for small wavelengths.

2. The Wave Drag Coefficient

In discussing the steady forces caused by sound waves, it has been found expedient to introduce a quantity called the wave drag coefficient and symbolized by D_W . This coefficient is defined as the magnitude of the force per unit local acoustic energy density* divided by the object area projected in the direction of the undisturbed particle velocity. The coefficient D_W may be thought to be the magnitude of the sum of a number of partial vector drag coefficients

$$D_W = \left| \sum_n d_n \right|$$

each d_n representing forces arising from one specific mechanism. The following partial drag coefficients are of interest: d_1 , arising from radiation pressure; d_2 , involving

* In some instances (Chapter VI for example) we have used twice the average local kinetic energy density in place of the energy density. This allows results obtained in travelling and standing waves to be compared against a common theoretical curve.

mean viscous forces; d_3 , describing the so-called Oseen-type forces.

In the experiments reported in Chapter VI, the Oseen-type forces are much greater than all the others, so that it is proper to set $D_W = |d_3|$.

3. Forces Produced by Acoustical Radiation Pressure

A technique is outlined in this section for finding the force caused by radiation pressure arising from the interaction of a collimated beam of sound with an object. The force is evaluated in terms of a surface integral of asymptotic scattering functions for the object. The expression for the force is valid for objects of any shape having arbitrary non-uniform boundary impedance. In addition, the method is simpler in its application than King's.⁽¹⁹⁾ Specific expressions are derived for rigid spheres and cylinders of infinite and zero mass.

We shall see that the effects of ordinary viscous and thermal losses at the surface of small objects may give rise to extra forces, induced by radiation pressure, which are several orders of magnitude greater than the values calculated by King. The exact value of the force on the object cannot be obtained directly since part is due indirectly to a transfer of momentum associated with the medium streaming by the object. The streaming is caused by the wave momentum absorbed in the viscous and thermal

boundary layer surrounding the object.

We seek first a relation between the average pressure p_E in fixed coordinates and the average Lagrange density L_{av} . Taking the time average of Euler's equation⁽²²⁾ gives:

$$\overline{\rho(u \cdot \nabla)u} + u \left[\overline{\nabla \cdot (\rho u)} \right] = -\nabla \bar{p}_E. \quad (1)$$

If this development is to be carried out to second order in u , the solutions u_0 and ρ_0 to the first order wave equation may be utilized. Thus Eq.(1) becomes:

$$\rho_0(\overline{u_0 \cdot \nabla u_0} + \overline{u_0 \nabla \cdot u_0}) = -\nabla \bar{p}_E. \quad (2)$$

By taking the time average of Eckart's⁽²²⁾ Eq.(11)* and assuming irrotational motion, one finds easily:

$$\rho_0(\overline{u_0 \cdot \nabla u_0} + \overline{u_0 \nabla \cdot u_0}) = +\nabla L_{av} \quad (3)$$

Thus

$$\bar{p}_E = -L_{av} + \text{constant}, \quad (4)$$

establishing the first relation required.

Next we look for a connection between the flux of momentum density (a tensor of rank two whose connection with radiation pressure was first recognized by Brillouin⁽²³⁾) and the Lagrange density. Introducing the flux of momentum density dyad $\rho_0 uu$, we note that the relation:

$$\nabla \cdot uu = u \cdot \nabla u + u \nabla \cdot u,$$

in connection with Gauss's theorem

$$\iiint \nabla \cdot (uu) dv = \oint d\bar{A} \cdot uu,$$

* This equation called by Eckart the conservation law of acoustic "momentum" is $\frac{1}{c_0^2} \frac{\partial J}{\partial t} + \rho_0 [u_0 \cdot \nabla u_0 + u_0 \nabla \cdot u_0] - \nabla L + \rho_0 u_0 \nabla \times (\nabla \times u_0) = 0$ where J is the acoustic energy flow (instantaneous intensity).

enables Eq.(3) to be written as

$$- \oint L_{av} \vec{dA} + \rho_0 \oint \vec{dA} \cdot \vec{uu} = 0, \quad (5)$$

establishing the second relation required.

The force on the object can be obtained from the pressure evaluated in the coordinates of the boundary of the object, which are fixed only if the object is rigid. (Continuity of pressure and velocity is assumed at the fluid-object interface; penetration of fluid into the object is ruled out). The average pressure on the boundary p_B may be obtained by applying the inverse stationary coordinate transform to the instantaneous pressure, in fixed coordinates, and subsequently performing the time average. This leads to the average boundary pressure:

$$\bar{p}_L = \bar{p}_E + \overline{d_B \cdot (\nabla p_E)} \quad (6)$$

in which d_B is the boundary displacement.

Next, if the simplifying restriction is made that the boundary moves only perpendicular to itself, the following relation holds on the boundary:

$$\vec{dA} \cdot \vec{uu} = \left[d_B \cdot (\nabla p_E) \right] \vec{dA}, \quad (7)$$

These results are now applied to obtain the force on an object located on the axis of a collimated monochromatic

The direct transform from moving to fixed coordinates is ⁽¹⁾
 (scalar in fixed coords.) = (scalar in moving coords.)
 - d (scalar in moving coords.)

incident beam. Eq.(5) is applied to the region bounded by the outer surface of the object and a concentric surface R enclosing the object. In two or three dimensional problems the surface R is conveniently chosen to be a cylinder or sphere respectively, having a radius large compared with the dimension of the object and the wavelength. The boundary conditions at infinity are assumed to be perfect absorption. One-dimensional problems have been treated in detail elsewhere⁽²³⁾ and will not be discussed here. The outer normal in both instances is considered positive. By virtue of Eqs.(4) (5), and (7), the left-hand member of Eq.(6) integrated over the surface of the object yields the force on the object:

$$\vec{F} = - \int_{\text{obj.}} L_{av} \vec{dA} + \rho_0 \int_{\text{obj.}} \vec{dA} \cdot \overline{uu}, \quad (8)$$

The surface surrounding the scattering obstacle is sufficiently far from the scattering region so that over most of this surface there is no interference between the incident and scattered waves: hence, on this outer surface, L_{av} will differ from zero only in an arbitrarily small region of interference. The integration over R of the left member of Eq.(5) yields, therefore,

$$\rho_0 \int_R \vec{dA} \cdot \overline{uu} . \quad (9)$$

Since, by Eq.(5) the sum of (8) and (9) must be zero we find

$$\vec{F} = -\rho_0 \int_R \vec{dA} \cdot \overline{uu},$$

or, since $L_{av} \simeq 0$ on R and $u \perp R$, the force may be expressed in terms of the field momentum vector P:

$$\vec{F} = - \int_R |\vec{P}| \vec{dA}, \quad (11)$$

or the field intensity:

$$\vec{F} = - \frac{1}{c} \int_R |\vec{P}| \vec{dA}. \quad (12)$$

A complex drag coefficient d_1 may be defined, the real part representing the component of the force per unit projected area which lies in the direction of the incident field momentum P_0 , and imaginary part the component at right angles to P_0 . It is convenient to express d_1^* in terms of the total power scattered π_s , the total power absorbed π_a , and the magnitude of the scattered intensity γ , all expressed per unit incident intensity. If θ is the angle formed by the incident and scattered intensities and s is the projected area of the object we find:

$$d_1^* = \frac{1}{s} \left[\pi_a + \pi_s - \int \gamma \cos \theta \, dA \right] - \frac{i}{s} \int \gamma \sin \theta \, dA. \quad (13)$$

If the scattering object has an axis of symmetry coinciding with the incident wave normal, d_1^* is real and

$$d_1^* = d_1 = \frac{1}{s} \left[\pi_a + \pi_s - \int \gamma \cos \theta \, dA \right]. \quad (14)$$

Eq.(14) was used for computing the values of d_1 for

progressive waves given in Table IV. Asymptotic expressions for γ , as given by Rayleigh⁽²⁴⁾ in the low frequency approximation, were used to calculate d_1 for spheres and cylinders of ∞ mass. The appropriate dipole term was subtracted for the case of 0 mass, the incorrect assumption being made that the obstacle moves with the fluid.

The coefficient d_1 for standing waves was evaluated by integrating the space maximum time-averaged pressure in fixed coordinates⁽¹⁾ over the surface of the obstacle.

King⁽¹⁹⁾ has obtained expressions for the radiation pressure on spheres. In the low frequency approximation our results agree exactly in the traveling wave case.

The force on rigid objects of any shape can be evaluated provided the object is small compared with the wavelength. To accomplish this, the technique applied by Lamb⁽²⁵⁾ to the scattering of sound by an obstacle of any form can be applied.

TABLE IV

Wave Drag Coefficient

a = radius of object

k = wave number

Object	Mass	Progressive Wave	Maximum Value in Standing Wave
Sphere	∞	$\frac{11}{9}(ka)^4$	$\frac{8}{3}ka$
	0	$\frac{8}{9}(ka)^4$	0
Cylinder	∞	$\frac{5\pi^2}{8}(ka)^3$	πka
	0	$\frac{3\pi^2}{8}(ka)^3$	0

We now consider absorption of energy by the boundary layer and its influence on the force communicated to the object. In order to have a definite problem at hand, we shall consider a rigid sphere with a radius much smaller than the wavelength. Let us, however, consider the forces which act on the outer surface of the acoustical boundary layer rather than at the surface of the sphere. To simplify the problem, only viscous losses will be considered. The effect of viscous losses will be to bring in the term $\frac{\pi a}{s}$ in the expression for the drag coefficient.

For a small sphere ($ka \ll 1$) the fraction of the incident energy which is lost through viscous action is, approximately, (25)

$$\frac{6\nu}{ca} \pi a^2$$

ν being the kinematic viscosity and c the velocity of sound. Thus that part of the coefficient due solely to viscous absorption, is

$$\frac{\pi a}{s} = \frac{6\nu}{ca} \quad (15)$$

The conditions for equality between the expression (15) and the coefficient arising from scattering by the rigid sphere is obtained by setting d_1 from Table IV equal to

Eq. (15):
$$\frac{11}{9}(ka)^4 = \frac{6\nu}{ca}$$

for traveling waves, and

$$\frac{8}{3} ka = \frac{6\nu}{ca}$$

for standing waves.

Recently several publications⁽²⁶⁾⁽²⁷⁾ have appeared in which the drift of aerosols under the influence of sound has been discussed in terms of radiation pressure. Thus it would be of interest to obtain numerical values for the equalities (16) and (17). For a frequency of 10,000 cps in air the radius for equality is of the order of 20 microns for standing waves and 100 microns for traveling waves.

The author has recently⁽¹⁾ predicted a steady force which should occur as a result of the temperature dependence of the viscosity. This we call the Stokes-type force and it is supposed to be exerted in a direction opposite to the intensity vector. The author derived an expression relating this force to the intensity of a sound wave in a gas. He assumed a temperature dependence of the viscosity given by simple kinetic considerations and thus based his derivation on the assumption that the viscosity varied with the 1/2 power of the temperature, (in reality the variation is according to a higher power but this does not influence the order of magnitude of the results.)

For a plane progressive wave the drag coefficient associated with the Stokes force is

$$d_2 = \frac{-3(\gamma - 3)v}{ca} \approx \frac{-5v}{ca} \quad (16)$$

where γ indicates the ratio of specific heats which has been assumed to be 1.4 for air. We now see that d_2 will be smaller than the d_1 of Eq.(15) and that, subject to the

uncertainty in the true value of d_1 , the direct measurements of d_2 may not prove feasible.

In the discussion of this section we have tacitly assumed that the instantaneous temperature of the object followed that of the medium. To have assumed otherwise would have added unnecessarily to the complexity of the problem.

4. The Oseen-type Forces

The force acting on a sphere moving at a constant velocity relative to a viscous medium can be written to include a term depending on the square of the velocity u :

$$\vec{\text{Force}} = 6\pi r \mu_0 \vec{u} [1 + k |u|] \quad (17)$$

where the first term is the well known Stokes law, and the second term involves a constant k that is usually determined experimentally. In steady flow, k is given approximately by Oseen's second approximation to the relation for the drag on a sphere. The relation (17) is usually expressed by giving the hydrodynamic drag coefficient which is defined to be the ratio of the force divided by the projected area of the sphere and the kinetic energy density of the fluid. If C is the drag coefficient then, to within Oseen's approximation, Eq.(17) may be expressed as:

$$C = 24R^{-1} \left\{ 1 + \frac{3R}{16} \right\} = 24R^{-1} + D \quad (18)$$

where R is the Reynold's number for the sphere. The degree to which Eq.(18) conforms to the facts can be seen in Fig. (30) which is taken from Prandtl and Tietjens⁽²⁸⁾. The dotted line is a plot of Eq.(18) whereas the solid curve represents experimental data. It can be seen that the deviation from Stokes' law is definitely noticeable for a Reynold's number of about 1. It is also evident that Eq.(18) does not fit the facts to well for $R > 1$. Goldstein⁽²⁹⁾ has obtained an expansion from which values of C can be calculated for R as high as 2. His expansion is

$$C = 24R^{-1} \left(1 + \frac{3}{16}R - \frac{19}{1280}R^2 + \frac{71}{20480}R^3 - \frac{30179}{34406400}R^4 + \frac{122519}{560742400}R^5 - \dots \right) \quad (19)$$

The first term in the series, $24R^{-1}$, is the value obtained by Stokes' and the second approximation, Eq.(18) was obtained by Oseen. Due to the complexity of Eq.(19) we shall not consider it further.

Inasmuch as Oseen's approximation appears to account in a crude way for the facts of steady flow, it is natural to ask to what degree the approximations will hold for non-steady flow. The point of view adopted in this and the succeeding chapter has been to adopt Oseen's approximation as a point of reference against which experimental results may be compared. In order to carry this program out we first assume Oseen's law to be instantaneously

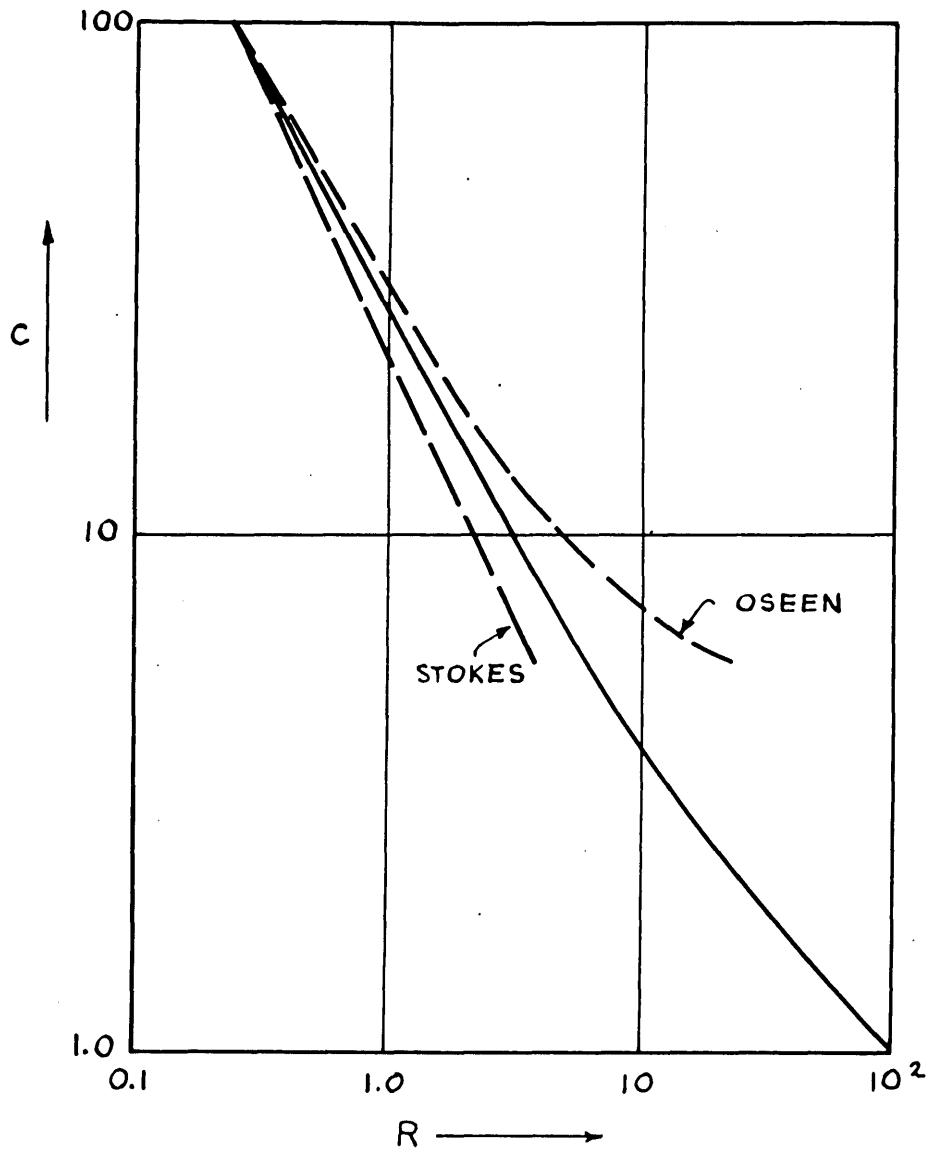


FIG. 30 - DRAG COEFFICIENT VS. REYNOLDS' NUMBER FOR SPHERE.

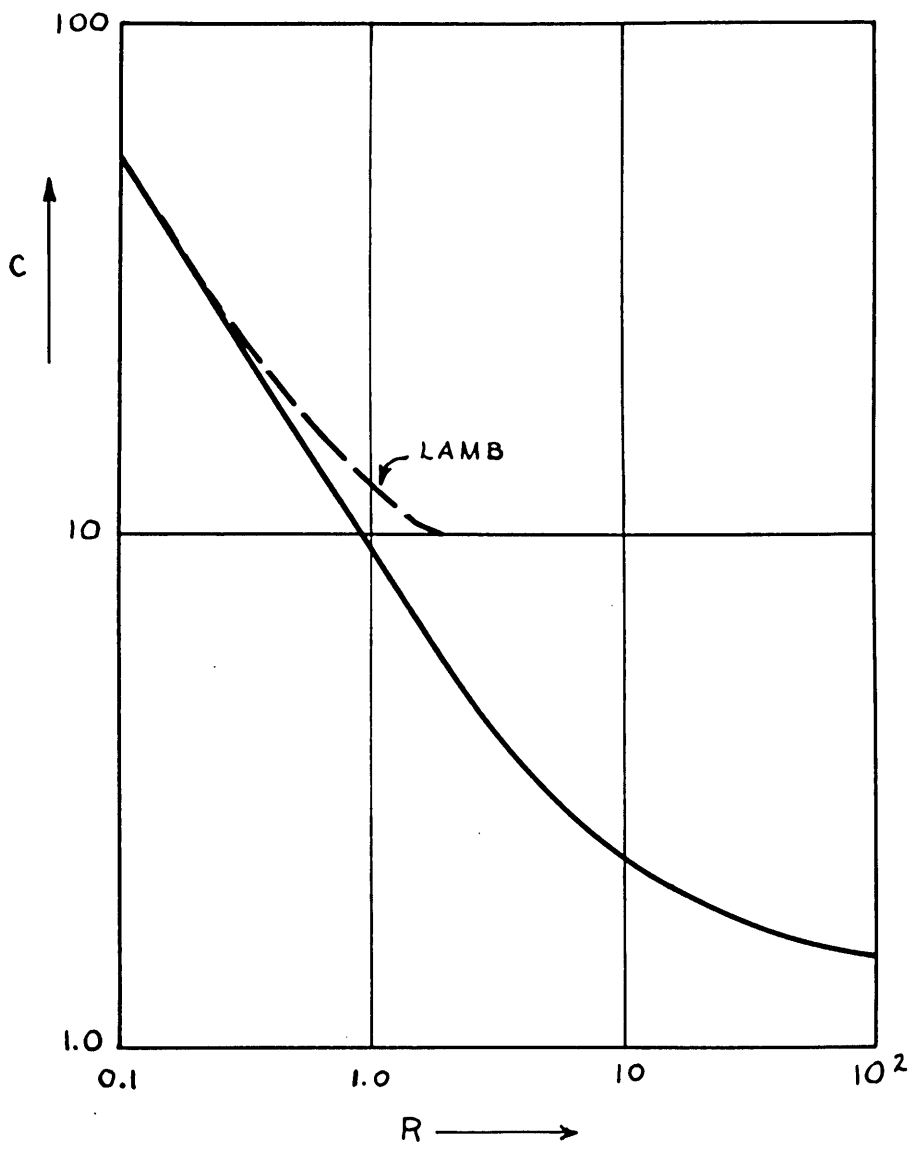


FIG. 31 - DRAG COEFFICIENT VS. REYNOLDS' NUMBER FOR CYLINDER OF INFINITE LENGTH.

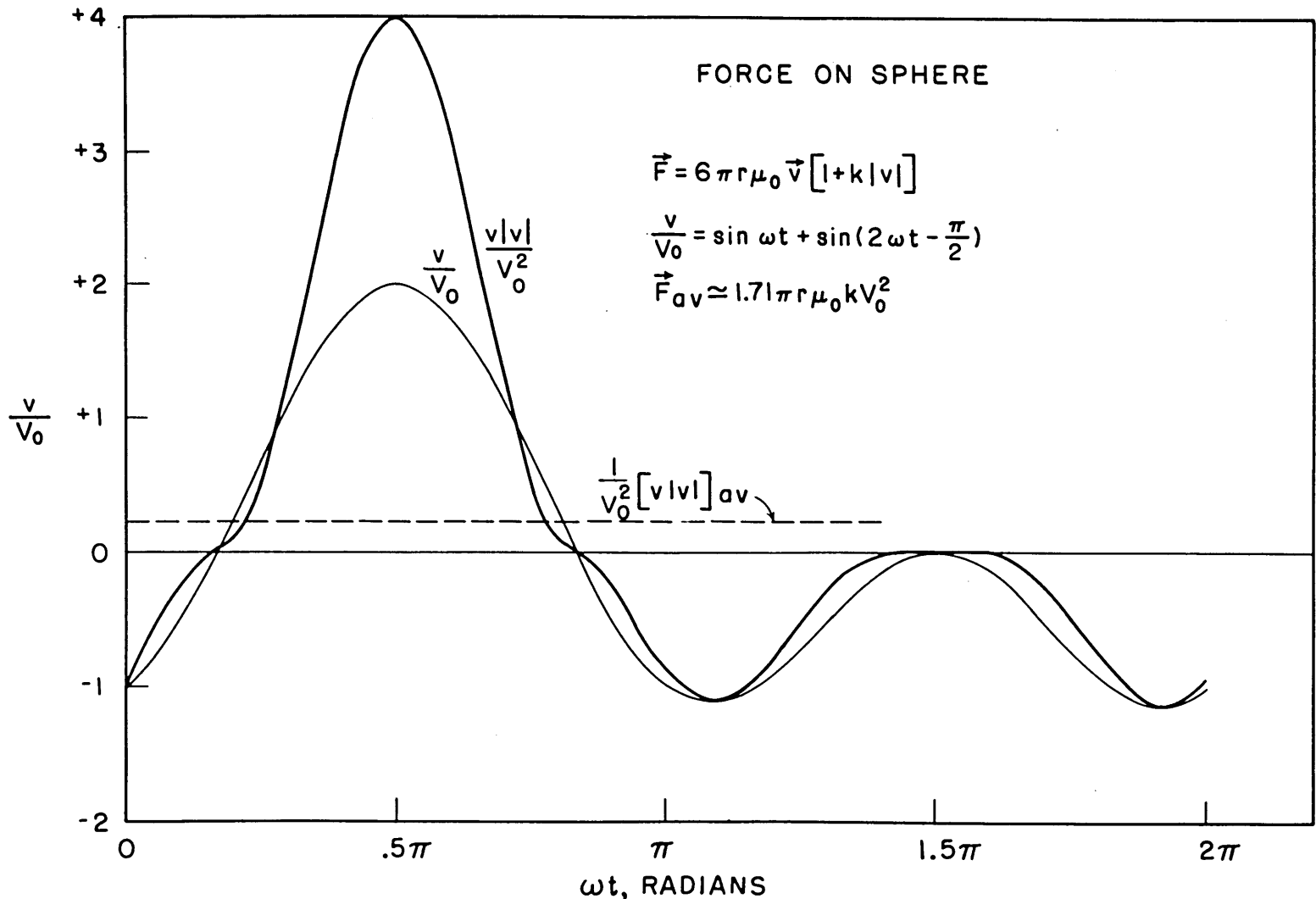
applicable and proceed to derive the consequences of this assumption for non-steady flow.

It may be worth pointing out that for most of the experiments we have done, the objects have been so small and the frequencies so low that the first order acceleration forces are of the same order or smaller than the first order viscous forces. The time average of the first order acceleration force is zero in a periodic wave. We neglect second order acceleration forces. The acceleration forces are tied up with the virtual mass of the sphere. It is possible that the virtual mass is very much reduced under the influence of large alternating amplitudes. This latter point is discussed further in Section 2 of Chapter VII.

It is easy to see that if u is periodic and has a zero average value, the first term in Eq.(17) contributes nothing to the average value of the force. Whether the second term contributes to the average or not depends on whether the average

$$\frac{1}{T} \int_0^T u |u| dt = \overline{u |u|} \quad (20)$$

is different from zero. Following Baerwald (see Appendix IV) we shall call the average represented by $\overline{u |u|}$ the Oseen-type moment. There are an infinite variety of periodic wave forms which have an Oseen-type moment different from zero. One of the simplest is obtained by combining two harmonically related waves in proper phase as indicated in Fig. 32. The average force on a sphere resulting from an assumption of



WAVE FORM WITH OSEEN-TYPE MOMENT

FIG. 32

Eq.(18) in conjunction with this wave has been worked out as a simple example. In this case k is easily expressed in terms of D , the difference between Oseen's value of C and Stokes' value for the same quantity

$$k = \frac{aD}{12\nu} = \frac{4.5a}{12\nu}$$

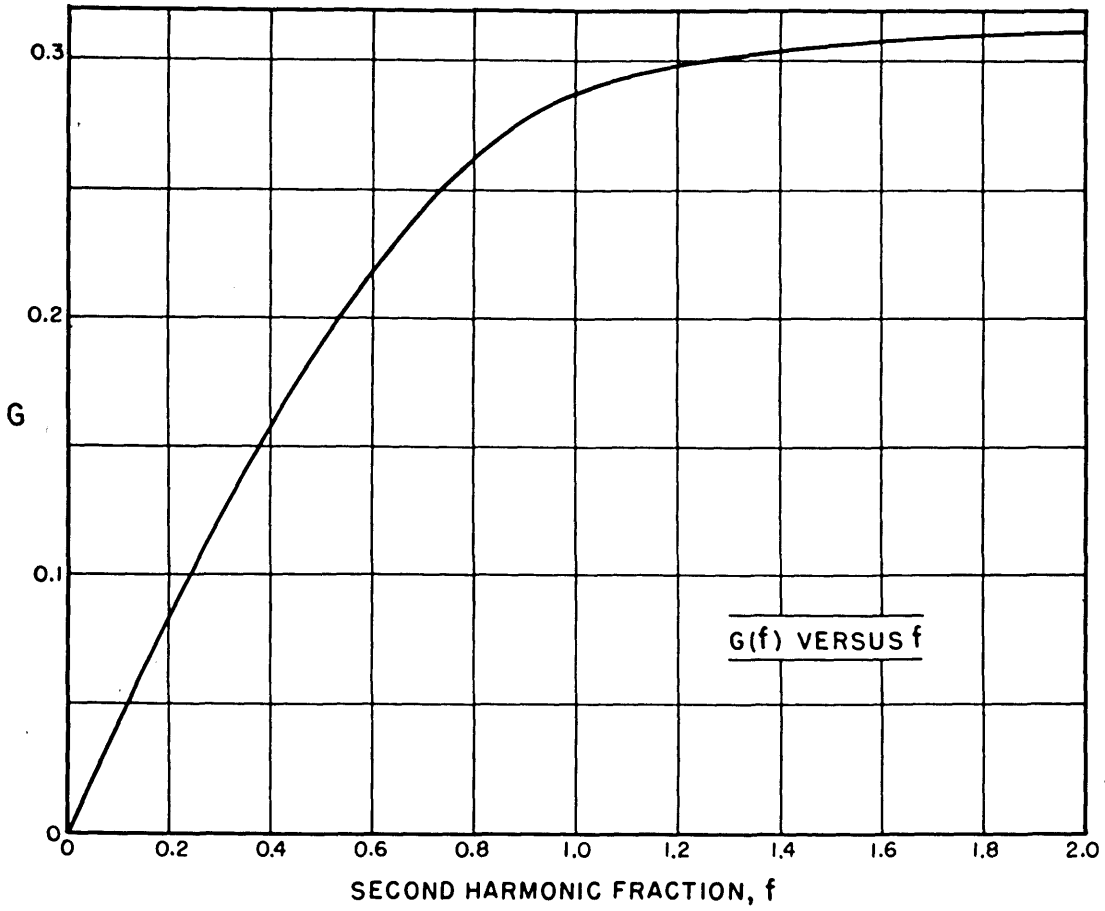
A more general wave than that depicted in Fig. 32 is obtained by considering as adjustable parameters f , the fraction of second harmonic and ϕ , the relative phase angle between the fundamental and second harmonic. Such a wave form would be the following:

$$u = u_0 \left[\sin \omega t + f \sin(2\omega t + \phi) \right]$$

This wave form is illustrated in the Figures 57 to 60 copied from one of Rider's handbooks⁽³⁰⁾. These figures can be used to adjust for desired waveform in case no calibrated phase controls are at hand. An expression for the Oseen-type moment of this more general wave is obtained in Appendix III for special values of f and ϕ . The results of Appendix III supplemented with calculations performed by the Joint Computing Group indicate that the normalized Oseen-type moment of this wave can be expressed as the product of two functions

$$\begin{aligned} \frac{\overline{|u|u|}}{u_0^2} &= G(f)\phi(\phi) \\ &= -G(f)\sin \phi \end{aligned}$$

Here $G(f)$ is a function of f alone and ϕ is a function only of the phase angle. The function G is plotted in Fig. 33.



NORMALIZED OSEEN MOMENT VS. HARMONIC FRACTION

FIG. 33

It is considerably neater to deal directly with the wave drag coefficient, d_3 instead of the force. For this more general wave, then, the coefficient d_3 turns out to be

$$d_3 = \frac{G\phi}{1+f^2} D = \frac{-4.5 G \sin \phi}{1+f^2} \quad (21)$$

for a plane progressive wave.

The factor $(1+f^2)$ in the denominator is proportional to the energy density in the wave. The function G is shown in Appendix III to be given by the following expression:

$$G = \frac{1}{\pi} \left\{ x \sqrt{1-x^2} + \frac{4}{3} f x (3-2x^2) - f^2 x \sqrt{1-x^2} [2x^2-1] - y(1+f^2) \right\} \quad (22)$$

where $x = \cos y$

and

$$y = 1/2 \cos^{-1} \left[\frac{1}{4f^2} (\sqrt{1+8f^2} - 1) \right]$$

Approximate and asymptotic expressions for G are easily found to be

$$G \rightarrow \frac{4f}{3\pi} \quad \text{as } f \rightarrow 0$$

$$G \rightarrow \frac{9\sqrt{3}}{8\pi} - 1/3 \approx .287 \quad \text{for } f = 1 \quad (23)$$

$$G \rightarrow \frac{1}{\pi} \approx .318 \quad \text{as } f \rightarrow \infty$$

From these relations we see that the drag coefficient varies inversely with the harmonic fraction, f , for small f , whereas for large f , d_3 varies inversely with the square of f . This means that d_3 will have a maximum with respect to f , as is evident from Fig. 43 in Chapter VI where the negative

logarithm of $D_W = |d_3|$ is plotted as a function of f , f being expressed in decibels.

H. G. Baerwald has recently checked the maximum value of our calculated d_3 and he has extended the calculations to a waveform containing three harmonic components. His results which were privately communicated to the author appear in Appendix IV. He found an appreciable increase in the wave drag coefficient upon addition of the third harmonic. Baerwald defined an "efficiency ratio" η which is the ratio of the Oseen-type moment to the power moment, u^2 . In terms of this ratio, our partial wave drag coefficient d_3 is equal to 2.25η . From Appendix IV we find that the maximum values of η are .325 for two harmonic components and .487 for three. In a letter to the author Baerwald comments as follows:

"I had expected an appreciable increase of the 'wave coefficient' upon addition of the third harmonic, as this would tend both to enhance the sharpness of the pulse shape at the in-phase point and to promote interference cancellation elsewhere. I wonder whether a different choice of two harmonics added to the fundamental would improve the result?"

The combination of a larger number of harmonic components is probably quite academic as far as application is concerned, and the corresponding calculation would be rather cumbersome and boring; I understand that there are quite a few harmonic synthesizers around and with such a gadget in combination with a cathode ray tube, photocell and some electronic circuitry, the whole matter could be tackled automatically in no time - but would it worth the effort?"

The experiments discussed in Chapter VI involve measuring the force on a pendulum fashioned by hanging a sphere from a

small cylindrical wire or thread. In order to know the force acting on the sphere, the force which is exerted on the cylinder must be known. Calculations similar to the ones just carried out for the sphere are difficult to duplicate for the cylinder because of the nature of the steady flow resistance law for cylinders. Lamb's⁽²⁵⁾ relation for the drag on a cylinder expressed in terms of the force per unit length is:

$$F/\ell = \frac{-4\pi\mu U}{\ln \frac{Ua}{2\mu} - 0.0772} \quad (24)$$

where ℓ and a are the length and radius, respectively of the cylinder, μ is the viscosity and U the velocity. This relation which holds only for small Reynold's number is plotted in Fig. 31. It is apparent that the drag coefficients for cylinders and spheres are not too dissimilar so that we might expect the Oseen-type forces due to sound waves to be about equally strong, on a unit area basis, for spheres and cylinders, at least in the range of Reynold's numbers depicted in the graphs. The analytic difficulty involved in computing the Oseen-type moment from Eq.(24) has prompted us to resort to an approximation. Instead of assuming the velocity waveforms to be compounded of two harmonically related sinusoids, we have used the rectangular wave depicted in Fig. 36. This wave, inserted into Eq.(24) leads to values of the drag coefficient (remember the projected area of a cylinder is $2r\ell$) which are

a function of the peak Reynold's number as indicated in Table V:

TABLE V

R_0	d_3
1	3.78
0.4	2.14
0.04	4.08
0.004	17.3
0.0004	94.2
0.00004	596

Finally we investigate the wave drag coefficient d_3 for a sphere in a moving stream of gas or liquid. In Appendix III the Oseen-type moments have been evaluated for a velocity wave consisting of a constant d-c term in addition to a sinusoidal component. In the event the amplitude of the alternating component is less than the d-c term the velocity may be written

$$u = u_0 \left[1 + f' \sin \omega t \right], \quad f' \leq 1 \quad (25)$$

where f' here indicated the modulation index. The Oseen-type moment of such a wave can be expressed as

$$\overline{u|u|} = (1 + f'^2/2) u_0^2 \quad (26)$$

In the event $f' > 1$ we may write for the velocity

$$u = u_0 \left[\sin \omega t + f \right], \quad f \leq 1 \quad (27)$$

for which case the Oseen-type moment is shown to be

$$\overline{u|u|} = \beta(f) u_0^2 \quad (28)$$

$$\text{where } \beta(f) = \frac{1}{\pi} \left[(1+2f^2) \sin^{-1} f + 3f \sqrt{1-f^2} \right]$$

and $\beta \approx \frac{4f}{\pi}$ for $f \ll 1$,

$$\beta(1) = 3/2$$

By means of Eq.(26) and the fact that Eq.(25) can be written as

$$u = (f'u_0) \left[1/f' + \sin \omega t \right],$$

$\beta(f)$ can be defined for any $f \geq 0$. A plot of β is given in Fig. (34).

We are not too much interested in the total force experienced by the object in a combined sonic and flow field. If we were, we would also have to take Stokes' law into account. What we want is the additional force caused by the interaction of the sonic and flow fields. Thus it is necessary to subtract from Eq.(28), f^2 , the Oseen moment of the d-c flow field. This leads to a differential β , called β_d and given by:

$$\beta_d = \beta - f^2 \quad (29)$$

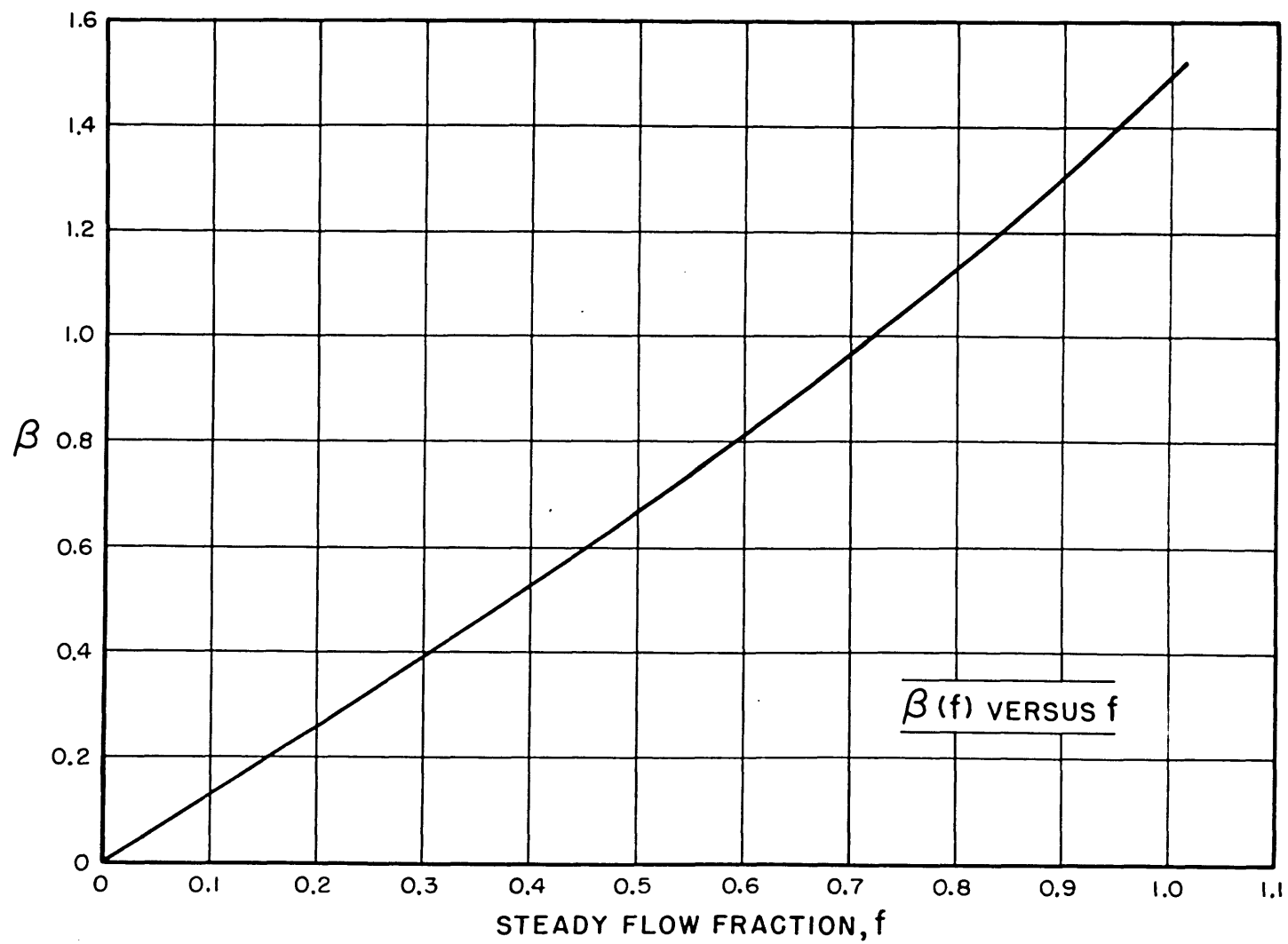
from which we can obtain the wave drag coefficient pertaining to a sinusoidal wave in the presence of steady flow:

$$d_3 = C\beta_d = 4.5\beta_d \quad \text{for } f \leq 1 \quad (30)$$

and

$$d_3 = \frac{C}{2} = 2.25 \quad \text{for } f \geq 1$$

Thus a d_3 has been found which represents the interaction force per unit project area divided by the acoustic (not including the steady flow kinetic energy) energy density. From Eqs.(30) it is seen that d_3 depends through β_d on the steady flow fraction f provided this fraction is less than unity.



NORMALIZED OSEEN MOMENT VS. STEADY FLOW FRACTION

FIG. 34

If $f > 1$ the drag coefficient is a constant. In the experiments described in Chapter VI the flow velocity was maintained at a fixed value, while f was varied by changing the sound pressure level. In the experiments combining flow and sound the condition $f \ll 1$ was realized so that over the available experimental range

$$\begin{aligned}d_3 &= 4.5 \beta_d && \text{and } f \ll 1 \\ &\approx 4.5\beta && \text{by virtue of Eq.(29)} \\ &\approx \frac{18f}{\pi} && \text{by virtue of Eq. (28)}\end{aligned}$$

The negative logarithm of d_3 obtained from Eqs.(30) has been plotted as a function of the sound pressure level in Figs.46 and 47, the values of the flow velocity being indicated along side the solid curves to which they pertain.

When dealing with one dimensional standing waves, the wave drag coefficient is a function of where in the wave one is. In waveforms consisting of a fundamental and second harmonic component the coefficient has positions of maxima and minima which occur roughly an eighth of a wavelength apart. In a perfect standing wave d_3 is zero at the velocity nodes of the fundamental and second harmonic components. The positions of maxima in d depend on the relative amplitudes to which the two modes are excited. If the second harmonic mode is excited to $1/3$ or less of the strength of the fundamental, the positions of the maxima in d become essentially independent of the relative amplitudes of

the two modes. In this case if x is the distance from the hard termination, the coefficient d_3 and hence the force vary according to

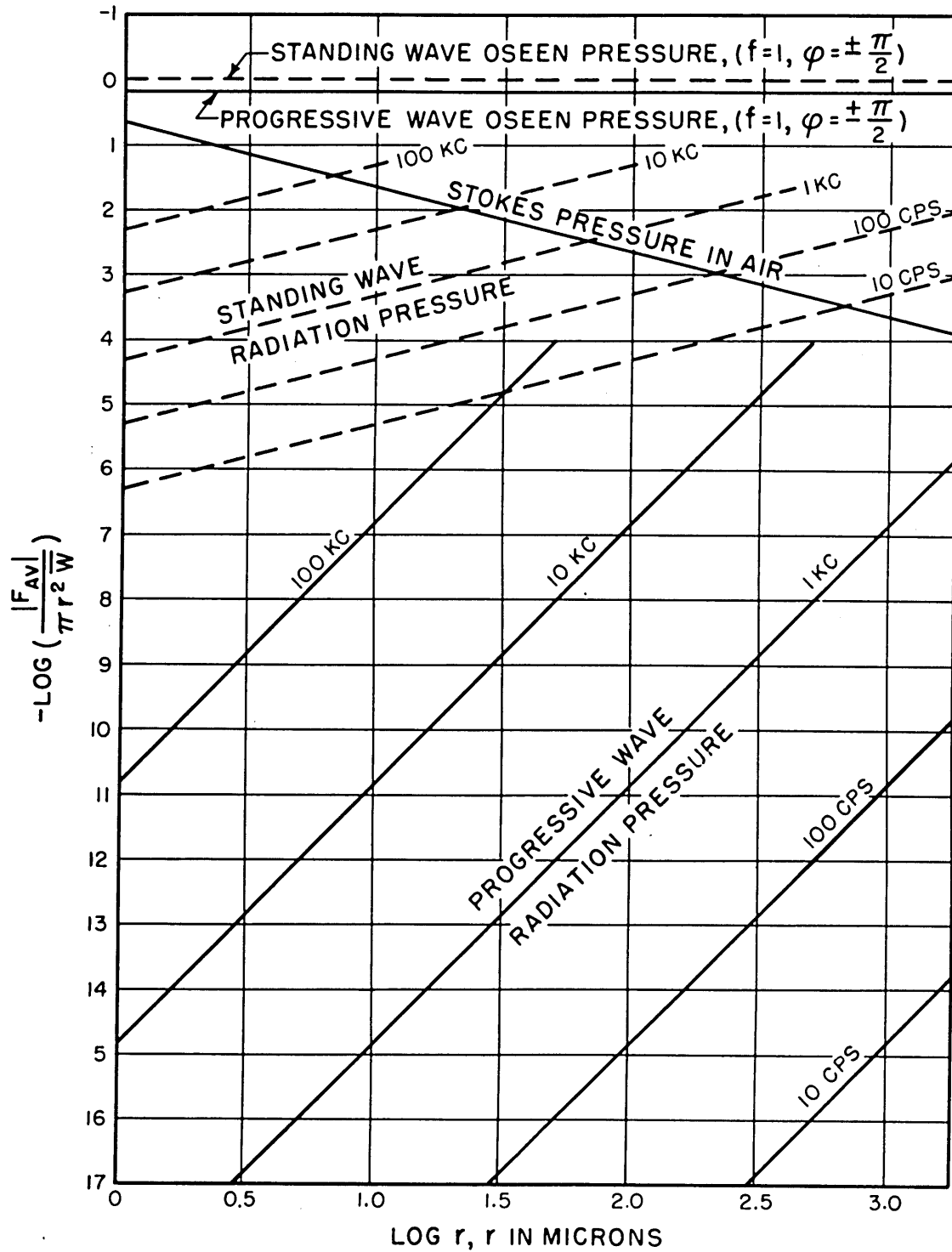
$$\pm \sin kx \sin 2kx$$

The sign in this expression depends on the relative phase angle between the harmonics, and the fundamental component. The modulus of the above quantity has maxima at $x = (\pm 0.152 + n/2)\lambda$, $n = 1, 2, \dots$. These results should be compared with the x dependence of the radiation pressure due to a single mode of wave number k . If a positive force lies in the $+x$ direction, then the classical radiation pressure force varies according to

$$\sin 2kx$$

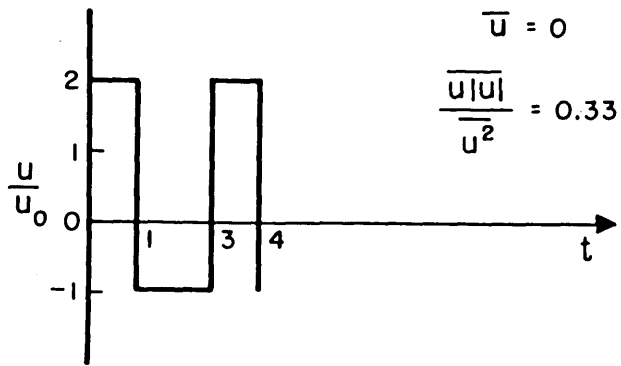
which has a maximum modulus at $x = (1/8 + n/4)\lambda$, $n = 1, 2, \dots$. Thus the behavior of the Oseen-type force in a standing wave is very similar to the radiation pressure force except that the Oseen force can act either in the same direction as radiation pressure or in the opposite direction.

In Fig. 35 we have compared the three types of forces discussed so far. The chart is primarily intended to convey orders of magnitude and it pertains to spheres and wave numbers for which $kr \ll 1$. Traveling waves as well as standing waves have been treated. The curves for radiation pertain to the classical radiation pressure. The order of magnitude of the radiation pressure when modified by viscous losses may approach that of the Stokes' type force as discussed in Section 3 of this chapter.



THE PARTIAL DRAG COEFFICIENTS COMPARED

FIG. 35



RECTANGULAR WAVE WITH AN OSEEN
MOMENT

FIG. 36

CHAPTER VI

AN EXPERIMENTAL DETERMINATION OF THE WAVE DRAG COEFFICIENT ON SPHERES AND CYLINDERS

1. Introduction

The measurements of the average force exerted on small spheres and cylinders in a plane wave acoustic field are described in this chapter. Due to basic limitations imposed by the available instruments, the measurements were restricted to spheres having a radius of about 100 microns (10^{-2} cm). Cylinders having a radius of 1/2 and 7 microns were investigated.

The experimental technique is discussed in Section 2. Most of the equipment associated with the orifice experiments was used in these measurements. Early measurements of the average force caused by a wave containing second harmonic distortion, are discussed in Section 3. In these early results the force on the fiber supporting the sphere was unjustifiably neglected, an omission which led to measured values of the force on the sphere which were too large. These early measurements were performed by Mr. Peter W. Sieck and the author who have jointly reported their preliminary⁽³¹⁾ findings. Measurements of the force on cylinders are reported in Section 7; the results of these measurements permitted the fiber force to be taken into account in subsequent measurements with spheres. All but the early measurements of Section 3 were performed by

Mr. Keith Hoyt and the author. The results of some of these measurements have recently been reported.⁽³²⁾

The experimentally determined variation of the force with the second harmonic fraction and with the phase angle between the harmonic components is discussed in Section 4, while the results of varying the sound pressure level are presented in Section 5. In Section 6 results are presented of measurements made on the forces arising from the interaction of a steady flow with sounds.

2. Experimental Technique

All measurements of force were obtained by observing the deflection of a pendulum which was suspended in the acoustic field. This pendulum was fashioned out of spheres and cylinders. Fig. 37 illustrates how a spherical particle was suspended so as to hang on the axis of the horizontal three inches in diameter. A loudspeaker is fixed to one end of the tube about 1 meter from the sphere. The opposite end of the tube is terminated with a 1-meter long pc fiberglass wedge (described in Section 2 of Chapter II) whose tip was 1 meter from the sphere.

The whole tube assembly is tightly sealed with modelling clay. Sound pressure measurements were obtained using one section of a Brush rochelle salt cell placed in the tube about two feet from the sphere. Before each measurement, this microphone was calibrated in situ at each frequency for which

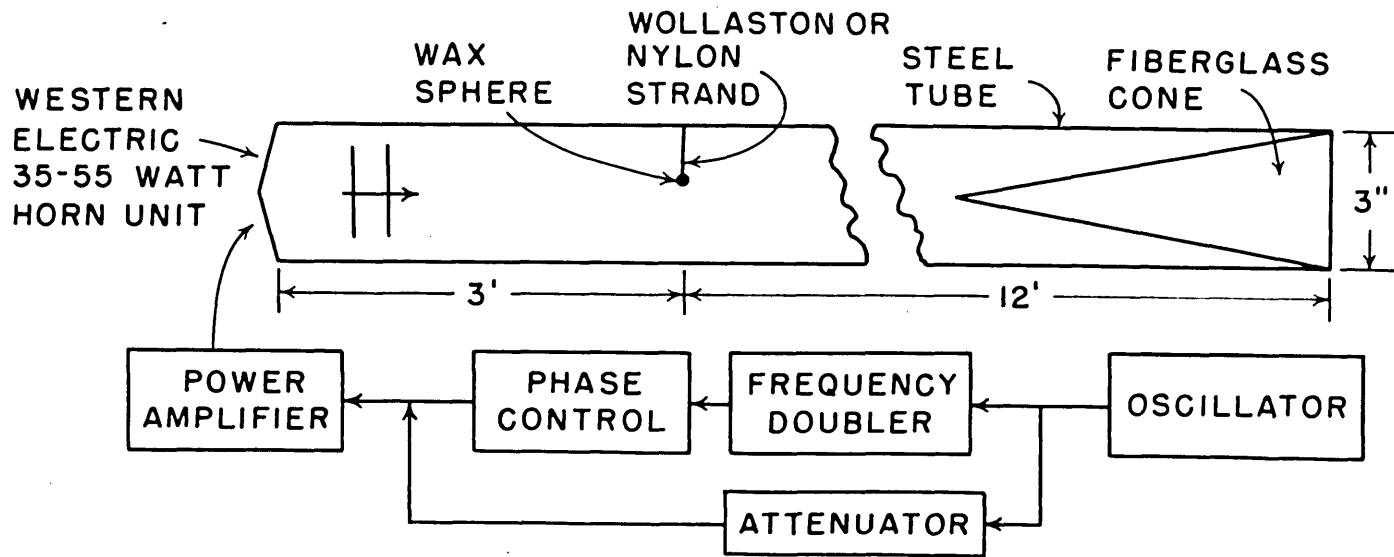


FIG. 37

measurements were to be obtained. The calibration was a comparative procedure utilizing a Western Electric 640-AA having its diaphragm flush with the inside walls of the tube.

The deflection of the pendulum was observed through a plane glass port in one section of the tube. The magnitude of the deflection was ascertained by viewing the foot of the pendulum through a low powered microscope equipped with an eyepiece which included a scale.

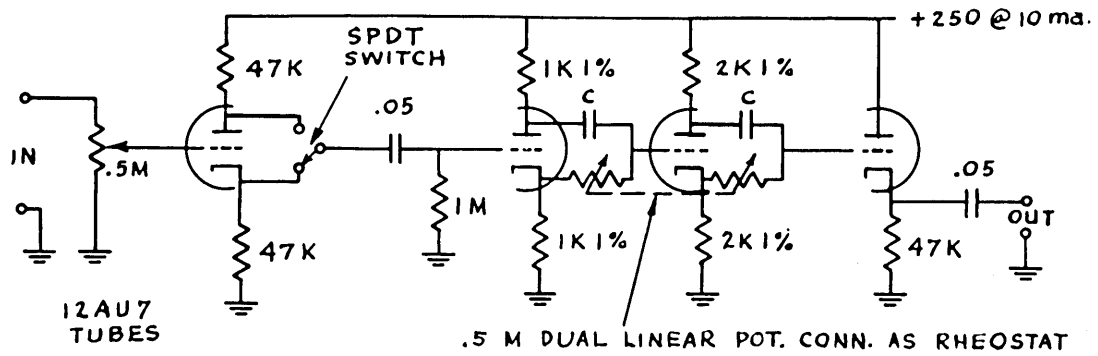
The basic equipment is illustrated in the Block Diagram of Fig 37. In the photograph of Fig. 18, the microscope can be seen in place, just to the right of the attenuators. The flow metering apparatus was used in connection with the interaction experiments described in Section 6. In the lower righthand corner, the 640-AA microphone can be seen projecting into the tube.

Two loudspeakers, each with their separate amplifiers, were sometimes used instead of one; this was usually done in measurements involving two harmonics. The two speakers, coupled to the left end of the tube, are partially visible in Fig. 18. The black spoked wheel-like object in the right center part of the photograph is an acoustical delay line employed to vary the relative phase between the two harmonic components. This delay line was used only when accurate values of the phase angle different from $\pm \pi/2$ were required as was the case for the results reported in Section 4.

In most of the experiment the relative phase of the second harmonic was adjusted so that $\phi = \pm \pi/2$; this was done by a convenient electronic phase shifting circuit due to Baruch⁽³³⁾. The schematic diagrams of the electronic phase control apparatus, and two of the frequency doubler circuits used are given in Figs. 38a, b, and c. The electronic doubler and phase shifter were incorporated on a single chassis. The crystal doubler was connected directly to the Western Electric 555 which drove the acoustic delay line. All phase adjustments were made with reference to $\phi = \pm \pi/2$; the $\pm \pi/2$ adjustment being obtained with the aid of an oscilloscope which was connected to the output of the microphone. This adjustment was not independent of amplitude; hence it was necessary to make the adjustment whenever the amplitude of either harmonic component was changed.

The 'maximum' available sound pressure level and the particle displacement amplitude measured for two kinds of loudspeaker units are plotted in Fig. 39. These measurements were made for progressive waves. If these maximum levels are exceeded, a fairly poor wave form is observed on the oscilloscope.

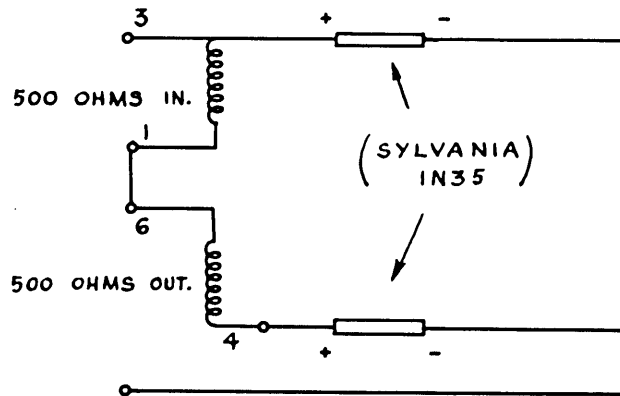
In all experiments the mass reactance of the spheres was sufficient to prevent the sphere from following the oscillatory motion of the medium;⁽¹⁾ this was not so for the supporting fiber.



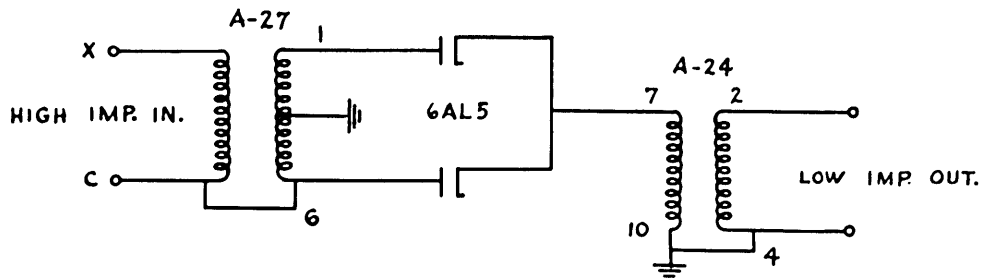
VALUES OF C. FOR FREQUENCIES IN THE RANGE GIVEN

f RANGE	C
70 CPS - 200 CPS	.01 μ f
150 CPS - 400 CPS	.005 μ f
350 - 700 CPS	.002 μ f ←
650 - 1000 CPS	.001 μ f
1000 - 3000 CPS	.0005 μ f ←

(a) PHASE SHIFTER



(b) CRYSTAL DOUBLER



(c) ELECTRONIC DOUBLER

FIG. 38 - SCHEMATIC DIAGRAM OF FREQUENCY DOUBLERS AND THE PHASE SHIFTER.

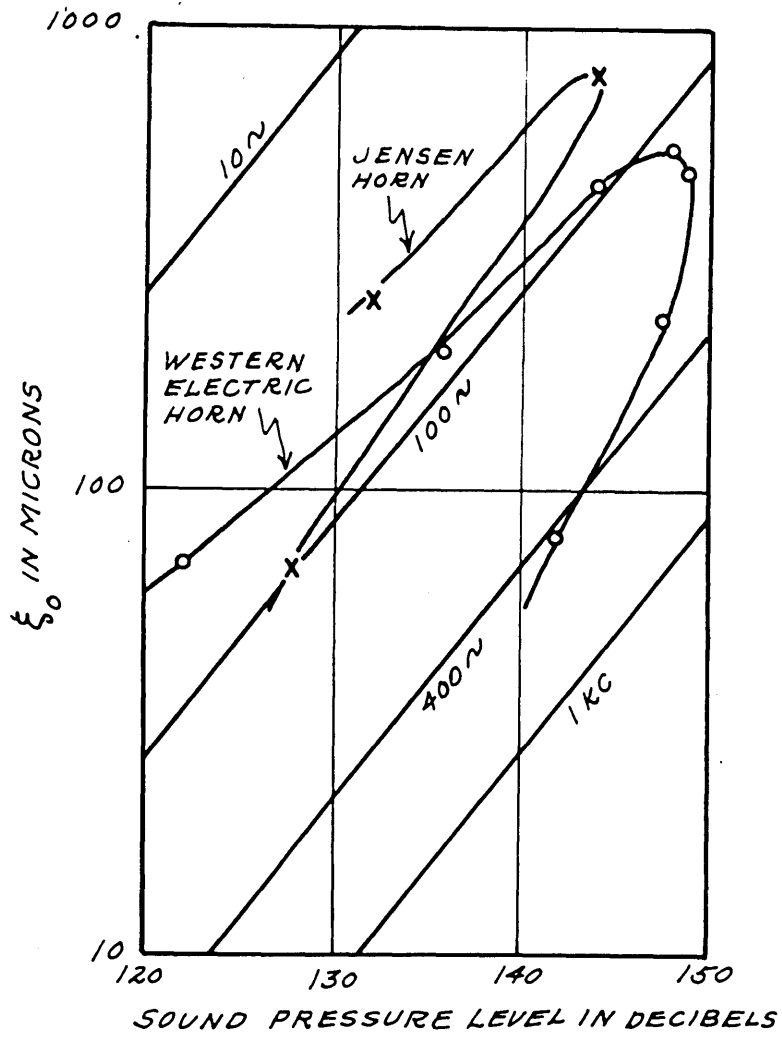


FIG. 39

In computing from the deflection of the pendulum the force exerted on the sphere from the deflection of the pendulum, it was necessary to correct for the weight of the supporting fiber as well as for the force exerted on the fiber by the acoustic wave.

For the measurements in a standing wave, the pendulum was maintained at a fixed distance of cm from the hard termination which replaced the pc cone. It was found necessary to adjust the frequencies slightly of the tube resonance, which reduced the steady circulations in the tube to a point where they did not cause disturbing forces on the pendulum.

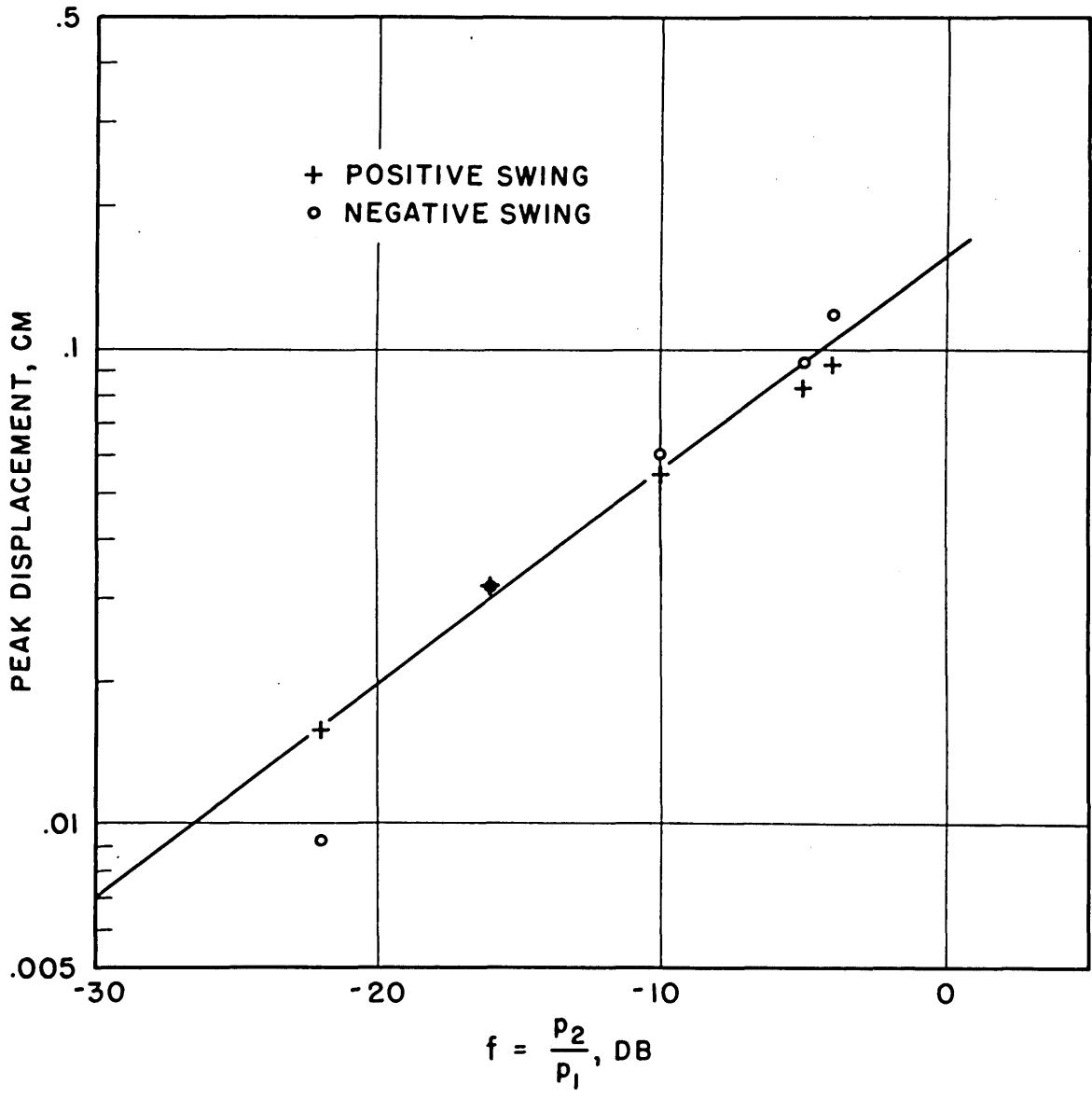
3. Early Experimental Results

The first experiments consisted of qualitative observations on the behavior of a wax sphere 137 microns in radius. The sphere was hung from a nylon strand 3.5 microns long, which had a radius of 7 microns. When the sound consisted of a combination of two tones, one having almost twice the frequency of the other, the sphere would oscillate about its equilibrium position with a period that corresponded to the period of the audible beats between the two tones.

Fine cork particles were introduced into the tube and the typical Kundt's dust figures were observed to form. That is, these cork particles distributed themselves into a series of fine striations, like ribs, across the bottom

of the tube. As described by Wood⁽³⁴⁾ for the case of a standing wave: "This rib-like structure is seen to consist of thin laminae formed of small dust particles in vigorous vibrations". However, for a traveling wave we observed that these ribs progressed slowly in the direction of propagation of the wave. By introducing a second harmonic component, the migration of the rib-like structures could be reversed in direction.

A quantitative measurement was next performed with the pendulum described in the first paragraph of this section. The results⁽³¹⁾ are given in Fig. 40. In this experiment the amplitude of the 400 cps fundamental sound pressure level was maintained constant at 131 decibels. Two oscillators were used and as the phase varies slowly, the particle is observed to oscillate slowly about its equilibrium position. The maximum values of the positive and negative swings are plotted (a positive swing is away from the source) as a function of the harmonic fraction in decibels. The equilibrium position of the particle is very closely the position assumed by the particle in the absence of a sound field; the reason the two positions are not exactly alike is due to the fact that any large amplitude wave is likely to contain second harmonic distortion which will give a 'background force'. The drag coefficient evaluated from these measurements at $f = -4\text{db}$ has been plotted in Fig. 43 as a star. This point lies above the theoretical



EARLY MEASUREMENT OF OSEEN TYPE FORCE

FIG. 40

curve and later experimental data, due to the fact that the force acting on the supporting fiber has been neglected. In analyzing subsequent data, corrections either were applied to account for this fiber force, or else it was ascertained that this force could be neglected in comparison with other experimental uncertainties.

A qualitative experiment was next performed to determine roughly the space dependence of this force along the length of a one-dimensional standing wave. The standing was set up in a transparent plexiglass tube with a hard termination. The phase was adjusted so as to render a force in a direction opposite to that which would be caused by radiation pressure. The pendulum was hung from a small magnet keeper whose position in the tube coincided with the position of an external magnet to which the keeper was attracted. Both the steady deflection of the pendulum from its equilibrium position, and the vibratory amplitude of the fiber were noted. These quantities are plotted in Fig. 41. It is evident that the second harmonic fraction is quite small, since the curve of fiber velocity amplitude shows no evidence of second harmonic distortion.

Other qualitative experiments were made in order to see if free spheres could be supported against gravity. It was found that polystyrene spheres from 5 to 20 microns in diameter could be supported in a field estimated to be of 150 db strength.

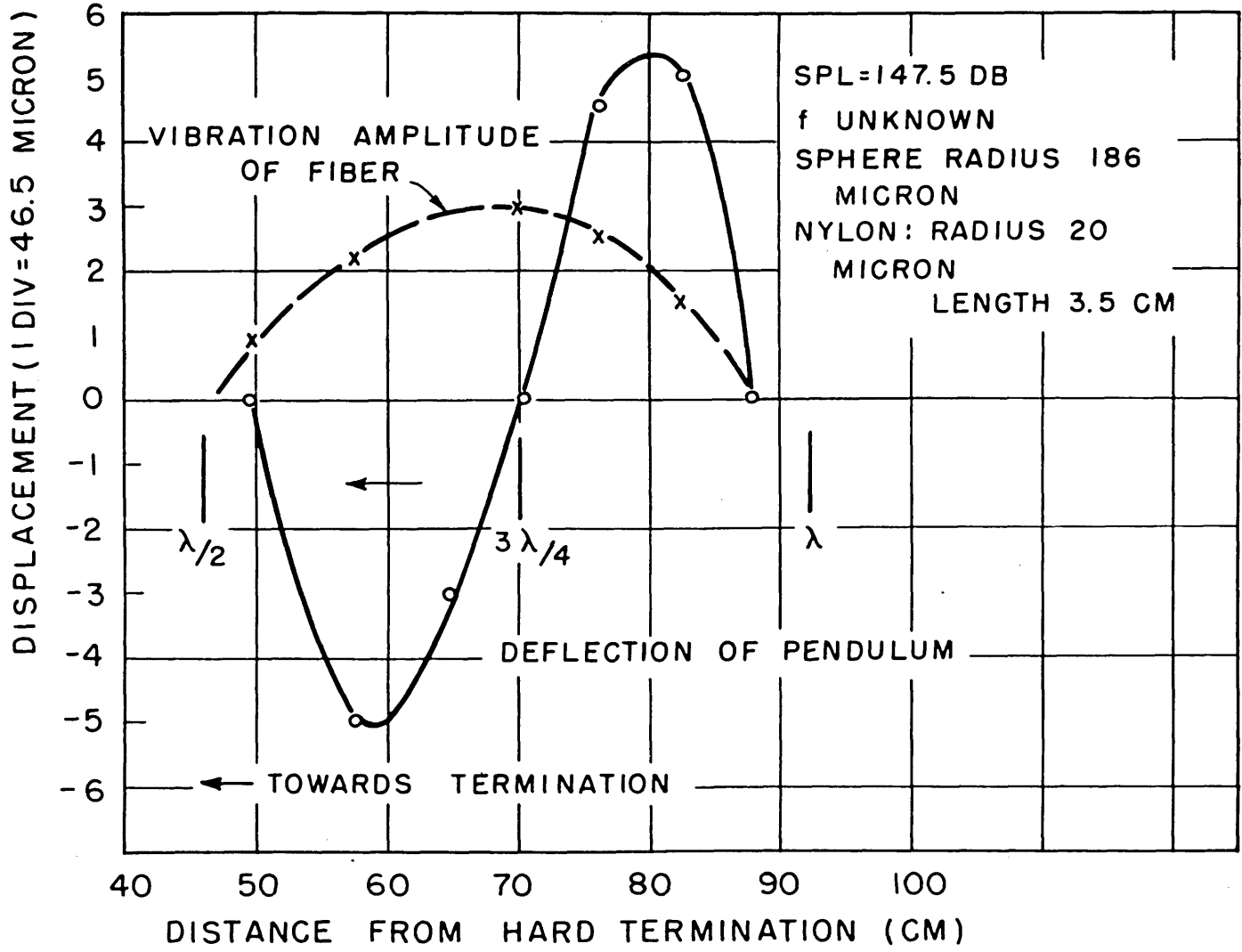


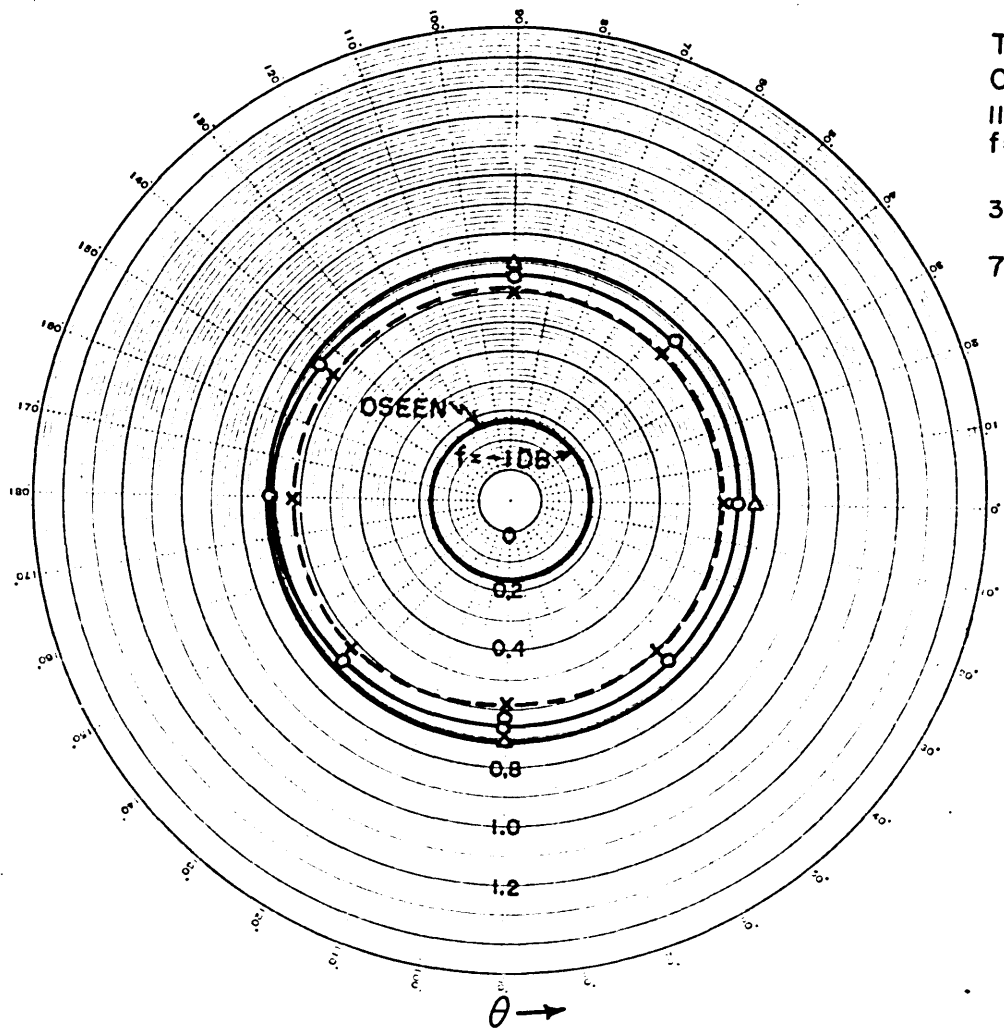
FIG. 41 - DISPLACEMENT OF PENDULUM IN A 375 C.P.S. STATIONARY WAVE.

A series of experiments were performed to determine whether asymmetry in the sphere or in its aspect or mounting influenced the force. The results are shown in Fig. 42, where $-\log|d_3|$ has been plotted for various angular orientations θ of the pendulum. The angle θ is an arbitrary angle of rotation of the supporting fiber about its own axis. It is evident that the force is independent of θ .

4. The Variation of $-\log|d_3|$ with f and ϕ

Detailed measurements were undertaken to determine the dependence of the partial drag coefficient, d_3 , on the fractional harmonic content f and on the phase ϕ . In Fig. 43 the experiments with f as variable are compared with the theory developed in the preceding chapter. The general shape of the experimental curve agrees with theory in having a broad maximum. The experimental maximum however comes at too large a value of f . Furthermore for f values less than -4db, the experimental values appear to be 0.5 greater than the theoretical curve.

As discussed in Section 5, d_3 has been found to vary both with the frequency and with the sound pressure level. In view of this fact the results presented in this section can be considered to constitute fairly good agreement with the simplified theory which does not itself explain why d_3 should vary with either the frequency or the intensity of the wave.



THE POLAR DEPENDENCE
 OF $-\text{LOG}|d_3|$
 112 MICRON ON NYLON FIBER
 $f = -1$

340 \sim , 136 DB (x) $+\pi/2$
 (o) $-\pi/2$
 740 \sim , 129 DB (Δ) $-\pi/2$

$\theta \rightarrow$
 FIG. 42

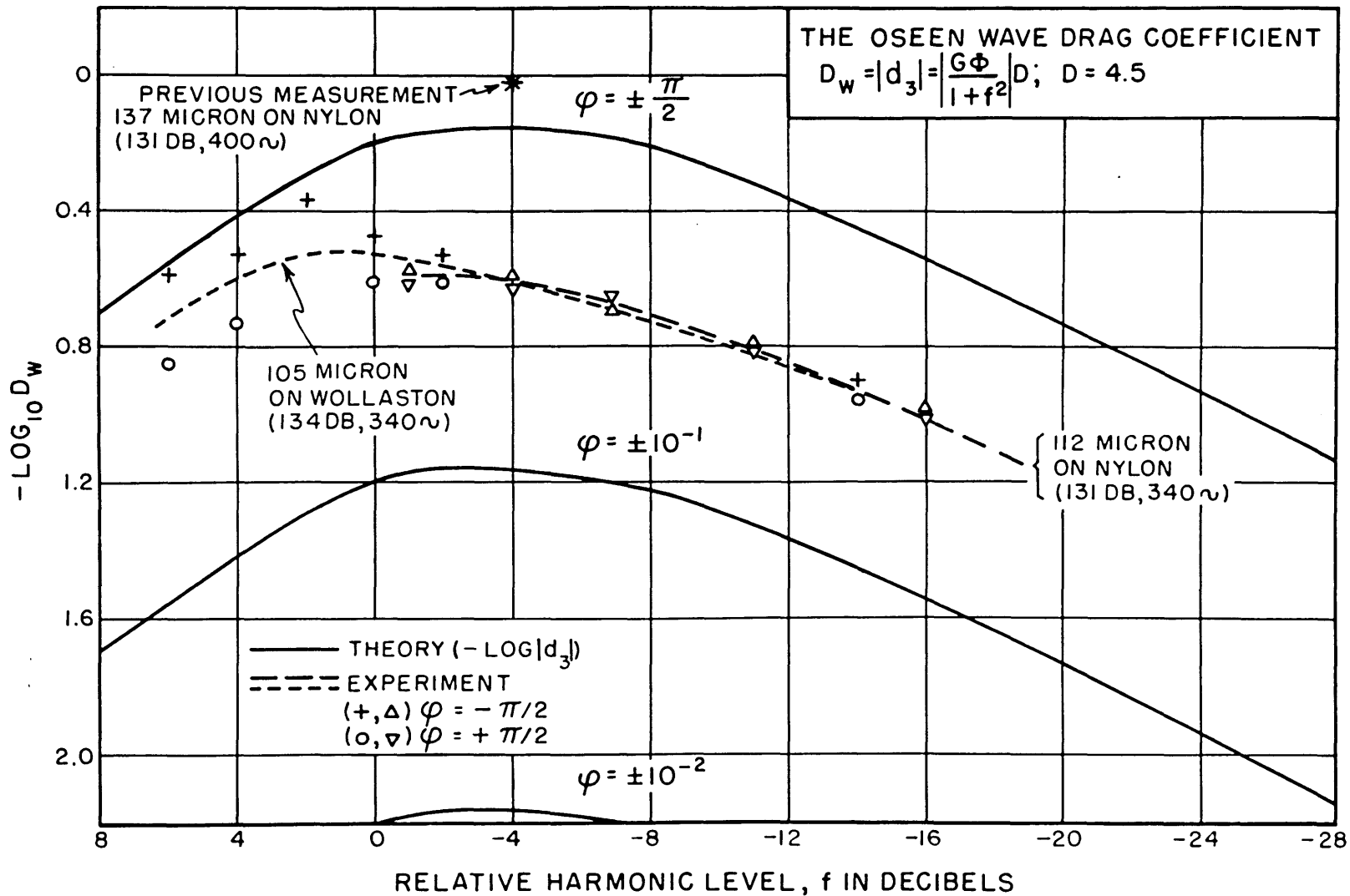
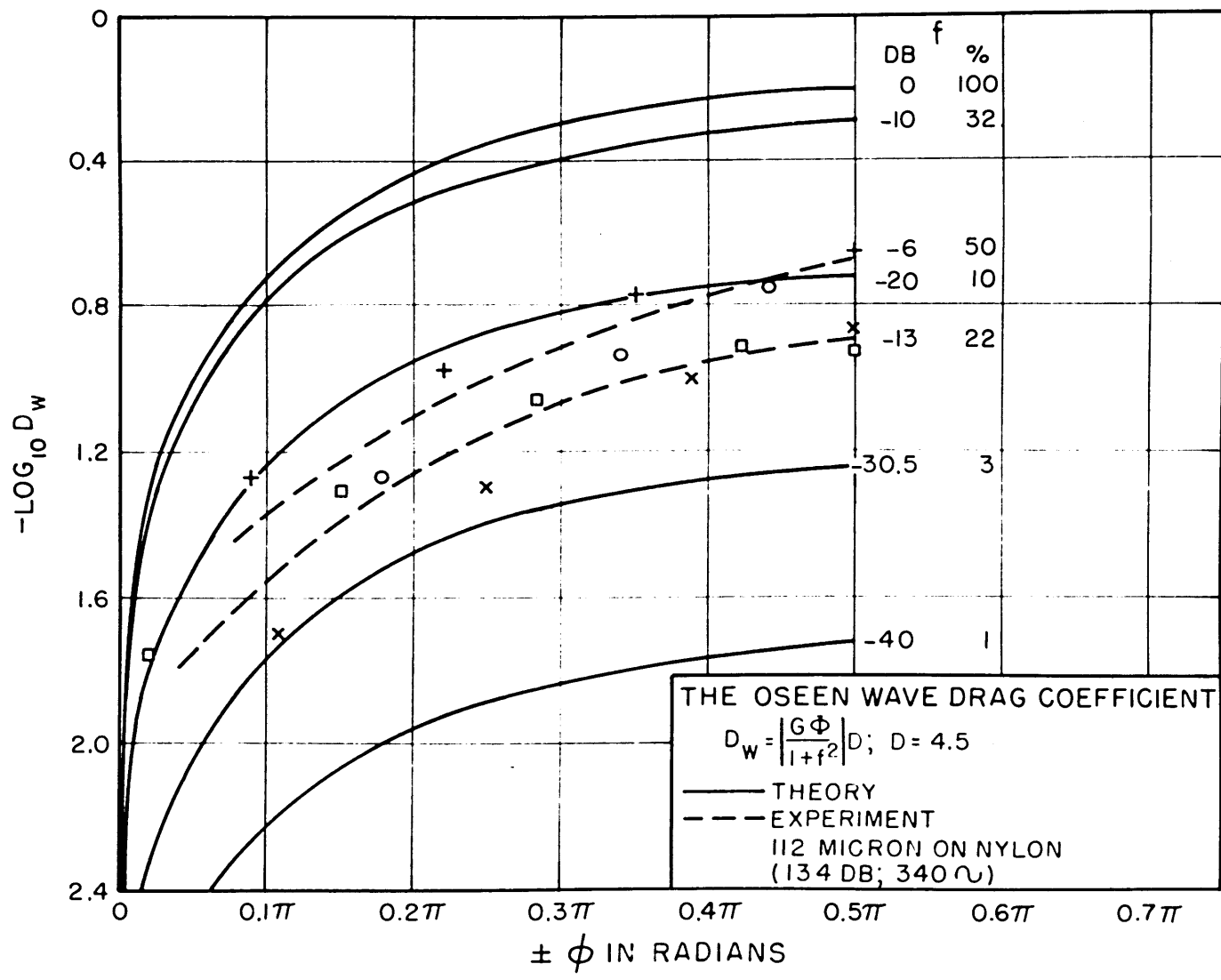


FIG. 43

In Fig. 44 some experimental data are given holding f constant and varying ϕ . Theoretical curves are plotted for varying percentages of the second harmonic distortion. The results of two experiments have been plotted. Data plotted as circles and plus marks were obtained with $f = -6\text{db}$ while the squares and crosses refer to data taken with $f = -13\text{ db}$. The plus and cross marks refer to data obtained with ϕ positive while the circles and squares signify negative phase angles. All the data plotted in Fig. 44 were obtained using a 340 cps fundamental sound pressure level of 134 decibels. As with the previous results these experimental points again show that the measured force is less than that predicted by theory. However, the shape of the experimental curve agrees reasonably well with the theoretical curves.

At this point it is well worth remembering that the scale in Figs. 43 and 44 is considerably expanded compared to the scale in Fig. 35. The complete extent of the abscissa of Figs 43 and 44 corresponds to about two divisions in Fig. 35. We see from this fact that the magnitude of the Oseen-type force will not depend critically on the phase angle ϕ . It is also possible for the Oseen force to be relatively strong even for waves having as low as 1 per cent second harmonic distortion.



THE OSEEN WAVE DRAG COEFFICIENT

$$D_w = \left| \frac{G\phi}{1+f^2} \right| D; D = 4.5$$

——— THEORY
 - - - EXPERIMENT
 112 MICRON ON NYLON
 (134 DB; 340 Ω)

FIG. 44

5. The Wave Drag Coefficient Versus Sound Pressure Level and Frequency

The measurements of the wave drag coefficient discussed in this, and subsequent sections, were taken as a function of the sound pressure level of the fundamental wave component. Three discrete fundamental frequencies were used; the frequencies being generally in the neighborhood of 200, 340, and 600 cps. The measurements involving second harmonic distortion were performed with a constant f of -3 decibels, that is the second harmonic distortion was 71 per cent. The data presented were evaluated by averaging the wave coefficient measured at $\phi = +\pi/a$ with that measured at $\phi = -\pi/2$.

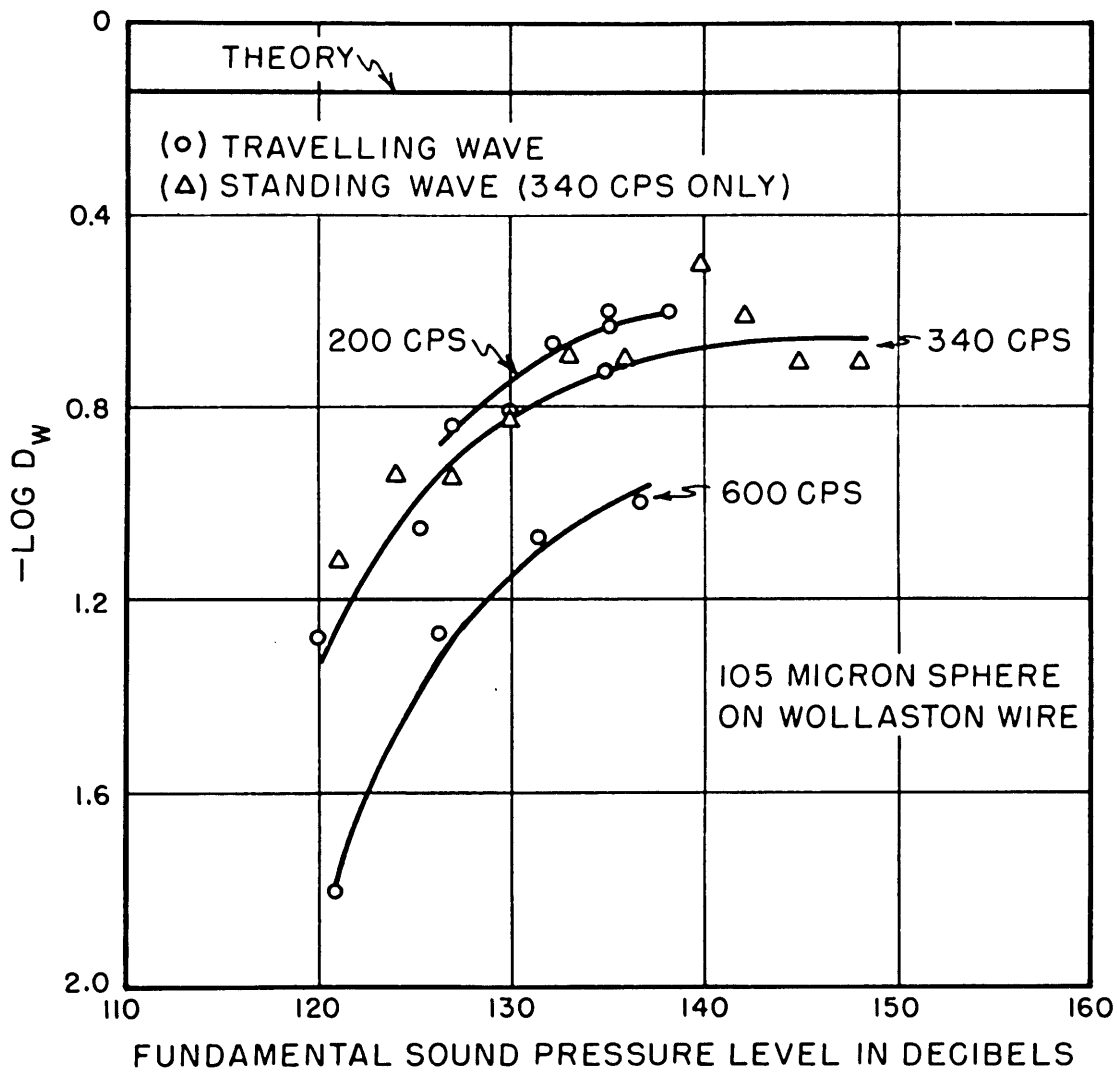
The experiments illustrating the interaction of steady flow with sound, were made by holding the steady flow velocity constant; this means that the flow fraction, f , is a function of the sound pressure level. The theoretical drag coefficient, therefore will be in this case a function of the sound pressure level.

Special attention should be paid to the way in which data obtained in standing waves has been presented. As mentioned in the footnote of Section 2, Chapter V, d_3 is here evaluated for standing waves by dividing the force, not by the energy density but by the local kinetic energy density multiplied by two. Furthermore by sound pressure level we mean the sound pressure level of an equivalent progressive wave which has the same average kinetic energy

density as the standing wave at the position of the object. These conventions permit us to represent on the same figure the measurements obtained in stationary as well as progressive waves.

In Fig. 45 results are given for measurements taken in a progressive wave containing a fundamental and a second harmonic component. The data pertain to a sphere 105 microns in radius supported on a 1 micron diameter platinum Wollaston wire. The results have not been corrected for the fiber force. Such a correction would add about 0.1 to the experimental curves.

A characteristic of these results is that $-\log D_w$ appears to be much greater than theory predicts (force too small) unless the medium displacement amplitude exceeds about 3 sphere diameters; in which case, within the limits imposed by the dynamic range of the experiment, $-\log D$ appears to level off to a value which depends on frequency. This constant value increases with increasing frequency. A linear extrapolation of $-\log D$ to zero frequency gives .45, a value about .3 greater than the theory (drag too small by a factor of 1/2). This extrapolation was made for a sound pressure level of about 140 db. One can estimate from Fig. 56 that a sphere of 105 micron radius in such a sound field, has a peak Reynold's number of about 10. From Fig. 30 it can be seen that the Oseen theory

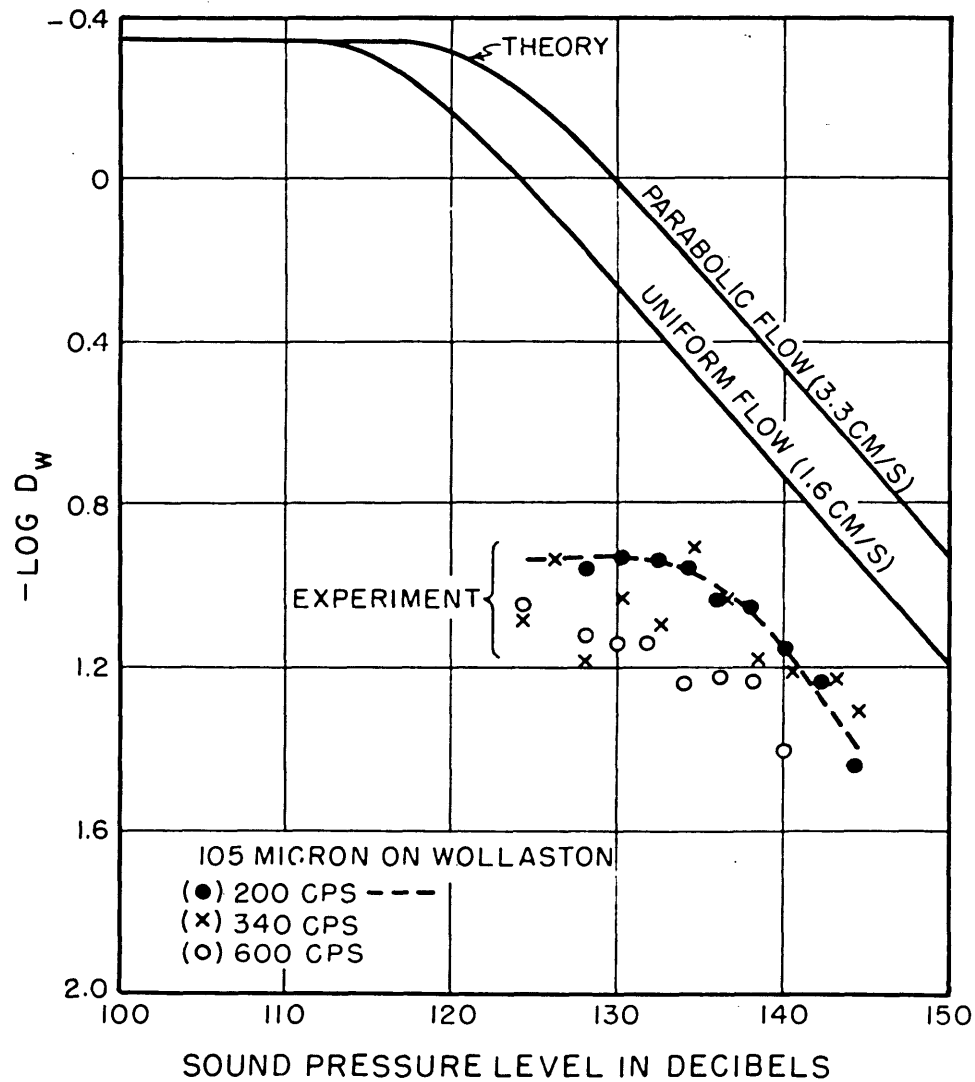


$$-\text{LOG} |d_3| \text{ FOR } f = -3 \text{ DB}$$

FIG. 45

predicts drags at a Reynold's number of 10, which are high by a factor of about 2. Thus, it appears that for sufficiently large particle displacement amplitudes, the zero frequency extrapolation of the average drag coefficient measured in a periodic velocity field is given fairly closely by the theory. The implications of this agreement are discussed in Section 1 of Chapter VII where indirect evidence is presented which suggests that the virtual mass of the sphere is reduced whenever $\xi > d$.

The differential force due to the superposition of a sound wave on a steady flow field has been measured, these results appear in Fig. 46 in terms of the negative logarithm of D_W (which might in this instance be called a differential drag coefficient indicative of the fact that it represents the difference in the force acting with and without sound). Theoretical curves are plotted for uniform and parabolic d-c flow distributions. Notice that the experimental values bear a relation to the theoretical curves which is very similar to that found in Fig. 45. Further results obtained in a stationary wave are given in Fig. 47. A correction for the fiber force cannot be applied to the data of Figs. 46 and 47 unless it is assumed that the same correction is applicable which pertains to the data of Fig. 45. No direct measurement of the differential drag coefficient for the supporting fiber was made.



WAVE DRAG COEFFICIENT
FOR A SIMPLE HARMONIC
WAVE WITH A SUPERPOSED
STEADY FLOW VELOCITY

FIG. 46

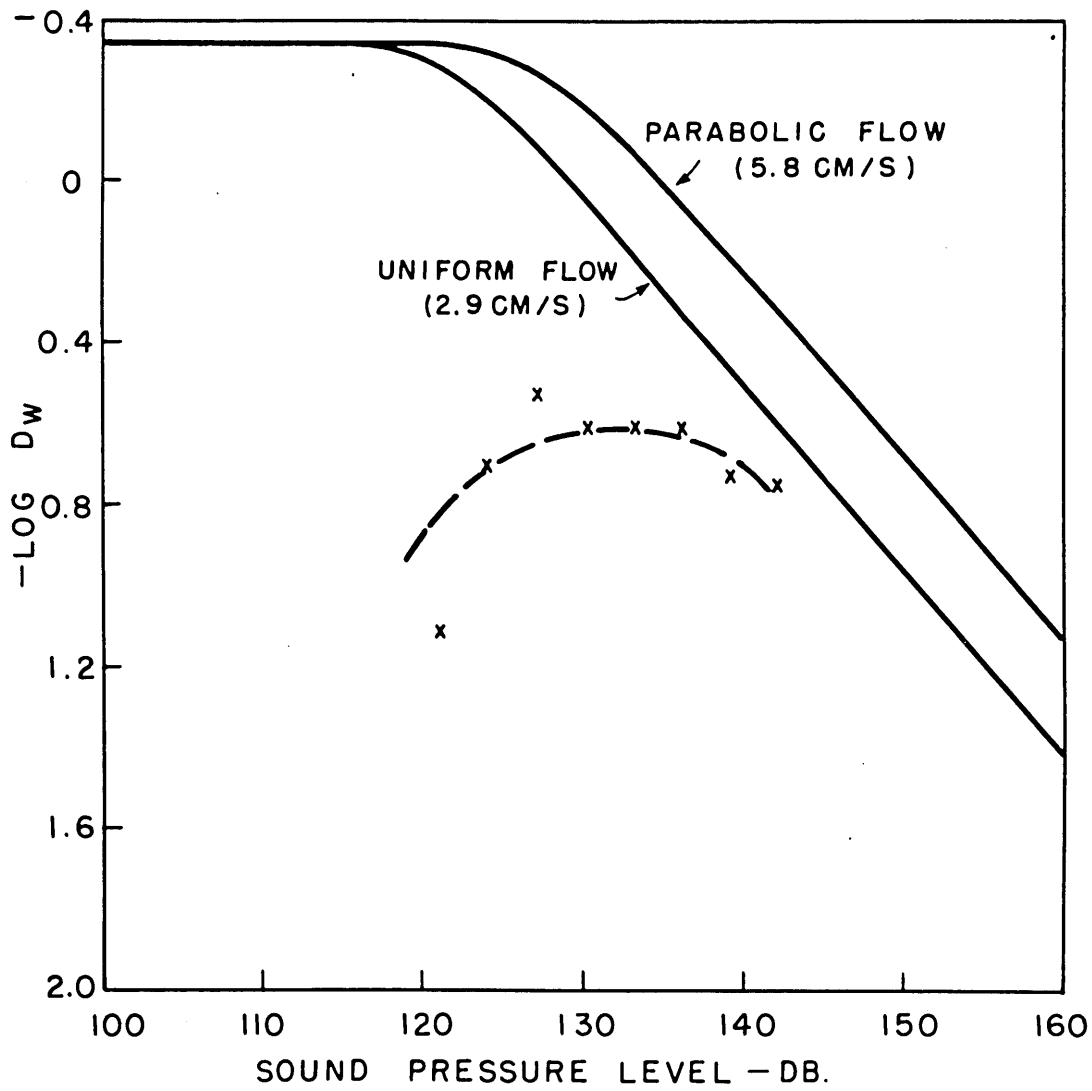


FIG. 47 - D_w IN STANDING WAVE AT 340 C.P.S.

The drag coefficient for the Wollaston Wire suspension was measured for a sound field containing second harmonic distortion ($f = -3\text{db}$). It was necessary to consider the oscillatory motion of the fine wire. The experimental points and the dashed curves in Fig. 48 represent data which have not been corrected for fiber motion. The corrected experimental curves are plotted in solid lines; The corrected curves are more in accord with the results presented previously for spheres than are the uncorrected curves. The nature of the correction for motion of the object is best understood by realizing that the corrected d_3 represents the force per unit average kinetic energy density times two, where the kinetic energy is evaluated in the coordinates of the oscillating wire. The ordinate then corresponds to the sound pressure level of an equivalent progressive wave whose energy density just equals $2T_{av}$. Stated another way, the corrected d_3 is the d_3 that would be measured if the wire were infinitely massive and thus incapable of oscillating with the medium.

Strictly speaking it is necessary to measure both the amplitude and the phase of the fiber oscillations with respect to the medium. Only amplitude was measured, and these results are given in Fig. 50. The correction for fiber motion was based on the assumption that the relative

velocity amplitude of the fiber and medium was equal to the medium velocity amplitude diminished by the fiber velocity amplitude. The validity of this assumption should be determined. Furthermore a curve such as Fig. 50 should be determined for several values of the sound pressure level.

The drag coefficient for a nylon fiber is given in Fig. 49. As can be seen from Fig. 51, the nylon fiber did not vibrate appreciably with the medium, and for this reason no correction was applied to the data of Fig. 49 for fiber motion.

The wave drag coefficient on a cylinder appears not to stabilize until the ratio ξ_0/d reaches roughly 10^2 at which point the peak Reynold's number at 300 cps is about 10^{-2} for the Wollaston wire, and about 2 for the Nylon strand. Thus the observation that the drag coefficient for the Nylon does not approach the theoretical value as closely as it does for the Wollaston wire may be due to the fact illustrated in Fig. 31 that the steady flow theory for cylinder represents reality rather poorly for a Reynold's number greater than one.

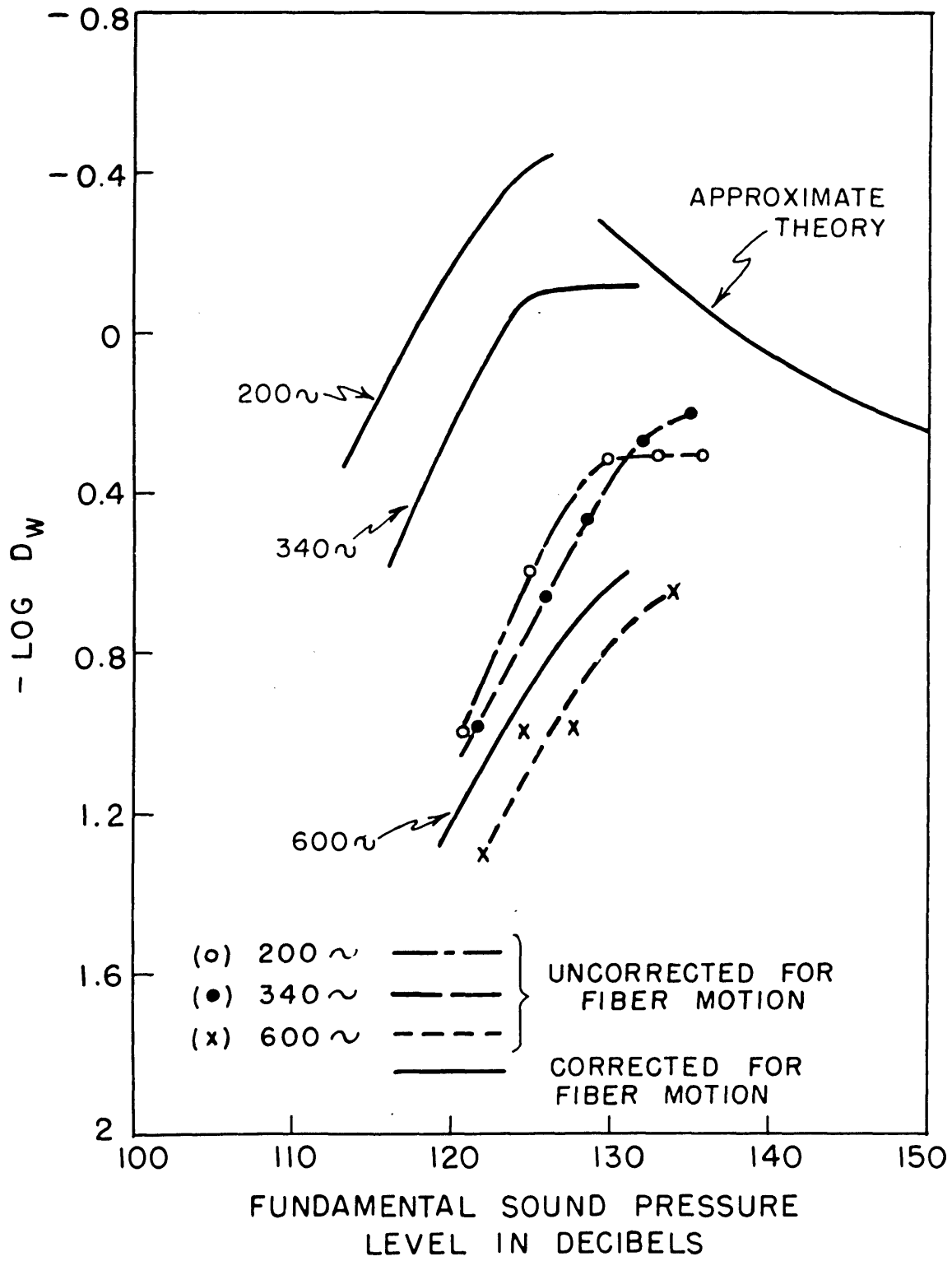


FIG. 48 - DRAG COEFFICIENT FOR 1 MICRON DIAMETER WOLLASTON WIRE

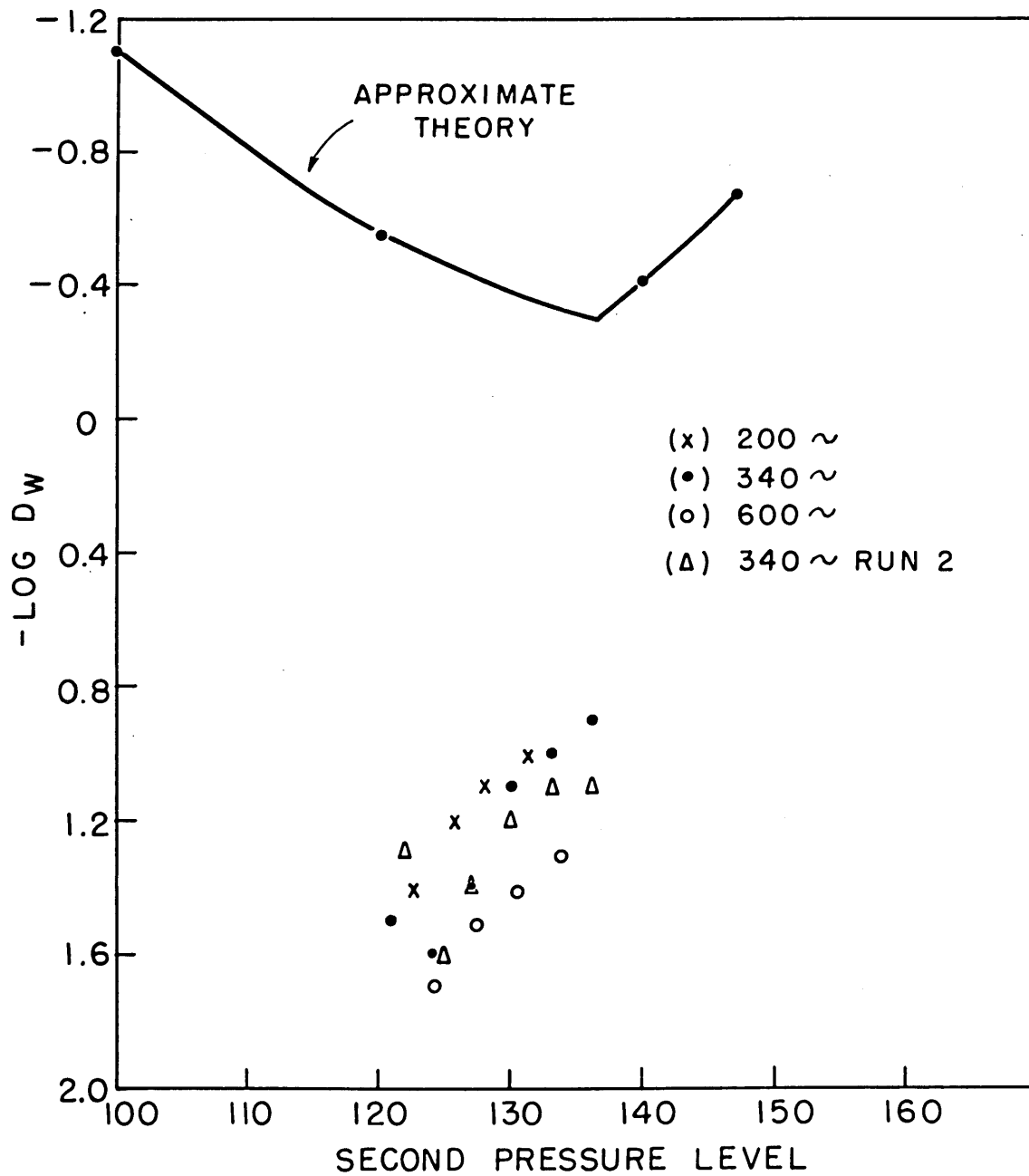


FIG. 49 - DRAG COEFFICIENT FOR 14 MICRON DIAMETER NYLON FIBER (UNCORRECTED FOR FIBER MOTION).

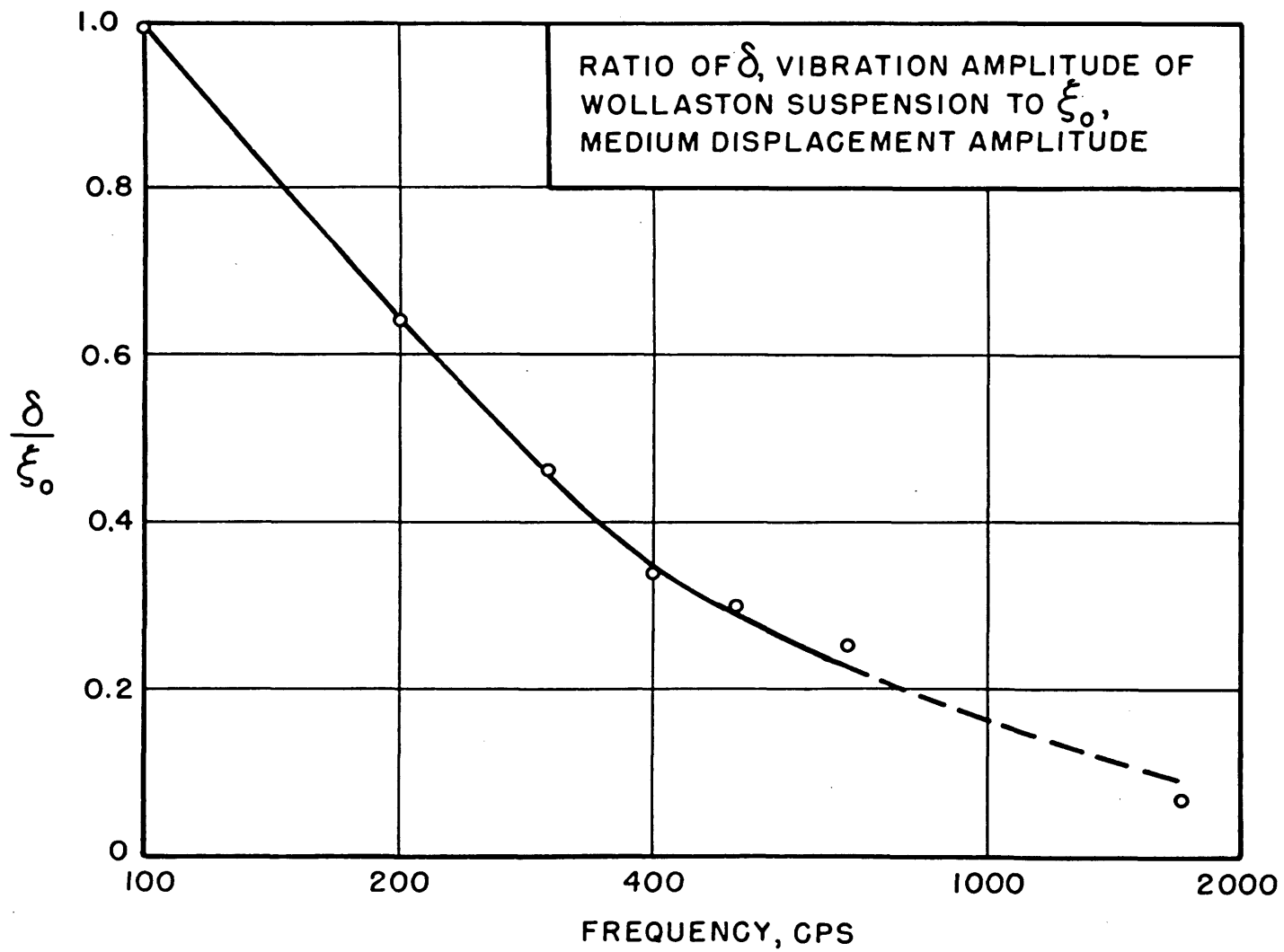


FIG. 50

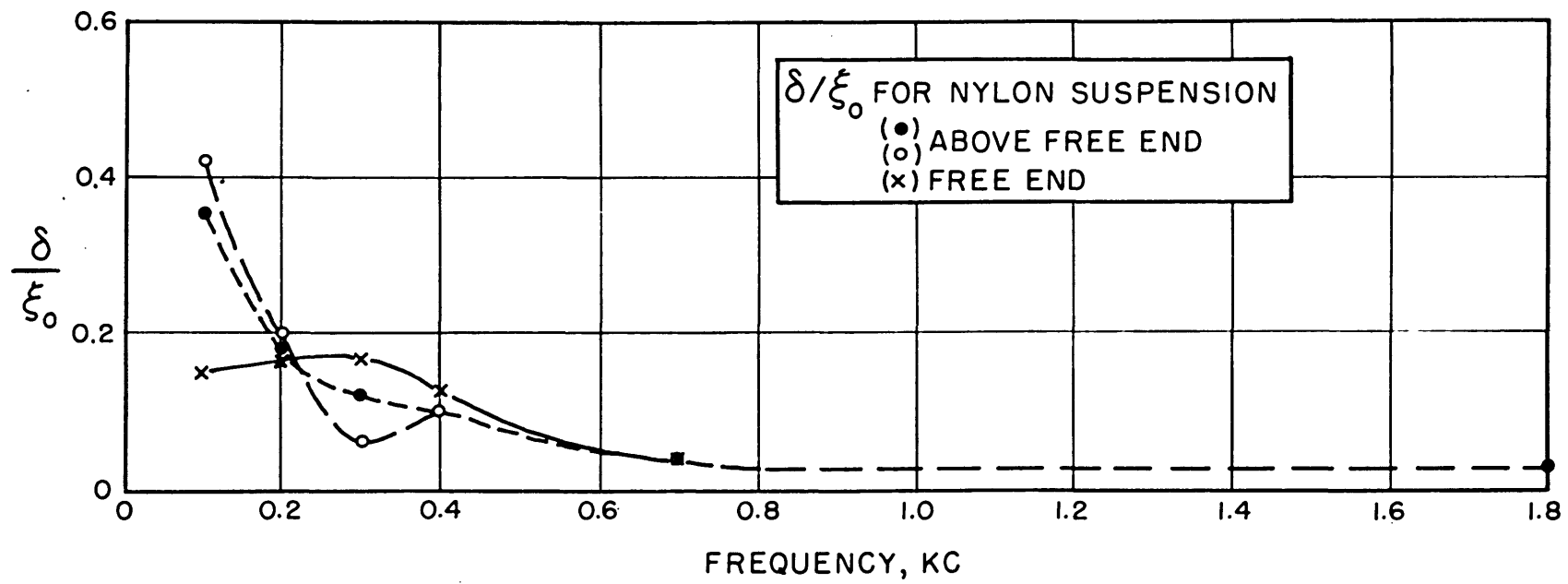


FIG. 51

CHAPTER VII
SIGNIFICANCE OF THE RESULTS

1. The Virtual Mass of an Oscillating Sphere

In this and the following sections we shall draw some conclusions about the oscillating sphere by comparing the non-linear behavior of the sphere with that of the orifice.

In Fig. 52 we have plotted on the same curve quantities proportional to the fractional reduction in the orifice as well as a quantity proportional to the drag coefficient for the sphere. The data are given for experiments carried out both with and without d-c flow velocity. The ordinate is a dimensionless particle displacement parameter obtained by dividing the effective displacement amplitude by the effective length of the object. In the absence of d-c flow the effective displacement amplitude is the amplitude of the fundamental component of the particle displacement. (This definition would need to be modified whenever the second harmonic exceeded the fundamental). When there is steady flow, the effective displacement amplitude is defined either as above, or as the ratio of the average distance travelled by the medium in one period of the wave, depending on which of the two definitions leads to the larger value. The effective length of the

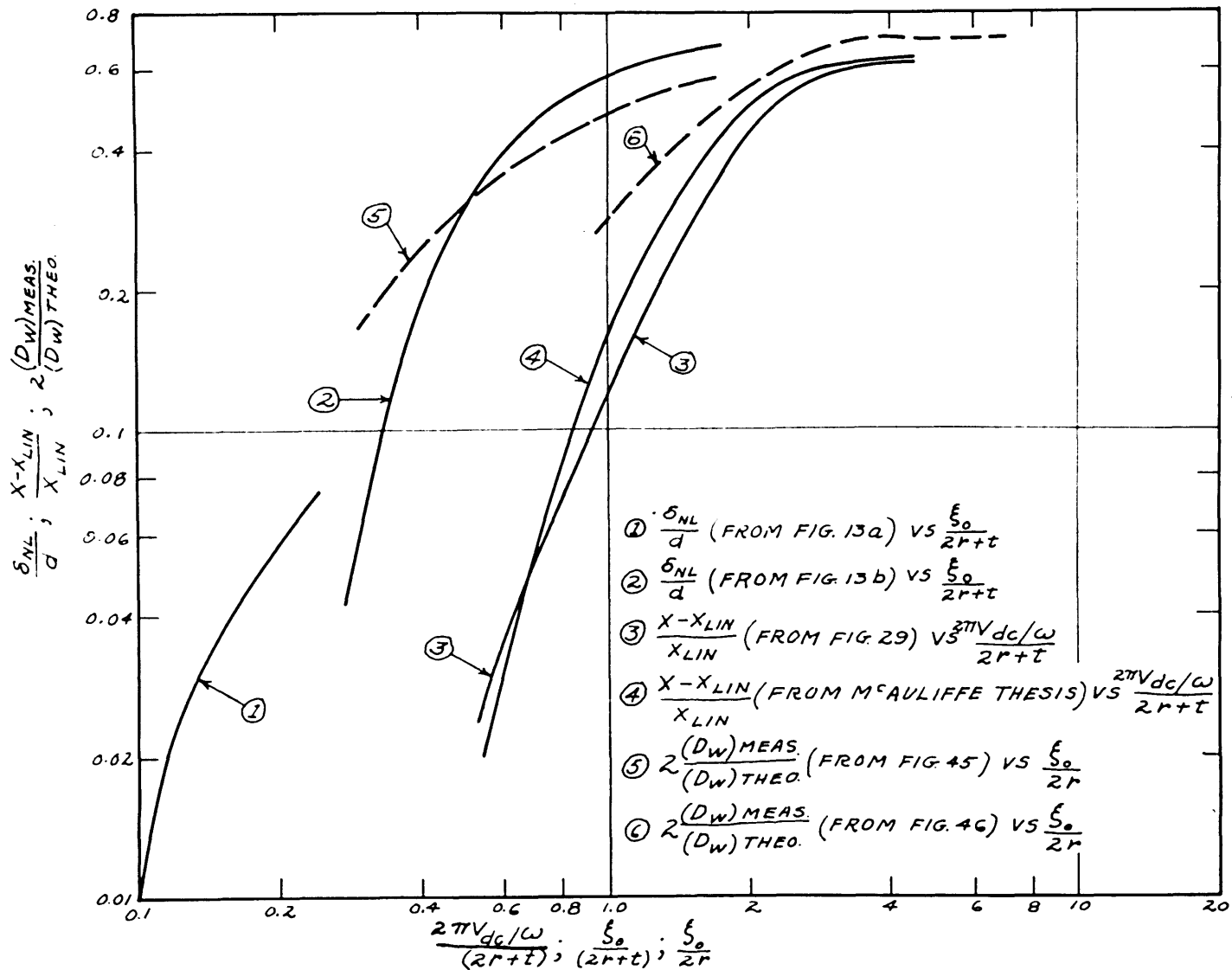


FIG. 52 — A COMPARISON OF THE INCREMENTAL REACTANCE FOR ORIFICES AND THE DRAG COEFFICIENT RATIO FOR SPHERES

orifice is the sum of the diameter and the thickness of the orifice. The effective length of the sphere is its diameter.

The quantities plotted in Fig. 52 are:

$\frac{\delta_{NL}}{d}$, the ratio of the reduction in the orifice mass δ_{NL} expressed as an effective end correction, divided by the diameter of the orifice;

$\frac{X - X_L}{X_L}$, the ratio of the reduction in the orifice reactance, from its linear value X_L , divided by X_L ;

$\frac{(2 D_W)_{\text{meas.}}}{(D_W)_{\text{theo.}}}$, the ratio of twice the measured wave drag coefficient for the sphere divided by the theoretical value for this quantity obtained in Chapter V.

For the rough comparison we wish to make, it is justifiable to consider $\frac{\delta_{NL}}{d}$ and $\frac{X - X_L}{X_L}$ as being a measure of the same quantity.

From the results plotted in Fig. 52 we see that the fractional reduction of the orifice reactance and quantity

$2 \frac{(D_W)_{\text{meas.}}}{(D_W)_{\text{theo.}}}$ for the sphere, vary in a similar way with the

particle displacement parameter. Both these quantities tend to approach a constant value which is reached approximately when the effective particle displacement is the same order of magnitude as the effective dimension of the object.

Since the reactance of the orifice is proportional to its kinetic mass, we see as mentioned in Section 6 of Chapter IV that the kinetic mass of the orifice is considerably reduced at large amplitudes.

We may now ask whether the virtual mass of the sphere is reduced at large amplitudes by the same mechanism which is responsible for reducing the kinetic mass of the orifice. There are two considerations which make this supposition plausible. We first examine ⁽³⁵⁾ the general hydrodynamic equation:

$$\frac{\partial u}{\partial t} + (u \cdot \nabla)u - \nu \nabla^2 u - \frac{1}{3}\nu \nabla(\nabla \cdot u) = -\frac{\nabla p}{\rho} + \overline{F}/\rho \quad (1)$$

where ν is the kinematic viscosity assumed to be constant, ρ is the density, and u the velocity. We assume all body forces, \overline{F} are zero and we assume that the fluid is incompressible; hence

$$\nabla \cdot u \equiv 0$$

and Eq.(1) becomes

$$\frac{\partial u}{\partial t} + (u \cdot \nabla)u + \frac{\nabla p}{\rho} - \nu \nabla^2 u = 0 \quad (2)$$

If the first two terms of Eq.(2) are omitted the remaining equation leads to Stokes' solution when applied to a sphere. The omission of the first term implies the steady state; while the omission of the second term linearizes the equation.

Oseen's extension ⁽²⁵⁾ of Stokes' solution provides

a rough approximation to the time independent solution of Eq.(2). Oseen's solution includes for a sphere the influence of the second order term. No solution in the literature has been found for the oscillatory case which includes the effects of the second order term.

The acceleration forces are represented by the term $\frac{\partial u}{\partial t}$. This term is also responsible for the radiation reactance of an oscillating sphere from Eq.(7) of Chapter III.

If it is true that at large amplitudes of oscillation the radiation reactance of the sphere is diminished (just as for the orifice,) one would conclude that the influence of the local acceleration term, $\frac{\partial u}{\partial t}$ had diminished correspondingly. Thus a treatment which neglected altogether the local acceleration forces, might be expected to agree approximately with experiments performed at large amplitudes, even though such a treatment represented poorly the results of experiments performed at low amplitudes. We have seen that the experimental results discussed in Chapter V bear out this point of view.

It is possible to apply the coherence criterion of Section 6 of Chapter IV to the virtual mass of the sphere. The kinetic mass of a sphere which is small compared with the wavelength, is $1/2$ mass of the fluid displaced by the sphere. This mass is for the most part concentrated in the vicinity of the sphere. When the particle displacement amplitude approaches the diameter

of the sphere, it is reasonable to assume that the coherence of this mass will be diminished. For flows having a low peak Reynold's number the reduction in the mass results from the irreversible nature of Oseen's solution. The wake formed periodically on either side of the sphere plays a role similar to the jet in the case of the orifice. The kinetic mass in the region of the wake will be diminished. Just as with the jet, the coherent reaction of the fluid which is undisturbed by the wake can be considered to take place across the free boundary separating the wake from the rest of the fluid; for this reason the radiation reactance of the sphere should not vanish completely as the particle displacement amplitude increases at least not until compressibility effects become important.

2. The Non-Linear and Differential Absorption Cross-Section of a Small Sphere

In addition to the usual viscous and thermal boundary losses, other losses at the sphere will occur either at large acoustic amplitudes (non-linear absorption) or at small amplitudes provided the sphere drifts through the medium (differential absorption).

By methods analogous to those employed to ascertain the non-linear losses in orifices, we find that the non-linear absorption cross-section for a sphere, based on the

Oseen force, is

$$\sigma_{NL} = 9a^2 u_0 / c \quad (3)$$

In the above formula a is the radius of the sphere, u_0 the particle velocity amplitude of the wave and c the velocity of sound.

The differential absorption cross-section for steady flow in the same direction as the wave vector, is

$$\sigma_D = 14.1 r^2 u_{dc} / c \quad (4)$$

provided the drift velocity exceeds the alternating velocity amplitude. The differential cross-section is proportional to the ratio of the drift velocity u_{dc} to the sonic velocity.

Now it must be emphasized that Eqs.(3) and (4) are based on Oseen's theory and we have seen that the application of this theory to periodic flows is approximately valid only for low frequencies and for large particle displacements. In the absence of direct measurements a better approximation to σ_{NL} and σ_D might be based on experimentally determined value of the wave drag coefficient. One might modify Eqs: (3) and (4) by multiplying them by the ratio of the experimental value of the wave drag coefficient to its theoretical value.

3. Floating Particles with Sound

The Oseen-type force can be used to support particles against gravity. For this purpose a wave compounded of the

fundamental and second harmonic components can be used. A chart, based on the theory of Chapter V, is given in Fig. 53 which relates the radius of the sphere to the total sound pressure level theoretically required to support the sphere. In actual experiments the sound pressure level would have to be greater for two reasons. First the actual wave drag coefficient at a constant sound pressure level decreases with increasing frequency. Secondly at sufficiently low frequencies the sphere will begin to oscillate with the medium; this has the effect of reducing the sound particle velocity with reference to the sphere and hence the force on the sphere is reduced. From these considerations we see that for a sphere with a specified radius and density, there is at any given sound pressure level an optimum frequency which will maximize the force acting on the particle.

4. Free Fall Velocity in a Sound Field

We expect that the terminal velocity of particles moving under the influence of a steady force will be modified in the presence of a large amplitude sound wave travelling parallel to the steady velocity of the particle. Subject to the same restrictions discussed above in Section 5, we have shown in Figs. 54 and 55 how the terminal velocity would theoretically be reduced in case the oscillating

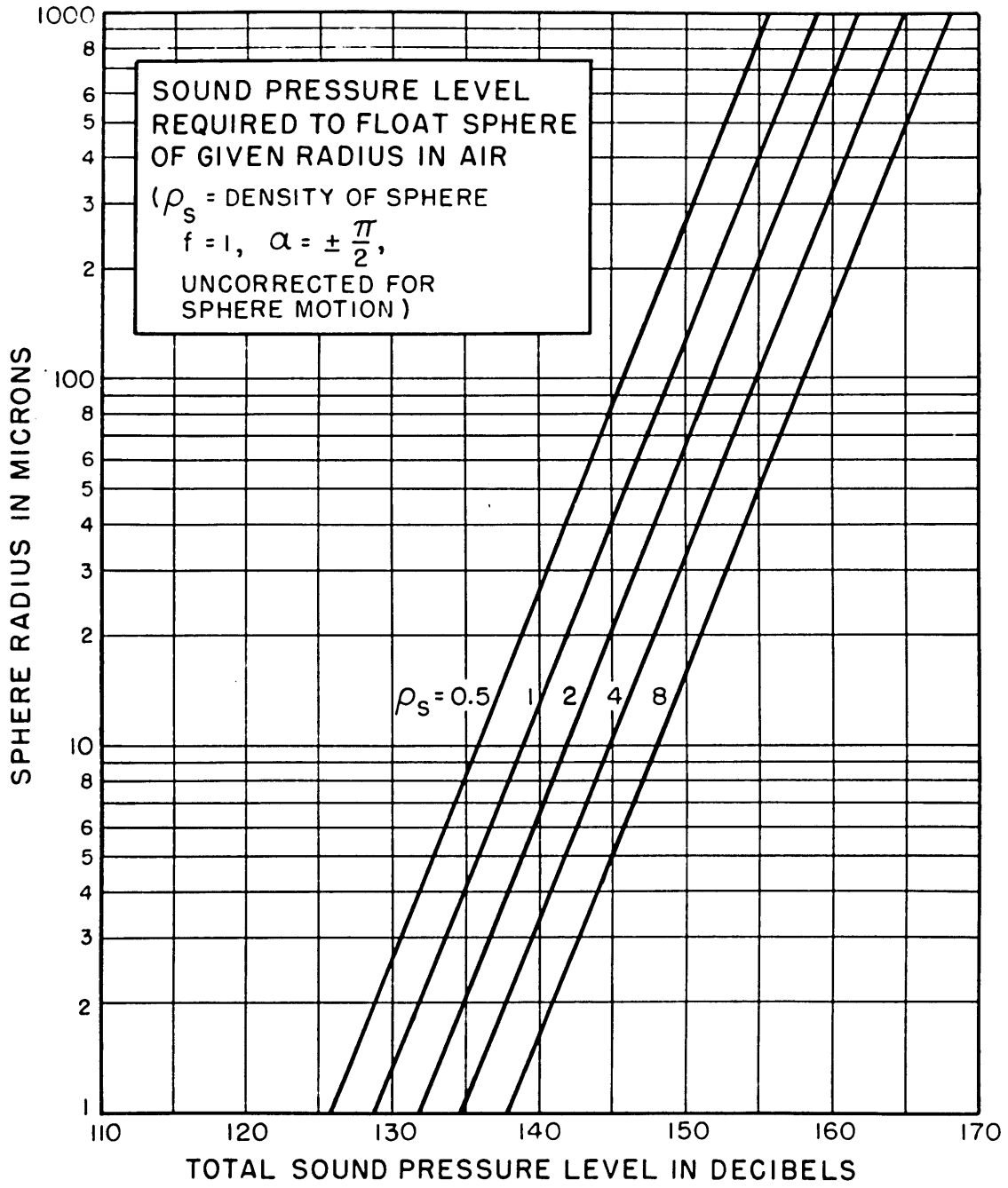


FIG. 53

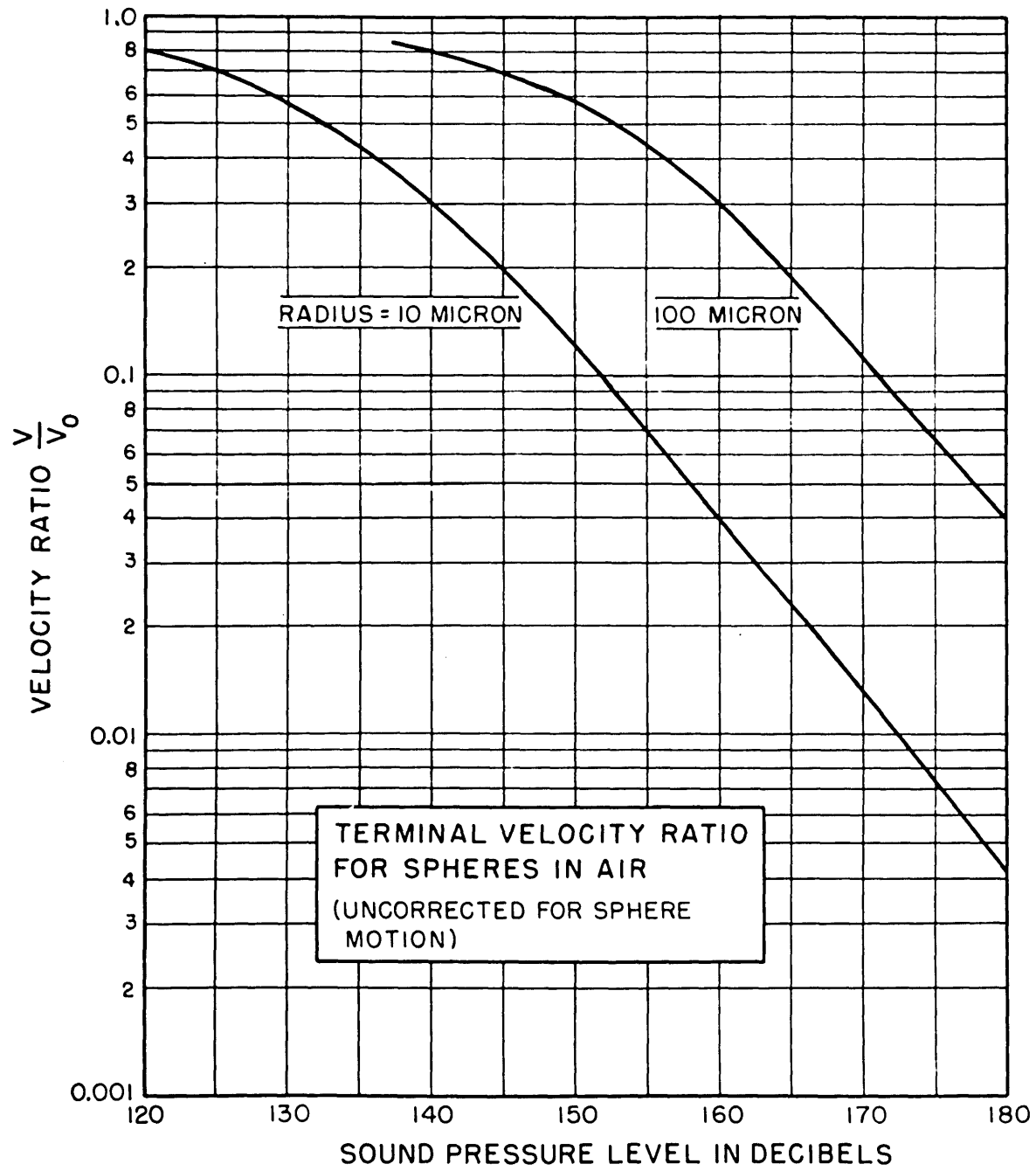


FIG. 54

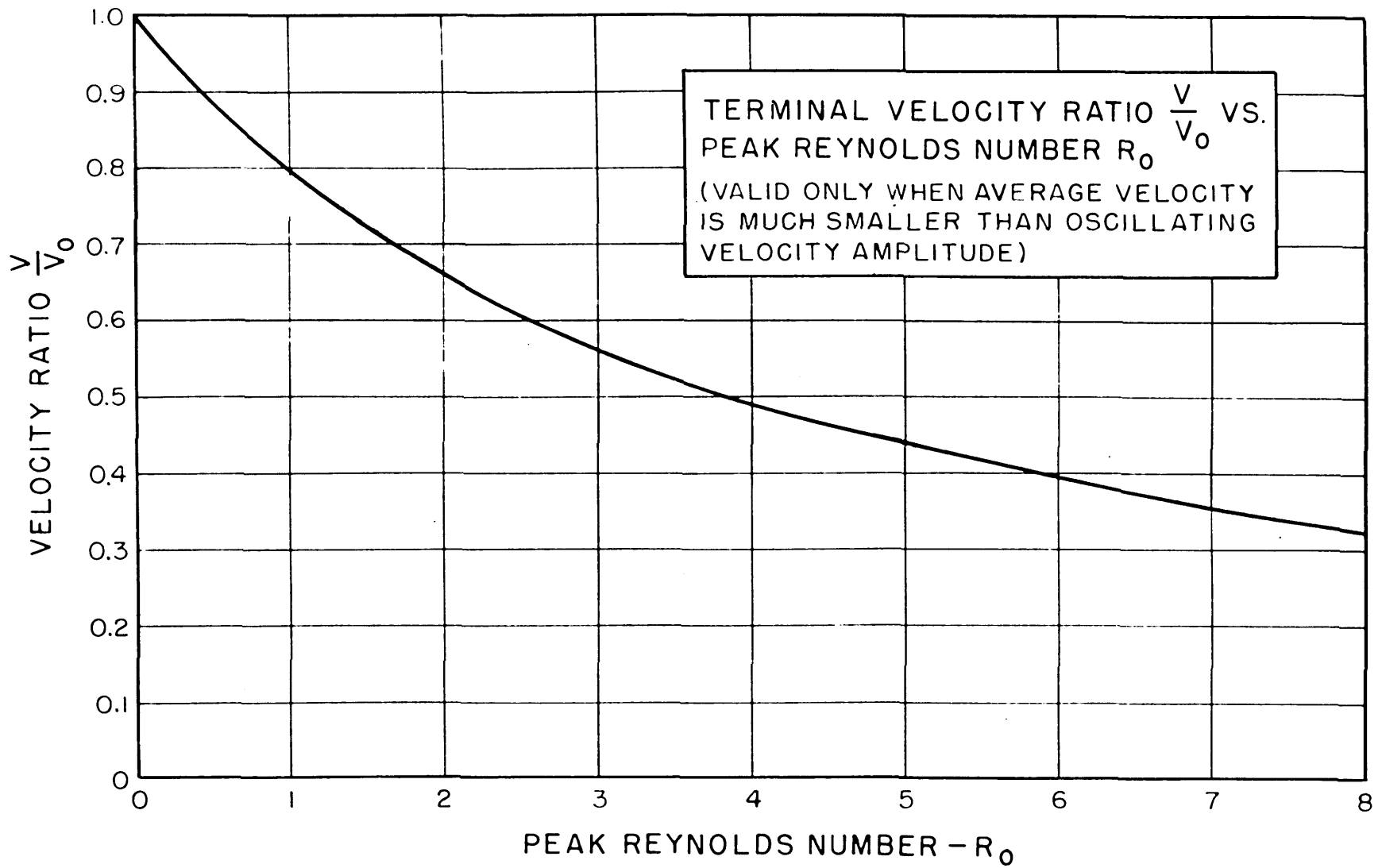


FIG. 55

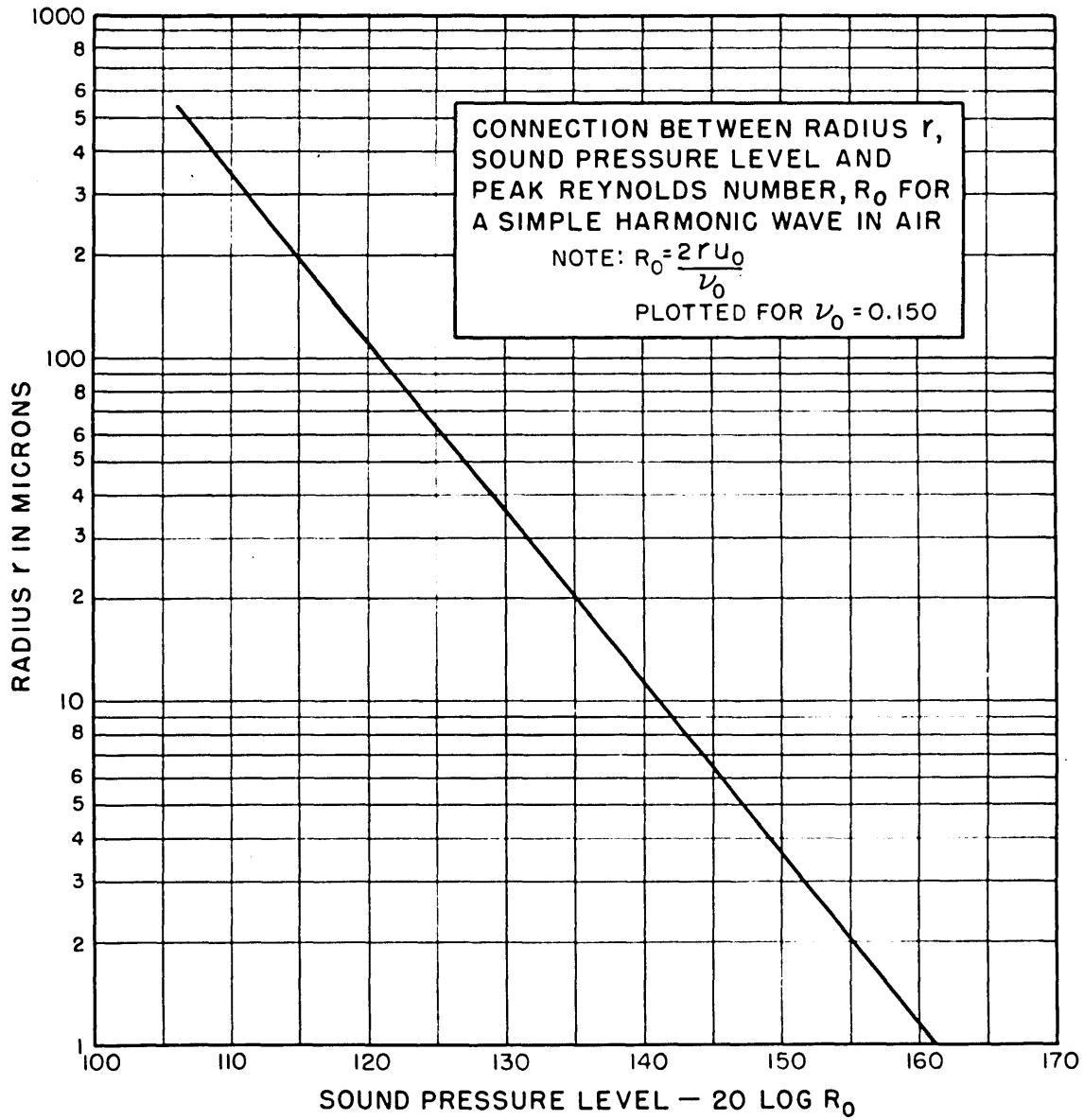


FIG. 56

velocity amplitude were considerably greater than the velocity of free fall. In this instance the wave has been assumed sinusoidal so that the additional retarding force is due to the interaction of the steady flow velocity with the sonic wave. Fig. 56 which is useful in connection with Fig. 55 enables the peak Reynold's number to be found for a sphere in a plane progressive sinusoidal wave

5. Recommendations For Future Work

One of the major results of this work has been the discovery that low frequency sound waves can produce strong forces on small particles. These so-called Oseen-type forces have been measured for a rather restricted range of the variables upon which they depend. It would be valuable to extend the measurements for a wider range of the variables. To accomplish this it would be useful to have sources providing up to 1 kilowatt of acoustical power. The forces generated in a periodic and inhomogenous velocity field could be measured by the techniques we have developed. For this measurement, the sphere could be suspended in a simple harmonic standing wave field. Andrade⁽³⁶⁾ has suggested that steady circulations induced in the vicinity of small objects have a great deal to do with the forces on particles in a standing wave.

The effects of asymmetric wave forms on diffusion

processes in gases and liquids would form an interesting problem for future work. Diffusion across semi-permeable membranes might be influenced by wave forms having a square root type moment.

Controlled experiments should be carried out to ascertain what part the Oseen-type forces play in the industrially established sonic agglomeration process.

APPENDIX I

A DERIVATION OF NON-LINEAR RESISTANCE FOR THE ORIFICE

The pressure, p , and the volume velocity, Q , being related as in $p = KQ^2$, we wish to show that if p varies sinusoidally, the non-linear resistance is $R_{NL} \approx KQ_0$. Here Q_0 stands for the peak volume velocity amplitude through the orifice.

If $p = P_0 \sin \omega t$, the magnitude of Q is

$$|Q| = K^{-1/2} \sqrt{P_0 |\sin \omega t|}$$

The instantaneous power is

$$\mathcal{P} = pQ = K^{-1/2} P_0^{3/2} |\sin^{3/2} \omega t|$$

from which the average power is obtained

$$\begin{aligned} \bar{\mathcal{P}} &= \frac{1}{T} \int_0^T \mathcal{P} dt = \frac{K^{-1/2} P_0^{3/2}}{\pi} B(5/4, 1/2) \\ &= \frac{KQ_0^3}{\pi} B(5/4, 1/2) \end{aligned}$$

The B function is expressible in terms of the Γ functions

$$B(5/4, 1/2) = \frac{\Gamma(5/4) \Gamma(1/2)}{\Gamma(5/4 + 1/2)} = 1.748$$

So that the resistance turns out to be

$$R_{NL} = \frac{2\bar{\mathcal{P}}}{Q_0^2} = 1.112 KQ_0 \quad (1)$$

The same result would have been obtained had one computed the fundamental component of Q and then divided by p .

APPENDIX II

ACOUSTICAL IMPEDANCE IN TERMS OF ENERGY FUNCTIONS

The acoustical (analogous) driving point impedance of a lumped acoustical network can be expressed in terms of the Lagrangian and dissipation functions of the system, a well-known procedure in electrical network theory. This approach can easily be extended further to the case of a continuous medium bounded by a surface of arbitrary impedance. The extension for a continuum is obtained by expressing the energy functions in terms of surface and volume integrals. The surface integrals may be interpreted in terms of an infinite number of terminal pairs serving to connect the "volume network" to the "surface network". This procedure facilitates the solution of certain perturbation problems.

For a one-terminal pair network, E is the complex voltage amplitude and I the complex current amplitude at the terminal. In the steady state

$$1/2E^*I = P_{av} + 2j\omega[V_{av} - T_{av}] = P_{av} + jQ_{av}, \quad (1)$$

in which P_{av} is the average power dissipated in the network, and V_{av} is the quadratic form defined on the loop basis:

$$V_{av} = \frac{1}{4\omega^2} \sum_{s,k=1}^l S_{sk} I_s I_k^* \quad (2)$$

Similarly

$$T_{av} = 1/4 \sum_{s,k=1}^l L_{sk} I_s I_k^*$$

$$F_{av} = 1/4 \sum_{s,k=1}^l R_{sk} I_s I_k^* = 1/2 P_{av},$$

where R, L and S are the resistance, inductance, and elastance loop parameter matrices respectively; I_s and I_k are the current amplitudes in the s^{th} and k^{th} loops respectively; Q_{av} is the reactive power supplied by the source. Defined in this manner, T_{av} and V_{av} are, respectively, the average kinetic and potential energy stored in the network.

In network theory, the driving point impedance of the network under discussion is given by (6)

$$Z(j\omega) = \frac{2P_{av} + 4j\omega(T_{av} - V_{av})}{I^2} \quad (3)$$
$$= \left[2P_{av} + 4j\omega(T_{av} - V_{av}) \right]_{I=1}$$

The current I can be identified with the volume velocity Q, and the voltage E with the pressure P at a simple source considered to be the input of an acoustical network. Z now becomes an acoustic impedance. In this analogy R, L and S are replaced by the analogous lumped resistance, mass and compliance.

Two further extensions will be made. The acoustic network is considered as a continuum, enclosed by a boundary with an arbitrary impedance ratio. The coupling of the continuum to the boundary can be effected by an infinite number of properly positioned terminal pairs. These two steps are formally represented by expressing the energy functions in terms of volume and surface integrals. The volume integrals for a dissipationless medium reduce to the volume integral of the time average of the Lagrangian density.

When the medium is isotropic, these integrals are:

$$T_{av}(\text{vol}) = \frac{1}{4\rho\omega^2} \int |\nabla P|^2 d\mathcal{V} \quad (4)$$

$$V_{av}(\text{vol}) = \frac{1}{4\rho c^2} \int |P|^2 d\mathcal{V}$$

By analogy with Eq. 1, the surface integrals result from integrating the complex power flowing into the boundaries:

$$P_{av}(\text{surf}) = 1/2 \operatorname{Re} \left[\int P^* U d\mathcal{S} \right] \quad (5)$$

$$T_{av}(\text{surf}) - V_{av}(\text{surf}) = \frac{-1}{4\omega} \operatorname{Im} \int P^* U d\mathcal{S}$$

where U is the complex particle velocity amplitude.

Eq.(5) can be written in terms of the boundary admittance , since $U = \eta P$:

$$P_{av}(\text{surf}) = 1/2 \operatorname{Re} \int \eta / P^2 d\mathcal{S}$$

$$T_{av}(\text{surf}) - V_{av}(\text{surf}) = \frac{-1}{4\omega} \operatorname{Im} \left[\int \eta |P|^2 d\mathcal{S} \right] \quad (6)$$

or, if η is independent of position,

$$P_{av}(\text{surf}) = 1/2 \operatorname{Re} [\eta] \int |P|^2 d\mathcal{S} \quad (7)$$

$$T_{av}(\text{surf}) - V_{av}(\text{surf}) = \frac{-1}{4\omega} \operatorname{Im} [\eta] \int |P|^2 d\mathcal{S}$$

The acoustic impedance is obtained by substituting $T_{av}(\text{vol}) + T_{av}(\text{surf})$ for T_{av} , $V_{av}(\text{vol}) + V_{av}(\text{surf})$ for V_{av} and $F_{av}(\text{surf})$ for F in Eq. (3).

The extension of this technique for systems that consist of lumped elements in addition to a continuum, or to the coupling of several continuous systems through one or more terminal pairs,

is possible. The above results have been obtained by analogy with a network theorem. A more rigorous development can be obtained from a simple application of Green's theorem.

Simple examples of the technique described above will be used to derive, first, the impedance of a spherically symmetric source and then a correction term for the kinetic energy contained within a hemisphere, leading to an approximate value for the end correction. The correction factor for the radiation mass of an orifice in a tube will also be obtained.

The complex pressure amplitude P due to a source of strength $Q_0 e^{j\omega t}$ is given by

$$P = \frac{j\omega\rho Q_0}{4\pi r} e^{-jkr - \alpha r} \quad (8)$$

where ω is the angular frequency, $k = \omega/c$, r is the distance from the source and ρ the density. The damping term α is introduced (after the fashion of the screening potential in the quantum mechanical treatment of the coulombfield) so that the integrals in Eq.(4) will converge. After performing the integration, α may be allowed to go to zero so that if the integration is carried out over the volume bounded by the source of radius r_0 and some arbitrary radius $R > r_0$ we obtain:

$$T_{av}(vol) = \frac{\rho Q_0^2}{16\pi} \left[k^2(R - r_0) + \frac{1}{r_0} - \frac{1}{R} \right] \quad (9)$$

$$V_{av}(vol) = \frac{\rho Q_0^2}{16\pi} k^2(R - r_0)$$

Obviously if all space outside the source is included, $R \rightarrow \infty$ in the integration and T and V become infinite, although the

difference T-V does not. P_{av} may be obtained from the first Eq.(5) evaluated over any fixed surface enclosing the source; this yields the radiated power.

If Eqs.(9) are introduced into Eq.(3) and $R \rightarrow \infty$, there results an expression for the reactance, X, of a spherical wave emitted by a source of radius r_0 :

$$X = (j\omega\rho)/(4\pi r_0) \quad (10)$$

In considering the radiation from a small piston ($r \ll \lambda$) in an infinite baffle, X will have twice the value given by Eq.(10) plus an additional term due to the kinetic energy of the fluid in the hemispherical cap covering the piston. This additional energy will be

$$1/2\rho 2/3\pi r_0^3 (U')^2 = 1/4\rho 2/3 \frac{bQ_0^2}{\pi r_0} \quad (11)$$

where $(U')^2$ is the space and time average of the square of the velocity with which the particles in the hemisphere move. The weighting constant b can be obtained approximately by averaging the square of the velocity of the piston with that at the surface of the hemisphere. This leads to $b = (1 + 1/4)/2 = 5/8$. Hence the extra kinetic energy becomes $(5\rho Q_0^2)/(48)\pi r_0$ which, inserted into Eq.(3), leads to the correction to the impedance $(5j\omega\rho)/(12\pi r_0)$. The approximate end correction is obtained by adding the above to twice the value given by Eq.(10):

$$X = 11/12 \frac{j\omega\rho}{\pi r_0} = 0.29 j\omega \frac{\rho}{r_0} .$$

This approximate value is 7.4 per cent higher than the classical value.

The approximate correction factor (7), δ , for the radiation mass in a circular tube of radius R_t is obtained by letting $R = R_t$ in Eqs.(9). The ratio of $(T_{av} - V_{av})_{R=R_t}$ to $(T_{av} - V_{av})_{R=\infty}$ gives immediately the low frequency approximation, $\delta = 1 - r_o/R_t$, where r_o is the orifice radius.

APPENDIX III

CALCULATION OF THE OSEEN-TYPE AVERAGE

1. Wave Form Comprising a Fundamental and Second Harmonic Component

We wish to obtain the average value of u^2 , where $u = \sin \omega t - f \cos 2\omega t$. We first find the zeros of u to be the solutions of

$$\cos 2\omega t = \frac{-1}{4f^2} \left[1 \pm \sqrt{1 + 8f^2} \right]$$

where the + sign preceding the radical pertains to the case $f < 1$, and both + and - are required when $f > 1$. We shall only treat the case $f < 1$. In this case the zeros of u in increasing order of ωt are at

$$\omega t_1 = \frac{1}{2} \cos^{-1} \left[\frac{1}{4f^2} (\sqrt{1 + 8f^2} - 1) \right]$$

$$\omega t_2 = \pi - \omega t_1$$

We then obtain readily

$$G = \frac{1}{2\pi} \left[- \int_0^{\omega t_1} u^2 d\omega t + \int_{\omega t_1}^{\omega t_2} u^2 d\omega t - \int_{\omega t_2}^{2\pi} u^2 d\omega t \right]$$

which yield Eq.(21) of Chapter V.

The average value β of $u|u|$ for the more general wave $u = \sin \omega t - f \sin(2\omega t + \phi)$, can be expressed as a product of $G(f)$ and $\phi(\phi)$. The evaluation of ϕ for $f = 1$ is trivial and leads to $\phi = -\sin \phi$. Calculations carried out by the Joint Computing Group show that β can be represented as a product of G and ϕ for any value of $f > 0$ although this has not been demonstrated analytically.

Fund. $\left\{ \begin{matrix} 0^\circ \\ 100\% \end{matrix} \right\} + 2nd \left\{ \begin{matrix} 0^\circ & \text{to} & +135^\circ \\ 5\% & & 100\% \end{matrix} \right\}$

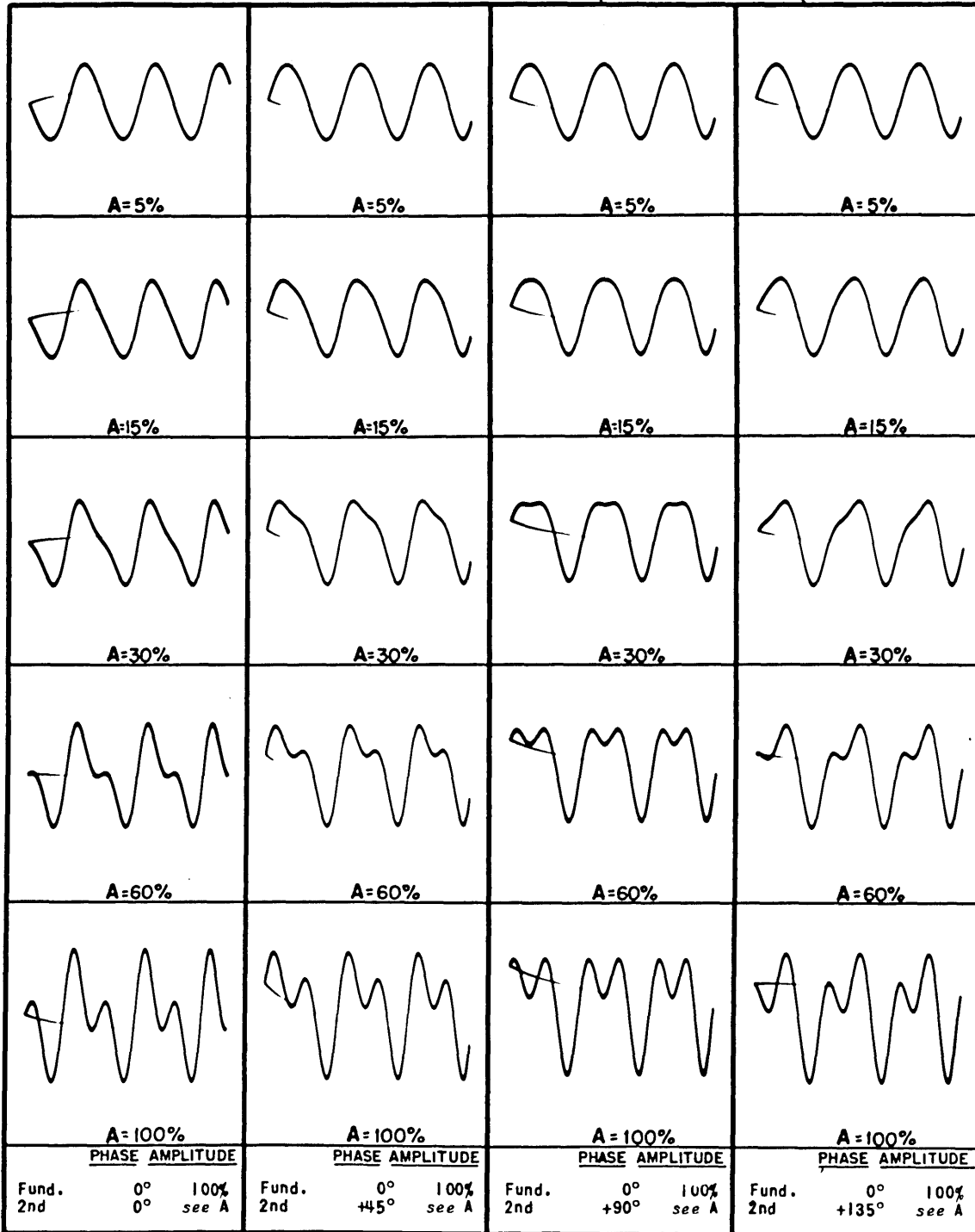


FIG. 57

Fund. $\left\{ \begin{array}{l} 0^\circ \\ 100\% \end{array} \right.$ + 2nd $\left\{ \begin{array}{l} 180^\circ \text{ to } -45^\circ \\ 5\% \text{ to } 100\% \end{array} \right.$

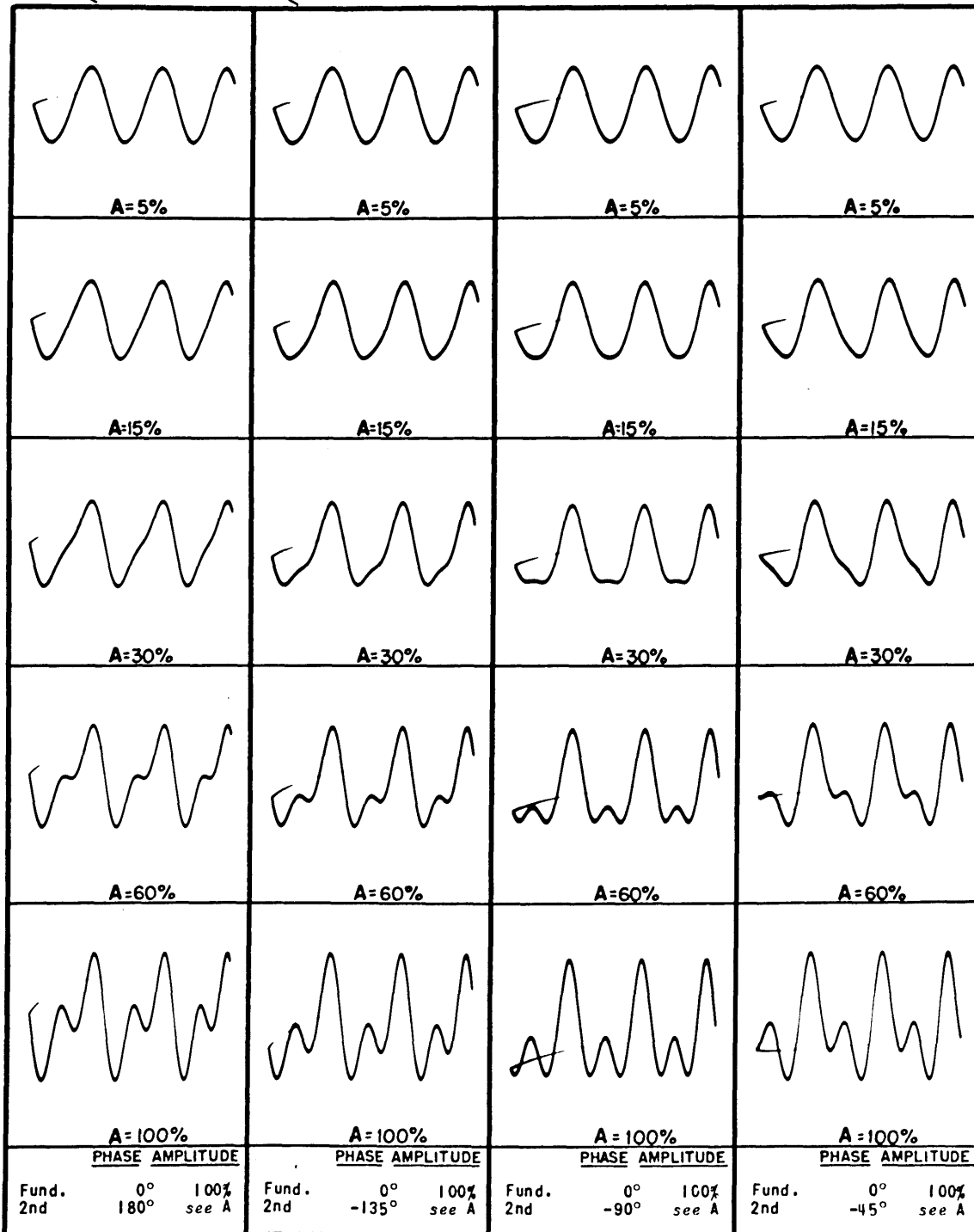


FIG. 58

Fund. $\left\{ \begin{array}{l} 0^\circ \\ 100\% \end{array} \right.$ + 3rd $\left\{ \begin{array}{l} 0^\circ \text{ to } +135^\circ \\ 5\% \text{ to } 100\% \end{array} \right.$

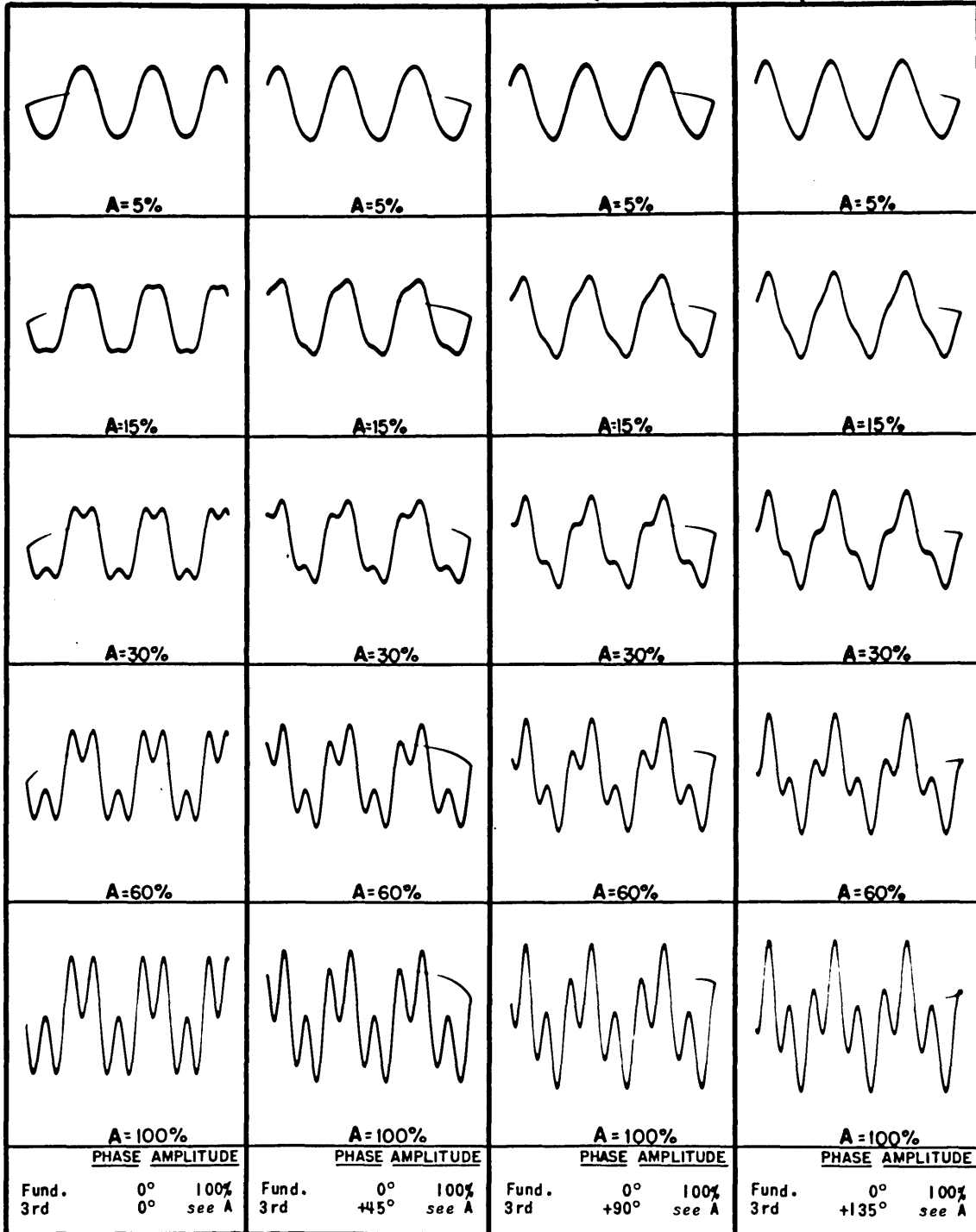


FIG. 59

Fund. $\left\{ \begin{array}{l} 0^\circ \\ 100\% \end{array} \right\} + 3rd \left\{ \begin{array}{l} 180^\circ \text{ to } -45^\circ \\ 5\% \text{ to } 100\% \end{array} \right\}$

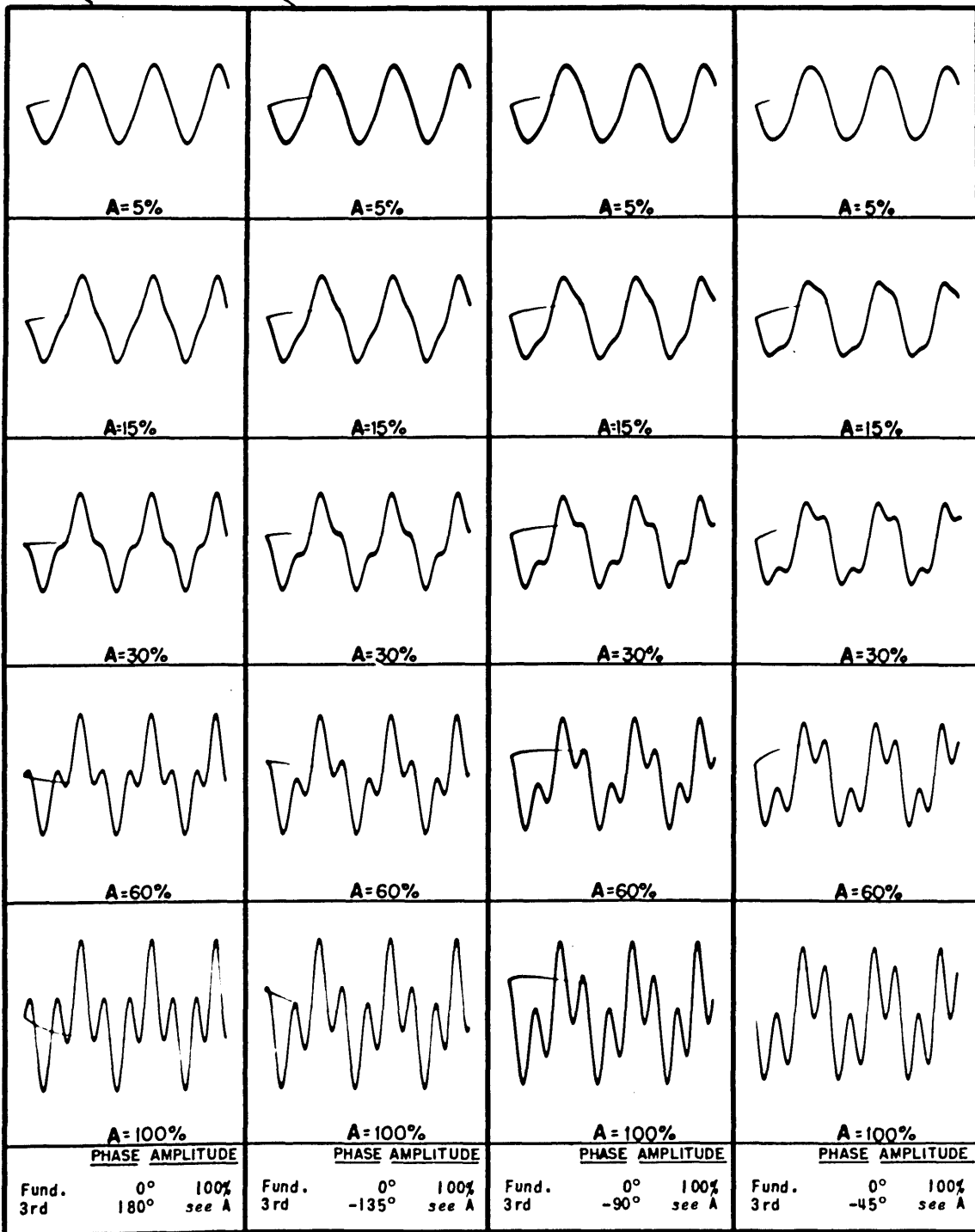


FIG. 60

APPENDIX IV

MAXIMIZING THE OSEEN-TYPE MOMENT

(by Dr. H.G. Baerwald)*

Consider a periodic function $u(x)$, e.g., with period 2π and with zero d-c component: $\bar{u} = \int_{(2\pi)} u dx = 0$. Consider the "power" moment $P = \overline{u^2}$ and "Oseen"-type moment $Q = \overline{|u|}$. We want to make the modulus of the "efficiency ratio" $\eta = \frac{Q}{P}$ maximal. As $\eta(u)$ is odd, we need consider only the case $\eta > 0$. Evidently, $\eta = 0$ and $\eta = 1$ are limiting values. It is also evident that: (1) in $(-\pi, +\pi)$, $\eta = 0$ for $u = \text{odd}$, i.e., only even functions $u(x)$ need be considered; (2) other things being equal, η becomes maximal if, in $(0, \pi)$, $u(x)$ has only one zero x_0 , being, e.g., > 0 for $0 \leq x < x_0$ and < 0 for $x_0 < x \leq \pi$; η will then approach the bound 1 for $x_0 \rightarrow 0$, i.e., if $u(x)$ is of the pulse type at 0, followed by a shallow negative trough. Simplest example, with $P = 1$:

$$u(x) = \begin{cases} \sqrt{\frac{1-\delta}{\delta}} & \text{for } 0 \leq |x| < \delta\pi \\ \sqrt{\frac{\delta}{1+\delta}} & \text{for } \delta\pi < |x| \leq \pi \end{cases} \quad Q = \eta = 1 - 2\delta$$

The present problem is to maximize η if $u(x)$ is composed of a finite number of harmonic components only. It is evident from the preceding that these must all be in phase at $x = 0$. As η is homogeneous of order zero, a common amplitude factor is irrelevant, and we may put

$$u_N(x) = \cos x + \sum_{n=2}^N P_{Nn} \cos nx, \text{ with } P_{Nn} = 0 \text{ for } n > N$$

* The Brush Development Company, Cleveland, Ohio.

The problem is to determine the p_{Nn} such that

$$\eta_N(p_{Nn}) = 1 - \frac{4}{\pi} \left[1 + \sum_2^N p_{Nn}^2 \right]^{-1} \int_{x_N}^{\pi} u^2 dx = \max.$$

x_N being the sole zero of u in $(0, \pi)$. As x_N should be small and, evidently, will be $< \frac{\pi}{2}$ it is apropos to put $x = \frac{\pi}{2} - \xi$, $\cos x = \sin \xi = y$ and $x_N = \frac{\pi}{2} - \psi_N$, $\sin \psi_N = \rho_N$; also to eliminate one of the unknowns p_{Nn} by introducing ψ_N (or ρ_N) into u . For $N \geq 3$, there is then a preliminary algebraic restriction on the possible values of ρ_N and p_{Nn} , namely that all roots of $\frac{u_N(y) - u_N(\rho_N)}{y - \rho_N} = 0$, which is an equation of degree $(N-1)$ only, must either be complex or, if real, absolutely > 1 .

The equation:

$$\left\{ 1 + 2\rho_N p_{N2} - (3 - 4\rho_N^2) p_{N3} - 8\rho_N(1 - \rho_N^2) p_{N4} \dots \right\} + \left\{ p_{2N} + 2\rho_N p_{3N} - 4(1 - \rho_N^2) p_{4N} \dots \right\} 2y + 4(p_{3N} + 2\rho_N p_{4N} \dots) y^2 + 8(p_{4N} \dots) y^3 + \dots = 0$$

with

$$0 = \rho_N + (2\rho_N^2 - 1) p_{2N} + \rho_N(4\rho_N^2 - 3) p_{3N} + (8\rho_N^4 - 8\rho_N^2 + 1) p_{4N} + \dots$$

the case $N = 2$:

$$\text{Here simply } u = \sin \xi - \frac{\sin \psi_2}{\cos 2\psi_2} \cos 2\xi;$$

$$\pi \eta_2 = \frac{\sin 4\psi_2}{\sin^2 \psi_2 + \cos^2 2\psi_2} \cdot (1 + \frac{1}{6} \cos^2 \psi_2) - 2\psi_2$$

$$\text{As } p_{22} = \frac{\sin \psi_2}{\cos 2\psi_2}, \quad 0 \leq \psi_2 \leq \frac{\pi}{6} \quad \text{for } 0 \leq p \leq 1$$

$$\psi_2 = \frac{\pi}{6} \text{ gives } \eta_2 = \frac{9\sqrt{3}}{8\pi} - \frac{1}{3} = .2869 \text{ with } \frac{d\eta_2}{d\psi_2} < 0;$$

$$\psi_2 = \frac{\pi}{8} \text{ gives } \eta_2 = \frac{13\sqrt{2}+1}{6\pi(2\sqrt{2}-1)} - \frac{1}{4} = .3124_5 \text{ with } \frac{d\eta_2}{d\psi_2} > 0;$$

then by successive interpolation:

$$(\psi_2)_{\text{opt}} = .4461 = .2840 \cdot \frac{\pi}{2} \text{ or } (p_{22})_{\text{opt}} = 6873 : (\eta_2)_{\text{max.}} = .3249_2$$

for $N > 2$, one may show that

$$0 < \psi_{N+1} < \psi_N \text{ and } \frac{\cos 2\psi_{N+1}}{\sin \psi_{N+1}} \cdot p_{N+1} < \frac{\cos 2\psi_{2N}}{\sin \psi_N} p_N \leq 1 (= 1 \text{ for } N = 2 \text{ only})$$

Thus we may put

$$u_N = \sin \xi - \frac{\sin \psi_N}{\cos 2\psi_N} (1 - \alpha_N) \cos 2\xi \dots, 1 > \alpha_{N+1} > \alpha_N > 0.$$

The case $N = 3$:

$$u_3 = \sin \xi - (1 - \alpha_3) \frac{\sin \psi_3}{\cos 2\psi_3} \cos 2\xi - \alpha_3 \sin \frac{1 + 2\cos 2\xi}{1 + 2\cos 2\psi_2}$$

then the restrictive algebraic condition is that the roots of

$$y^{-2} + 2 \sin \psi_3 \frac{1 + \frac{2}{1-\alpha_3} \cos 2\psi_3}{1 + 2 \cos 2\psi_3} y^{-1} + \frac{4 \frac{\alpha_3}{1-\alpha_3} \cos 2\psi_3}{1 + 2 \cos 2\psi_3} = 0$$

are either complex or both absolutely > 1 , This means either:

$$\left\{ 1 - \alpha_3 + 2\cos 2\psi_3 \right\}^2 \sin^2 \psi_3 - 4\alpha_3(1-\alpha_3)\cos 2\psi_3(1+2\cos 2\psi_3) < 0$$

or:

$$2 \sin \psi_3 \left| \frac{1 + \frac{1+\alpha_3}{1-\alpha_3} \cos 2\psi_3}{1 + \frac{2}{1-\alpha_3} \cos 2\psi_3} \right|$$

Preliminary inspection leads to the expectation that $\alpha > 1$ and

that though $\psi_3 > \psi_2$, $\psi_3 \neq \frac{\pi}{4}$. With

$$\pi \eta_3 = \frac{\sin 4\psi_3(1+2\cos 2\psi_3)}{30} \cdot R(\cos 2\psi_3, \alpha_3) - 2\psi_3 \text{ with}$$

$$R = \frac{5(1+2\tau_3)(13+\tau_3) - 2(1+27\tau_3 - 4\tau_3^2)a_3 - (63+\tau_3-2\tau_3^2)a_3^2}{(1+2\tau_3)^2 \{ (1-a_3)^2(1-\tau_3) + 2\tau_3^2 \} + 2a_3^2\tau_3}; \tau_3 = \cos 2\psi_3$$

trial and interpolation gives the optimum result:

$$(\psi_3)_{\text{opt}} = .68_7, (\alpha_3)_{\text{opt}} = .75_2, \text{ whence:}$$

$$\underline{(\rho_2)_{\text{opt}} = .80_4}, \underline{(\rho_3)_{\text{opt}} = .54_1}; \text{ then } \underline{(\eta_3)_{\text{max}} = .487^{(+)}}$$

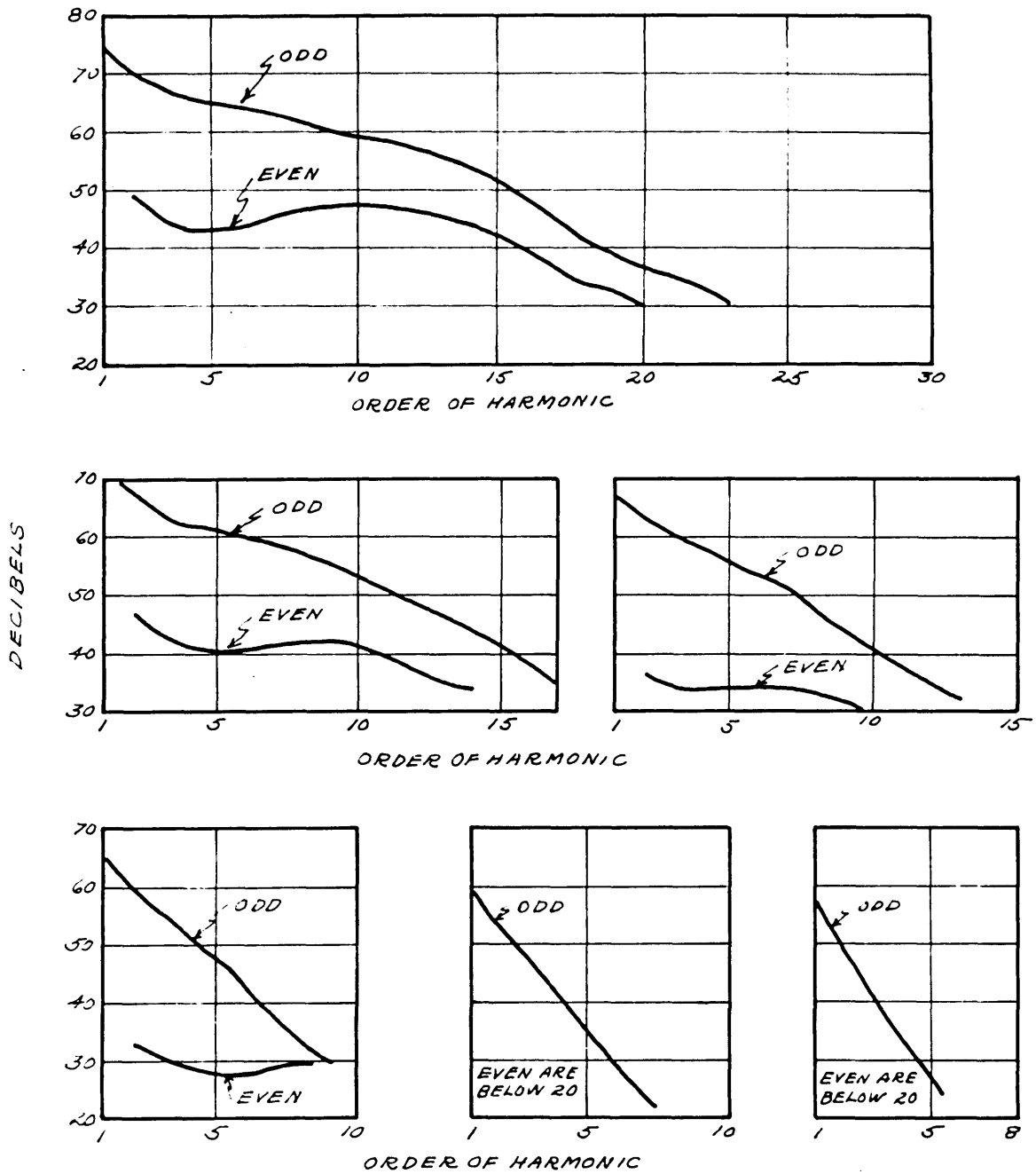
This represents a substantial improvement over $N = 2$. Naturally, η being an extremum, its value is not too sensitive to small deviations of p_{Nn} from their optimum values. No numerical investigation was made for cases $N > 4$. The seemingly plausible approach of approximating the initially introduced \mathcal{J} -function, with optimally adjustable parameter $\mathcal{J}_N = \mathcal{J}(N)$, by u_N via least squares, which would represent a numerically far simpler procedure, practical even for larger N , proves to be unexpectedly weak for $N = 2$ and 3 , i.e., with results rather far off $\eta_N \text{ max.}$, and is therefore not recommended.

APPENDIX V

THE GENERATION OF HARMONICS BY ORIFICES

The results of the harmonic measurements discussed in Section 7 of Chapter IV, appear in the following group of figures. All the measurements but the one represented in Fig. 72 were obtained by driving the orifice at 180 cps.

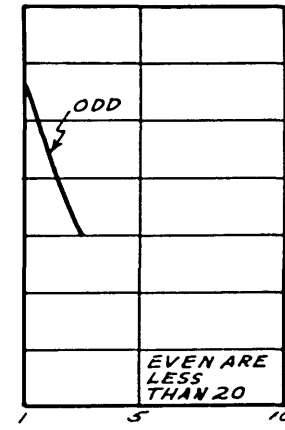
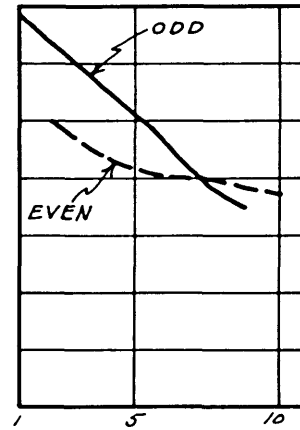
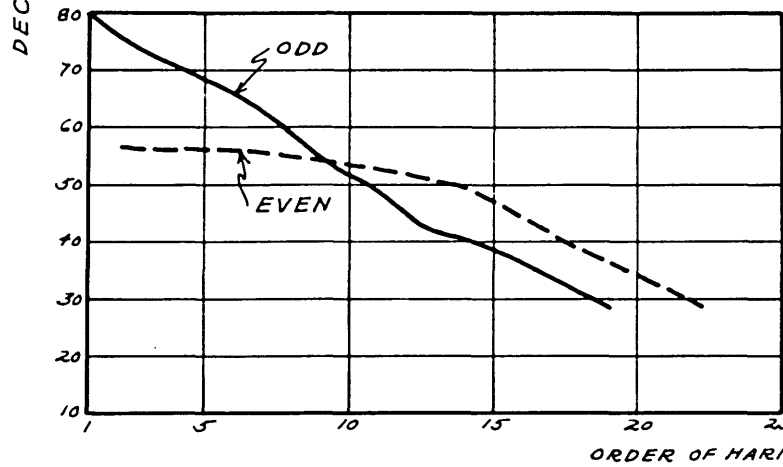
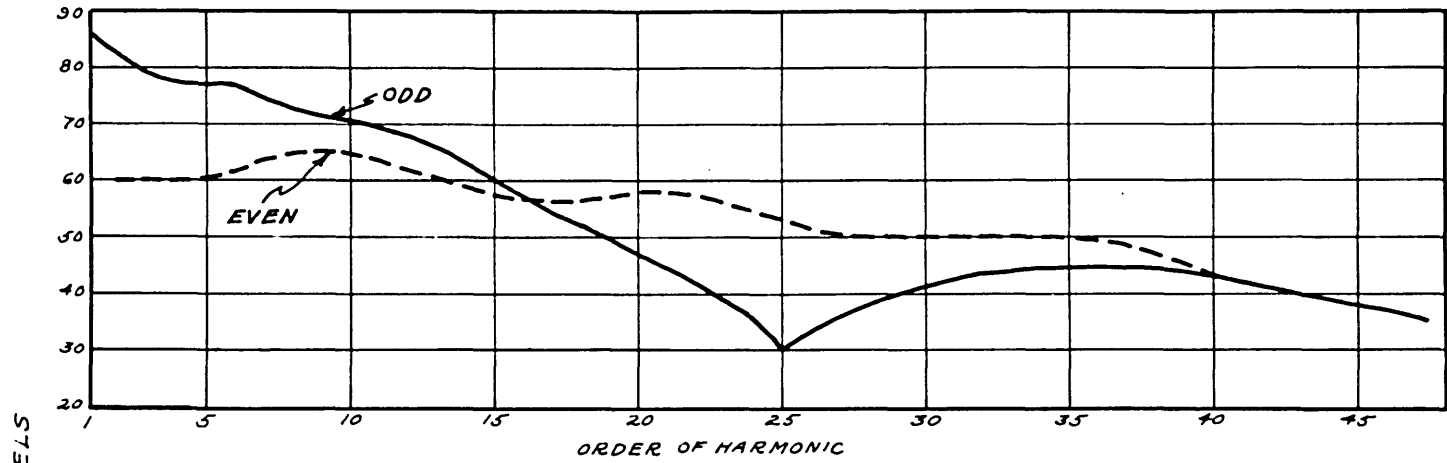
ORIFICE DIAMETER 0.25 CM
 ORIFICE THICKNESS 0.0508 CM



SOUND PRESSURE LEVEL 7 CM FROM ORIFICE
 1ST HARMONIC IS 180 CPS

FIG. 61

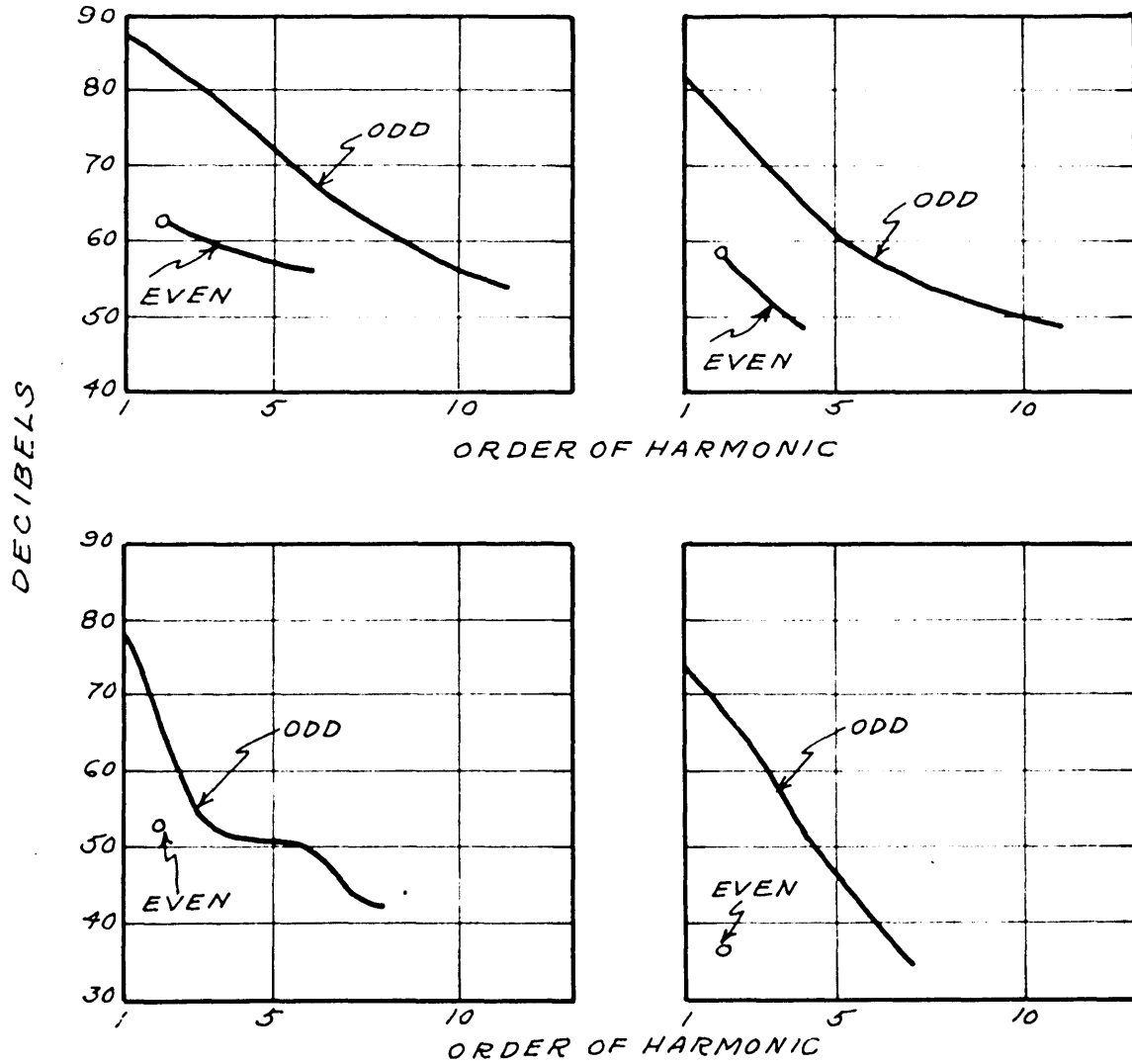
ORIFICE DIAMETER 0.357 CM
ORIFICE THICKNESS 0.09 CM



SOUND PRESSURE LEVEL 7 CM FROM ORIFICE
1ST HARMONIC IS 180 CPS

FIG. 62

ORIFICE DIAMETER 0.357 CM
 ORIFICE THICKNESS $\frac{1}{8}$ "



SOUND PRESSURE LEVEL 7 CM FROM ORIFICE
 1ST HARMONIC IS 180 CPS

FIG. 63

ORIFICE DIAMETER 0.357 CM
 ORIFICE THICKNESS $\frac{1}{4}$ "

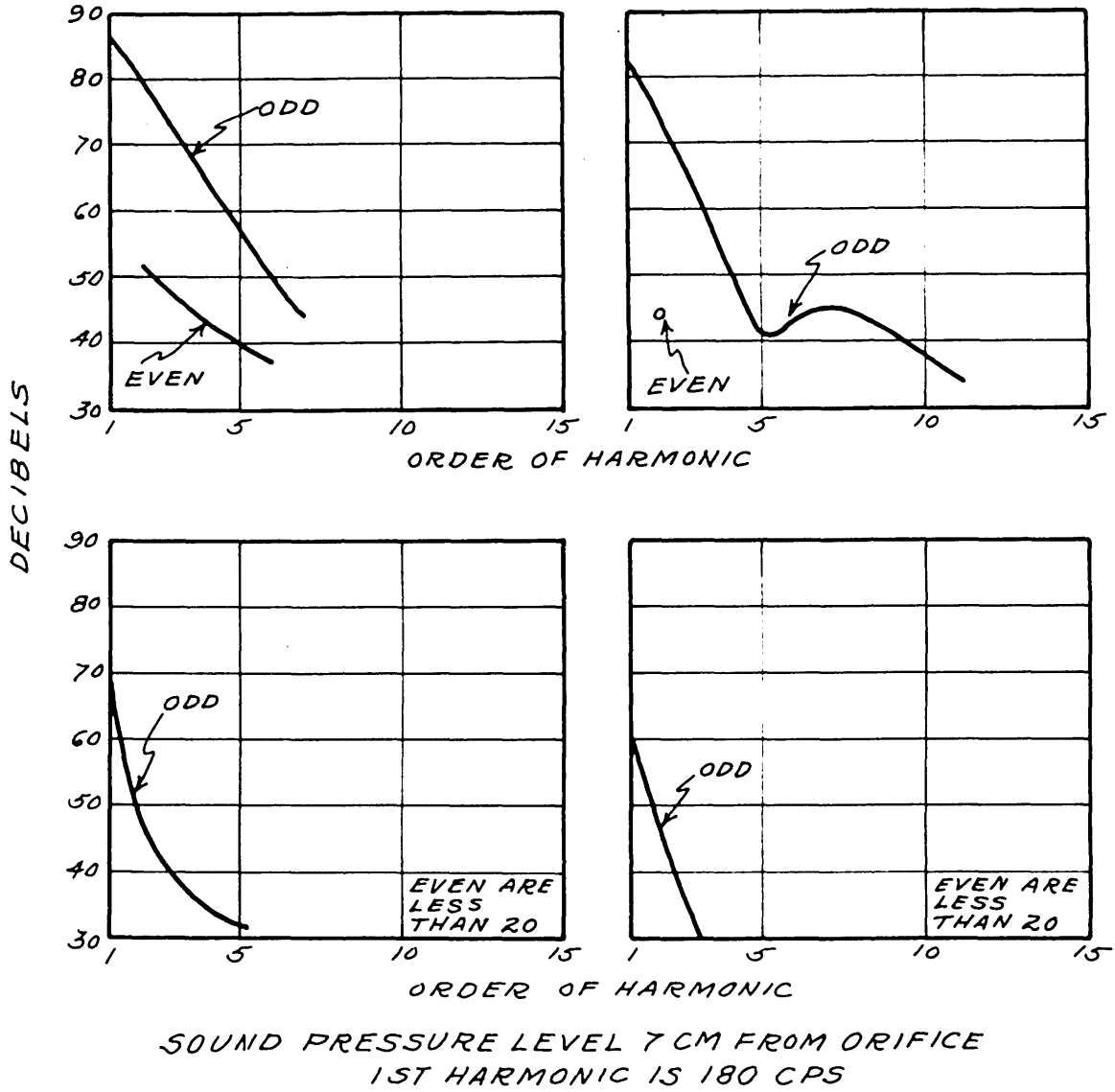
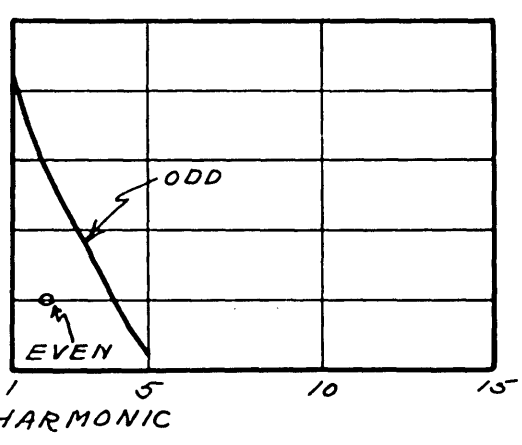
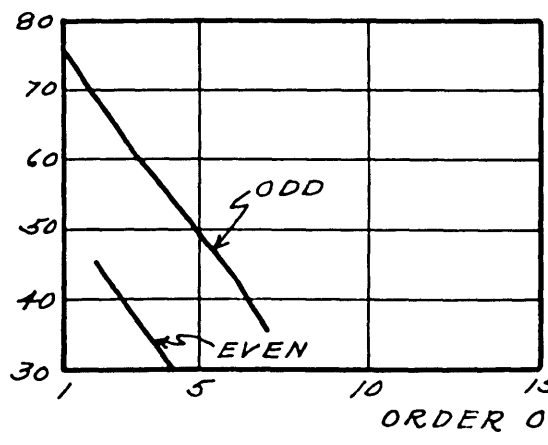
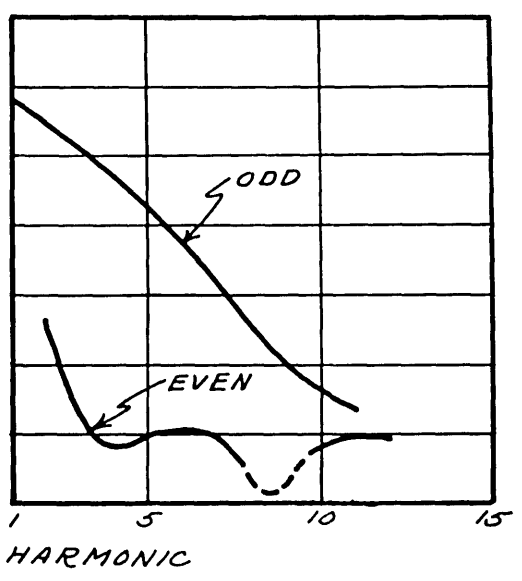
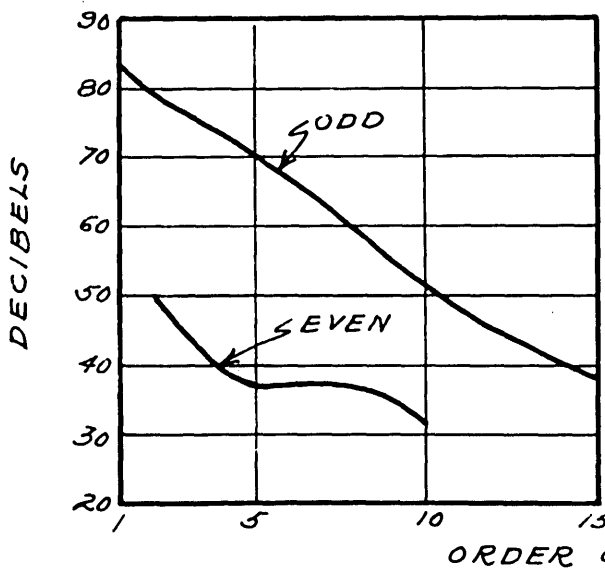
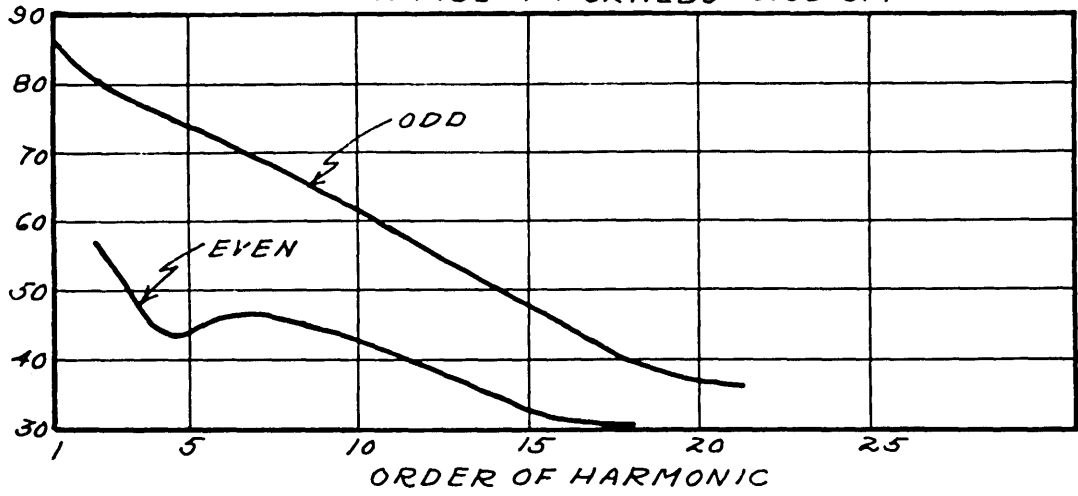


FIG. 64

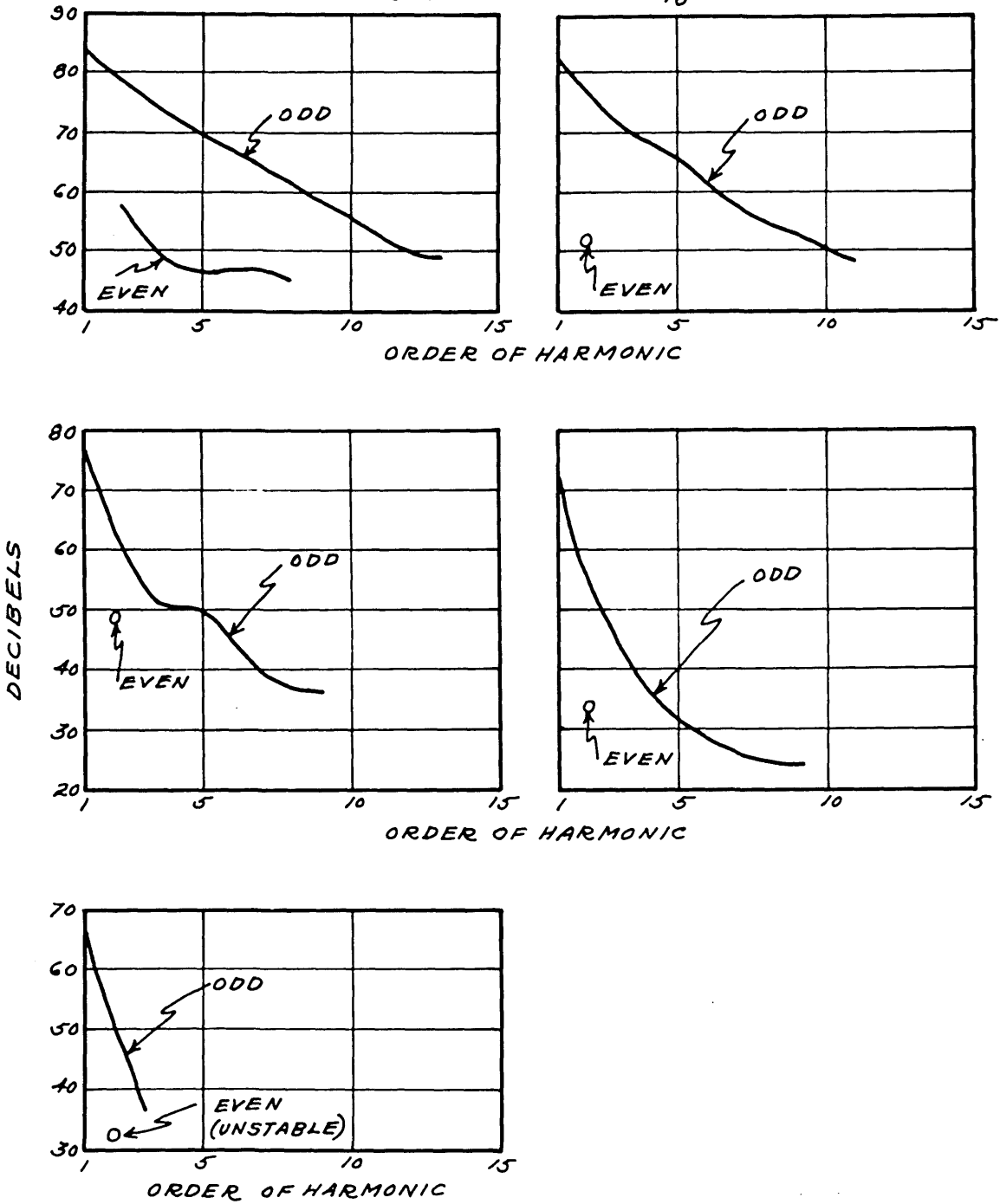
ORIFICE DIAMETER 0.5 CM
ORIFICE THICKNESS 0.05 CM



SOUND PRESSURE LEVEL 7 CM FROM ORIFICE
1ST HARMONIC IS 180 CPS

FIG. 65

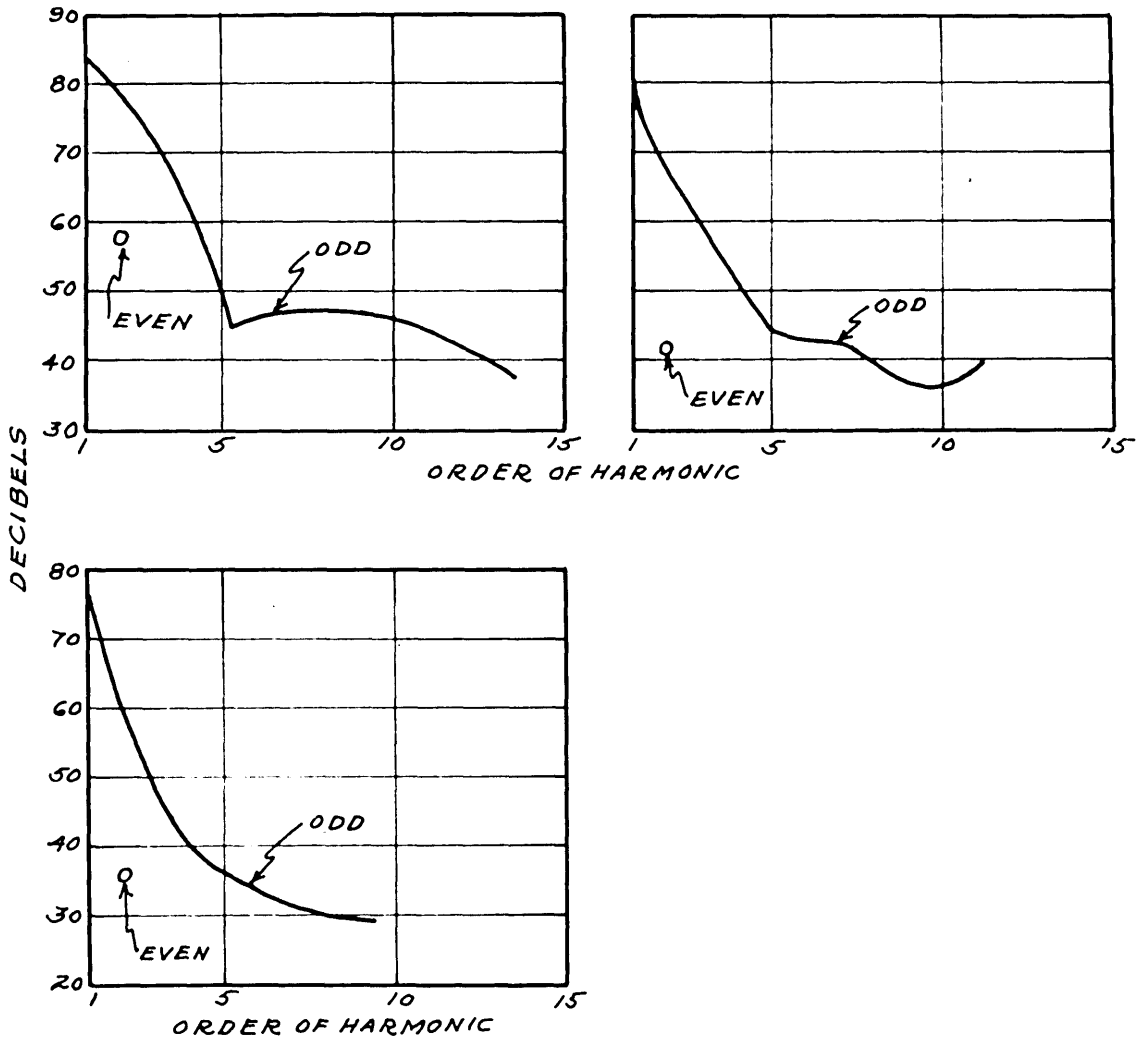
ORIFICE DIAMETER 0.5 CM
ORIFICE THICKNESS 1/8"



SOUND PRESSURE LEVEL 7 CM FROM ORIFICE
1ST HARMONIC IS 180 CPS

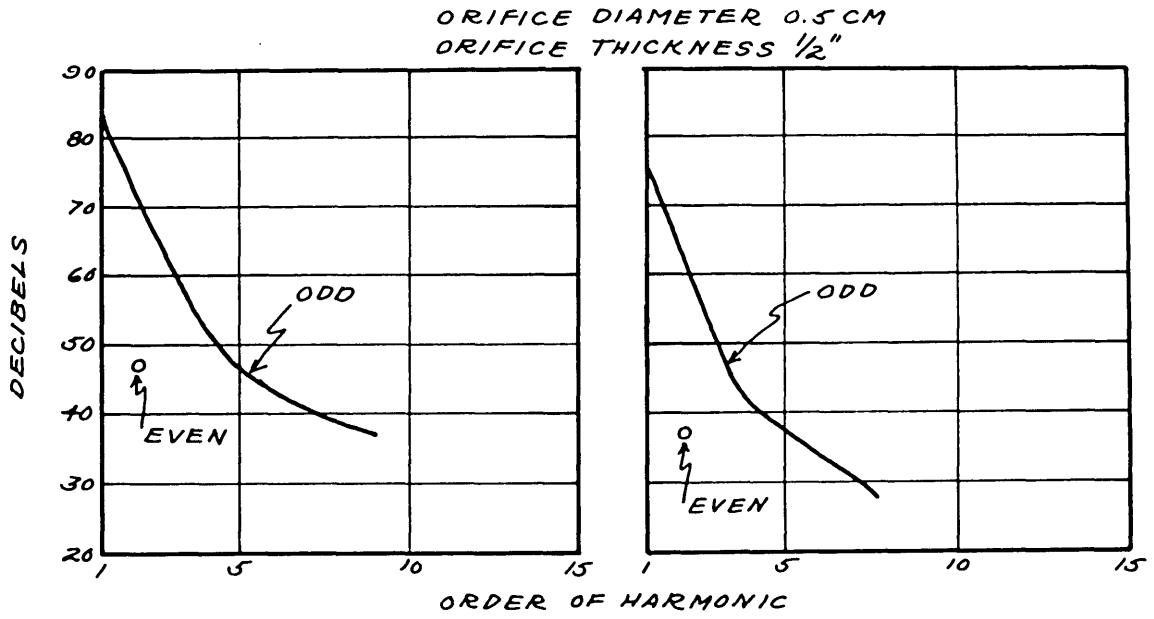
FIG. 66

ORIFICE DIAMETER 0.5 CM
ORIFICE THICKNESS $\frac{1}{4}$ "



SOUND PRESSURE LEVEL 7CM FROM ORIFICE
1ST HARMONIC IS 180 CPS

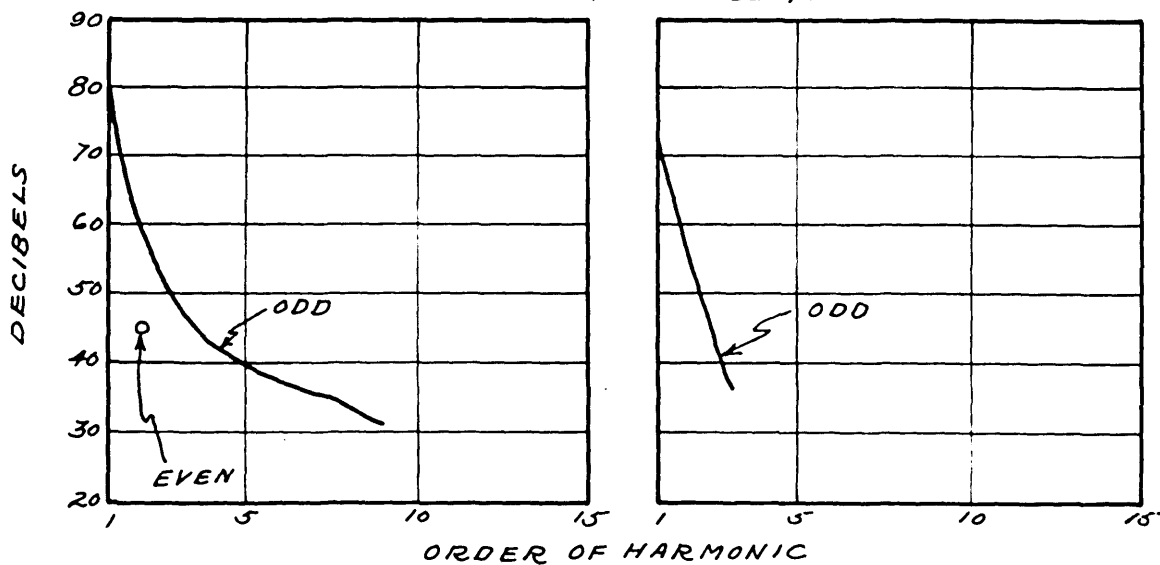
FIG. 67



SOUND PRESSURE LEVEL 7CM FROM ORIFICE
1ST HARMONIC IS 180 CPS

FIG. 68

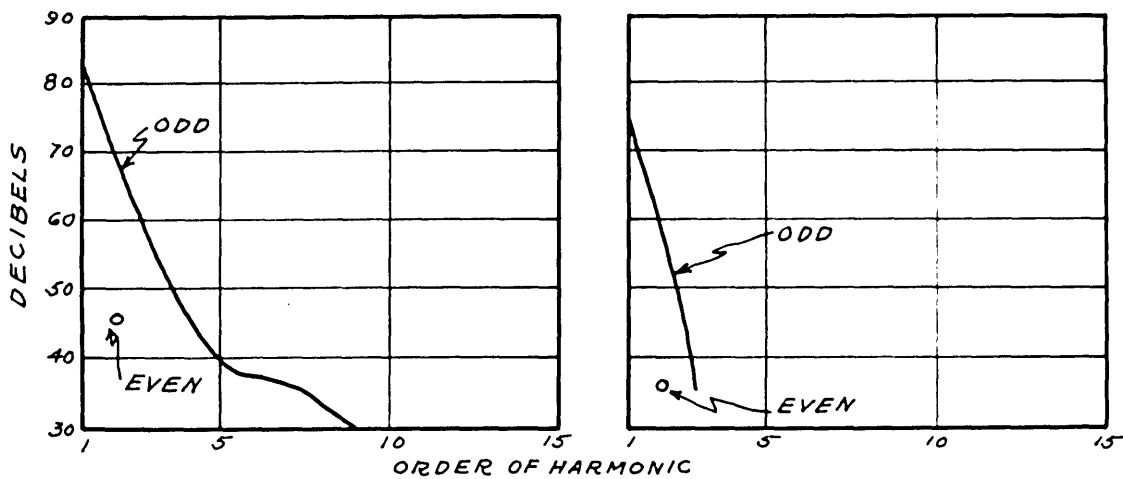
ORIFICE DIAMETER 0.5 CM
ORIFICE THICKNESS $\frac{3}{4}$ "



SOUND PRESSURE LEVEL 7 CM FROM ORIFICE
1ST HARMONIC IS 180 CPS

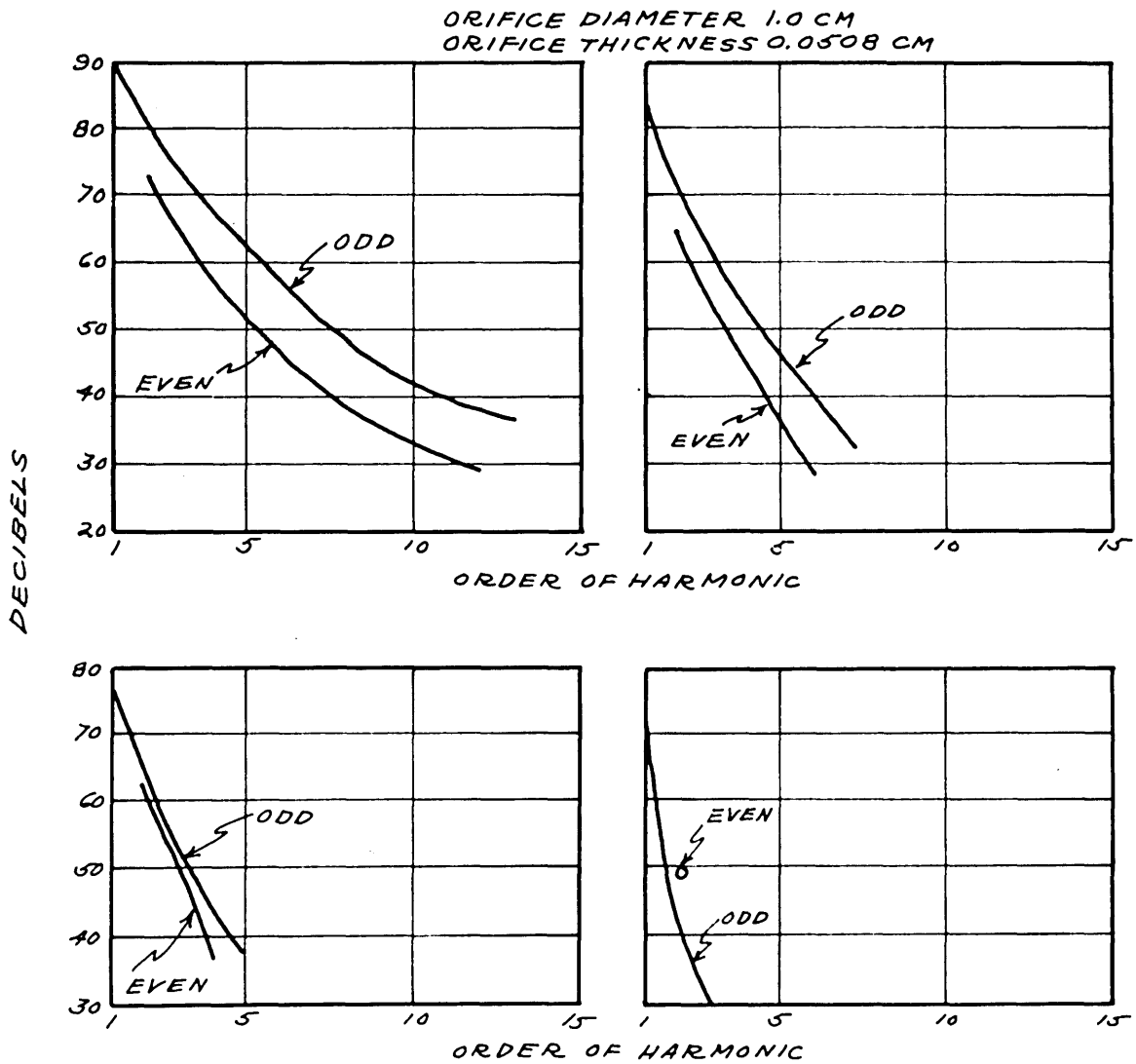
FIG. 69

ORIFICE DIAMETER 0.5 CM
ORIFICE THICKNESS 1/8"



SOUND PRESSURE LEVEL 7CM FROM ORIFICE
1ST HARMONIC IS 180 CPS

FIG. 70



SOUND PRESSURE LEVEL 7 CM FROM ORIFICE
1ST HARMONIC IS 180 CPS

FIG. 71

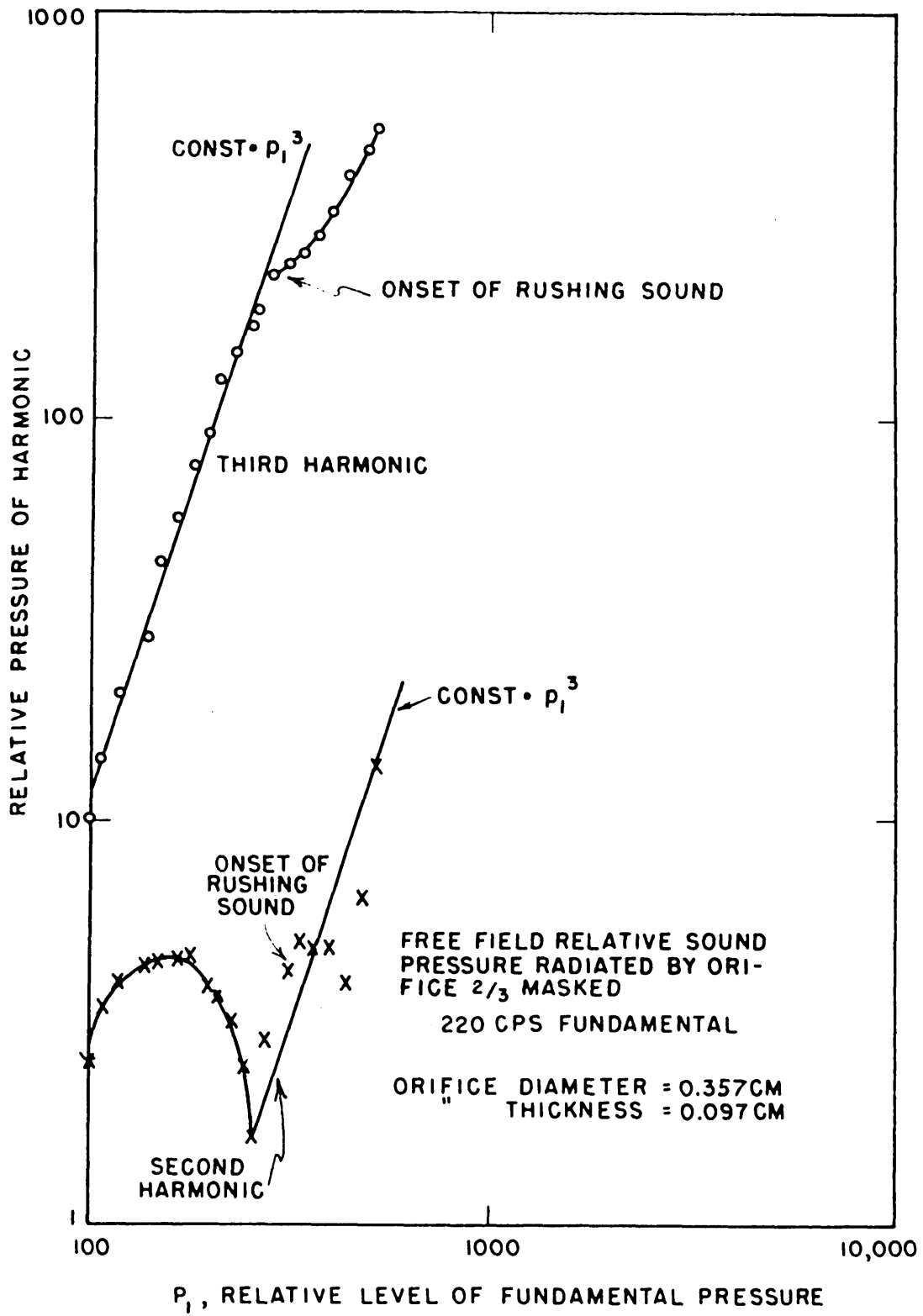
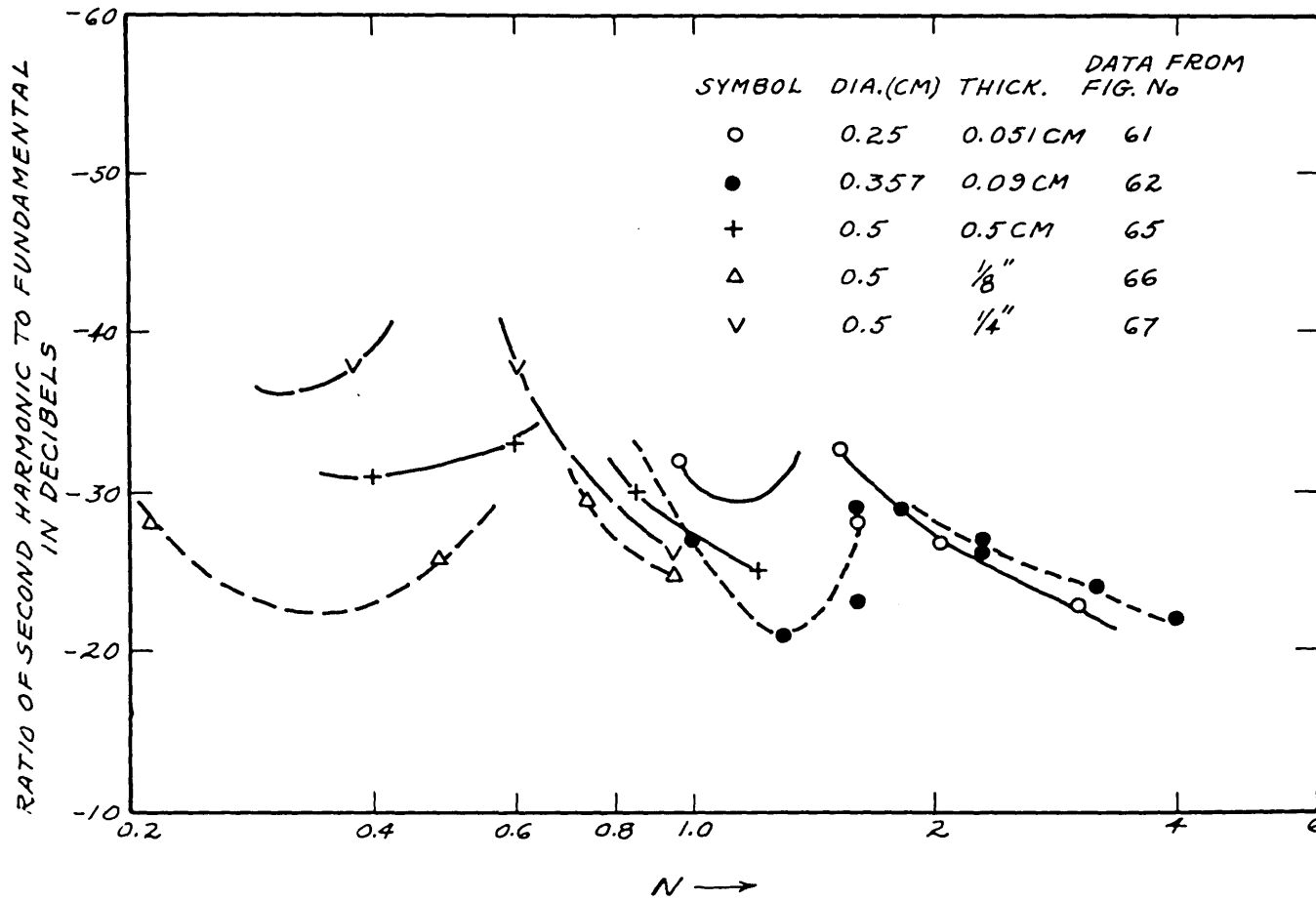
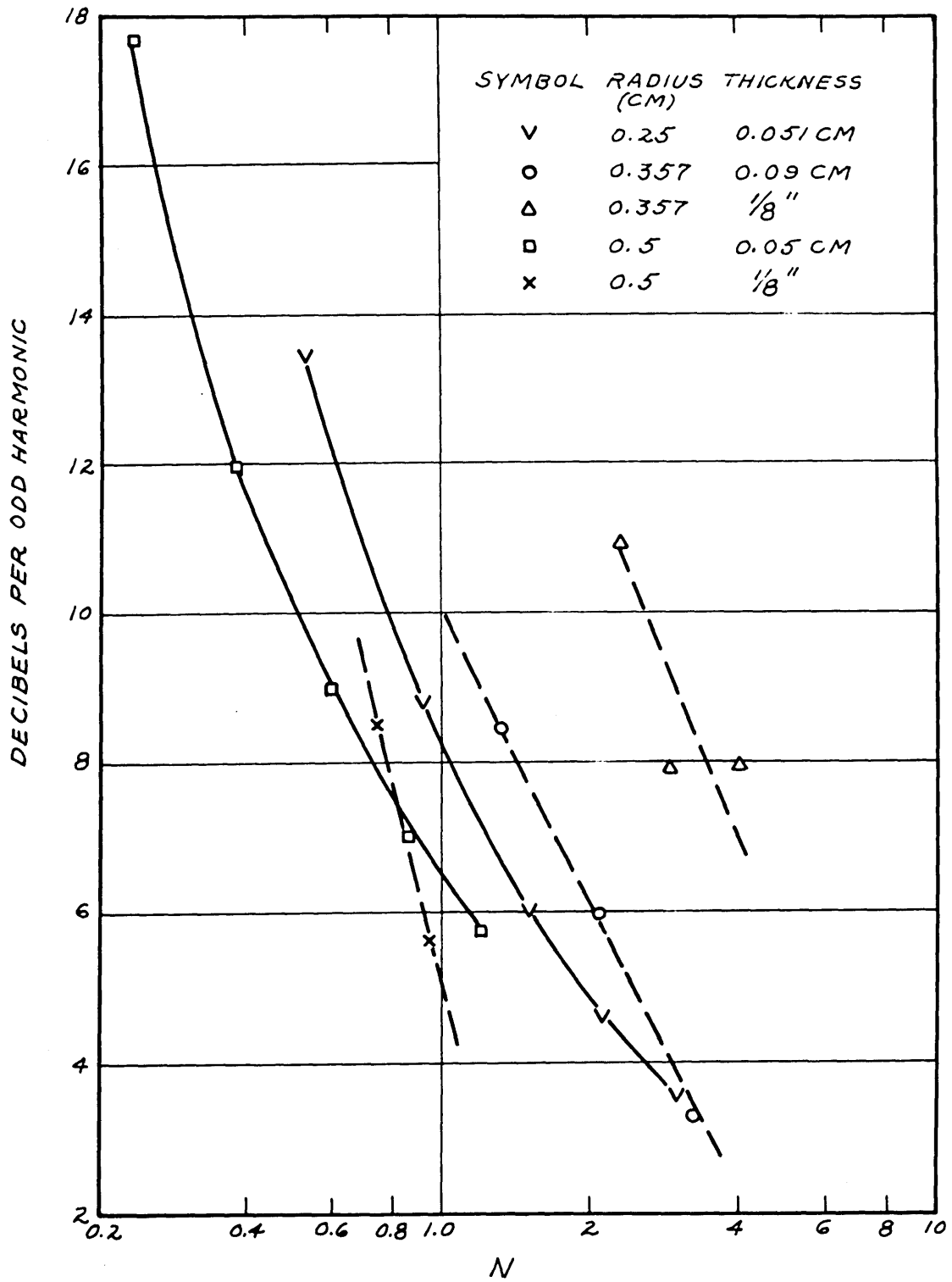


FIG. 72



RATIO OF THE SECOND HARMONIC TO THE FUNDAMENTAL COMPONENT
OF THE SOUND GENERATED BY AN ORIFICE

FIG. 73



APPROXIMATE DECAY RATE OF THE ODD HARMONICS

FIG. 74

BIBLIOGRAPHY

1. P. J. Westervelt, "Mean pressure and velocity in a plane acoustic wave in a gas," *J. Acous. Soc. Am.* 22, 319 (1950).
2. P. J. Westervelt, "Plane waves of finite amplitude", M.I.T. Physics Department Masters Thesis, June 1949.
3. Tchen Chan-Mou, "Mean value and correlation problems connected with the motion of small particles suspended in a turbulent fluid", The Hague: Martinus Nijhoff, 1947.
4. Fluid Meters, Their Theory and Application, A.S.M.E. fourth ed., Part I (1937).
5. Brown and Associates, Unit Operations, New York: John Wiley and Sons (1950).
6. L. J. Sivian, "Acoustic impedance of small orifices," *J. Acous. Soc. Am.* 7, 94 (1935).
7. Karl U. Ingard, "Scattering and absorption by acoustic resonators," M.I.T. Physics Department Ph.D. Thesis, May 1950.
8. R. C. Jones, "Fifty horsepower siren," *J. Acous. Soc. Am.* 18, 371 (1946).
9. Applied Fluid Mechanics, M. P. O'Brien and G. H. Hickox, New York: McGraw-Hill (1937).
10. R. H. Bolt, S. Labate, and U. Ingard, "The acoustic reactance of small circular orifices," *J. Acous. Soc. Am.* 21, 94 (1948).
11. U. Ingard and S. Labate, "Acoustic circulation effects and the non-linear impedance of orifices," *J. Acous. Soc. Am.* 22, 211 (1949).
12. E. J. Lindahl, "Pulsation and its effects on flow-meters," *Transactions of the A.S.M.E.*, 69, 8, November 1946.
13. P. J. Westervelt, "The generation of harmonics by small circular orifices," Abstract No. 40, November 1949 meeting of the Acous. Soc. Am.
14. P. J. Westervelt and P. W. Sieck, "The correlation of non-linear flow and differential resistance for sharp-edged orifices," M.I.T. Acoustics Lab. Quarterly Progress Report, April-June 1950.

See also: Errata to the above reference in Quarterly Progress Report for October-December 1950.

15. P. J. Westervelt and P.W. Sieck, "The correlation of non-linear flow and differential resistance for sharp-edged orifices," Abstract G1, June 1950 meeting of the Acous. Soc. Am.
16. C. Earl McAuliffe, "The influence of high speed air flow on the behavior of acoustical elements," M.I.T. Department of Naval Architecture M.S. Thesis, September 1950.
17. L. L. Beranek, "Precision measurement of acoustic impedance," J. Acous. Soc. Am. 12, 3 (1940).
18. L. Brillouin, "Sur les tensions de radiations," Annales de physique X, t.4, 528-586 (1925).
19. L. V. King, "On the acoustic radiation pressure on spheres," Proc. Roy. Soc. London A147, 215, 225 (1934).
20. L. Cremer, Archiv d. Elektr. Ubertragung 2, 136 (1948).
21. F. R. N. Nabarro, "The force on a body moving uniformly through a gas containing a sound wave," the Philosophical Magazine 41, 1270 (1950).
22. C. Eckart, Phys. Rev. 73, 68 (1948)
23. L. Brillouin, Les Tenseurs en mecanique et en Elasticite, New York: Dover Publications, 1946, pp. 278-304.
24. Rayleigh, The Theory of Sound, New York: Dover Publications, 1945, Vol. 1 and 2.
25. Lamb, Hydrodynamics, New York: Dover Publications, sixth ed., 1945.
26. H. W. St. Clair, M. J. Spendlove and E. V. Potter, "Flocculation of aerosols by intense high-frequency sound," Reports of Investigations, United States Department of the Interior - Bureau of Mines, R.I. 4218, March 1948.
27. Dudley Thompson, Ultrasonic Coagulation of Phosphate Tailing, Bulletin of the Virginia Polytechnic Institute, Engineering Experiment Station Series No. 75.
28. Prandtl and Tietjens, Applied Hydro and Aero Mechanics, New York: McGraw Hill, first ed., 1934.

29. Modern Developments in Fluid Dynamics, ed. Goldstein, Oxford: Clarendon Press, 1943, pp. 491-492.
30. Rider and Uslan, Encyclopedia on Cathode Ray Oscilloscopes and their Uses, John F. Rider Publisher, Inc. New York, 1950.
31. Peter Westervelt and P. W. Sieck, "The steady force exerted on a small sphere in a plane progressive wave containing a second harmonic component," J. Acous. Soc. Am. 22, 677 (A) (1950).
32. P. J. Westervelt and K. Hoyt, "Steady forces produced by sound waves (experimental)," M.I.T. Acoustics Lab. Quarterly Progress Report, October-December 1950.
33. J. Baruch, Electrical Engineering Thesis, M.I.T. 1950.
34. A. B. Wood, A Textbook of Sound, London: G. Bell and Sons, second ed., 1944.
35. Sonic Agglomeration of Natural Fog, Final Report - Part III, Navy Department Office of Research and Invention Contract Number N6-ori-100 with Task Order I Project Designation Number NR-063-23, Ultrasonic Corp., Cambridge, Mass. 1948.
36. E. N. Andrade, "On the circulations caused by the vibration of air in a tube," Proc. Roy. Soc. A134, 445 (1931).

BIOGRAPHICAL NOTE

Peter Jocelyn Westervelt was born at Albany, New York, on December 19, 1919 of parents William Irving Westervelt and Dorothy Jocelyn Westervelt. He attended the public school system of Winnetka, Illinois until entering the North Shore Country Day School in 1934 from which he graduated in 1938. He entered the Massachusetts Institute of Technology in 1938 where he was an undergraduate student until 1940 when he joined the M.I.T. Radiation Laboratory. In 1941 he transferred to the M.I.T. Underwater Sound Laboratory where he remained until the end of World War II. He re-entered M.I.T. in 1945 from where he obtained his B.S. degree in 1947. He continued a course of graduate studies at M.I.T. leading to the M.S. degree in 1949. From 1949 to date he has been pursuing a course of graduate study at the Massachusetts Intitute of Technology leading to a Ph.D. He is a member of Sigma Xi.

His publications to date are the following:

P.J. Westervelt, "Mean pressure and velocity in a plane acoustic wave in a gas," J. Acous. Soc. Am. 22, 319(1950).

R.H. Bolt, P.E.Doak and P.J. Westervelt, "Pulse statistics analysis of room acoustics," J. Acous. Soc. Am. 22, 328(1950).

A.W. Nolle and P.J. Westervelt, "Resonant bar method for determining the elastic properties of thin lamina," J. Appl. Phys. 21, 304 (1950).